Report no. changed (Mar 2006): SM-319-UU

SACLANTCEN MEMORANDUM
serial no.: SM-319

SACLANT UNDERSEA RESEARCH CENTRE MEMORANDUM

VERY LOW FREQUENCY AMBIENT NOISE MEASUREMENTS IN THE IONIAN SEA DATA REPORT

F. Desharnais, H.G. Urban and G.L. D'Spain

September 1997

Report no. changed (Mar 2006): SM-319-UU

SACLANT Undersea Research Centre
Viale San Bartolomeo 400
19138 San Bartolomeo (SP), Italy

tel: +39-187-540.111
fax: +39-187-524.600

e-mail: library@saclantc.nato.int

NORTH ATLANTIC TREATY ORGANIZATION

Very low frequency ambient noise measurements in the Ionian sea data report

F. Desharnais, H. G. Urban,
and G. L. D'Spain

The content of this document pertains to work performed under Project 042-1 of the SACLANTCEN Programme of Work. The document has been approved for release by The Director, SACLANTCEN.

Jan L. Spoelstra
Director

intentionally blank page

Very low frequency ambient noise measurements in the Ionian sea - data report

F. Desharnais, H. G. Urban, and G. L. D'Spain

Executive Summary: Very low frequency ambient noise can be the limiting background interference to the passive detection of targets. Measurements of very low frequency ambient noise were carried out in the Ionian Sea in June 1992. This memorandum introduces all relevant data collected during the sea trial. This includes environmental data, shipping traffic, seismic events and a brief description of acoustic data. Its purpose is to provide a comprehensive overview on data that can be further analyzed in accordance with the scientific objectives of the intended research.

The Ionian Sea experiment was designed to provide information in the very low frequency range, i.e. 0.5 to 50 Hz of the ambient noise. The principal instrumentation was an advanced sensor system of free floating glass spheres also called Swallow floats. They were equipped with a hydrophone and three geophone sensors to measure pressure and particle velocity of the underwater acoustic wave field.

The experiment was a joint operation between SACLANTCEN and the Marine Physical Laboratory (MPL) of Scripps Institution of Oceanography, USA. The sensor system had been developed by MPL for the measurement of very low frequency noise in the deep sea and previously been used in the Pacific and the Atlantic Oceans.

The objective of the experiments was to make VLF measurements of ambient noise in the Mediterranean Sea and to compare the data with previously collected data from the Pacific and the Atlantic Ocean. A further objective was to provide data for a further investigation of the ambient noise spectrum that is not completely understood and which may eventually be exploited for SONAR operation.

The pre-analysis of data shows good quality throughout, the environmental conditions were ideal and the collaboration with the MPL was excellent.

intentionally blank page

Very low frequency ambient noise measurements in the Ionian sea - data report

F. Desharnais, H. G. Urban, and G. L. D'Spain

Abstract: This memorandum describes an experiment and provides a data summary and quality assessment of very low frequency data of ambient noise collected in the Ionian Sea in June 1992. The experiment was a joint operation between SACLANTCEN and the Marine Physical Laboratory (MPL) of Scripps Institution of Oceanography, USA. The sensor system had been supplied by MPL, it consisted of 11 Swallow floats that are neutrally buoyant freely drifting glass spheres which were equipped with sensors to measure acoustic pressure and 3-dimensional particle velocity in the frequency range between 0.5 and 25 Hz. The data of the four sensors can be combined to yield the time averaged acoustic intensity vector, i.e. magnitude and direction of the acoustic propagation obtained in a single point in space. The acoustic data are complemented by a set of environmental data including seismic events, very low frequency propagation and commercial ship surveillance. All the data are of excellent quality, well documented and therefore, can be used to further investigate the very low frequency ambient noise field in the Mediterranean Sea.

Keywords: ambient noise, very low frequency, Swallow floats

Contents

1. Introduction 1
2. Description of the experiments 2
   2.1. Vertical directionality of ambient noise 2
   2.2. Horizontal directionality of ambient noise 2
   2.3. Swallow float experiments 3
3. MPL Swallow float results 5
   3.1. MPL Swallow float general description 5
   3.2. Basic concept 6
   3.3. Localization 8
   3.4. Gain, compass, battery voltage 9
   3.5. Acoustic data 11
4. Conclusions 19
References 20
Figures 21
Annex A - Time and position tables 133
Annex B - Environmental data 135
Annex C - Projector log 138
Annex D - Shipping traffic 139
Annex E - Earthquake information 142
Annex F - MPL Swallow float deployments - sea trial notes 144

1 Introduction

In June 1992 SACLANTCEN and the Marine Physical Laboratory, Scripps Institution of Oceanography, USA, (MPL) conducted a joint sea trial (IONEX 92) on board NRV *Alliance*. The main objective of the sea trial was to make acoustic ambient noise and propagation loss measurements in the very low frequency range of 0.5 to 25 Hz. It was the first time that SACLANTCEN had used Swallow[1] float technology to gather very low frequency ambient noise data.

Swallow floats are free floating, deep water drifting units which contain four acoustic sensors: one hydrophone (pressure sensor) and three orthogonal geophones (particle velocity sensors). The free floating ability reduces flow noise to a minimum, resulting in very good data quality in the frequency range from 0.5 Hz to 25 Hz. The information from the four sensors can be combined to compute the averaged acoustic intensity vector. Using the floats, it is possible to measure both the magnitude and the directionality of the ambient noise field at a single point in space.

Two sets of Swallow floats were used during the experiment. A first set of two were prototypes built at SACLANTCEN. A second set of eleven, used as the primary set, were developed at MPL. The sea trial experiments were conducted in a similar manner to previous Swallow float deployments executed by MPL. To complement the Swallow float measurements, other experiments involving vertical and horizontal arrays were carried out to assess the directionality of the ambient noise field in the higher frequency range.

This report introduces all relevant data collected during the sea trial. This includes non-acoustic data (environmental data, shipping traffic, etc.), a brief description of the acoustic data collected with equipment other than the MPL Swallow floats, and selected very low frequency data collected by the Swallow floats. The emphasis is on the set of very low frequency data, which will be discussed in terms of reliability and consistency compared with previously acquired data.

[1] named after the oceanographer J.C. Swallow

2 Description of the experiments

Three types of experiment took place during the sea trial (June 1992): two to measure the vertical and horizontal directionality of the ambient noise field (involving the deployment of the vertical and horizontal arrays respectively), and one Swallow float experiment involving the SACLANTCEN and the MPL Swallow floats. The objectives of the experiments were to measure the level and directionality of ambient noise at very low frequencies. The Centre's standard ambient noise measurement procedures using the vertical and the horizontal arrays were intended to complement the very low frequency measurements and to assess the directionality of the ambient noise in the higher frequency range.

The nominal position of the experiments was 37°40'N 18°20'E (Fig. 1), in the Ionian Sea. Except for one deployment of the horizontal array, all deployments were in this area. Hardware deployment timetables, including data recording periods, are in Annex A. The environmental data for all the experiments are given in Annex B.

2.1. VERTICAL DIRECTIONALITY OF AMBIENT NOISE

The experiments were carried out at the beginning and at the end of the sea trial (Annex A).

The measurements were made with the SACLANTCEN vertical array, deployed from NRV *Alliance*, and the data were transmitted to the ship *via* a radio link.

The vertical array is composed of two nested arrays of 32 elements each. The separation between the elements is 1 m for the low-frequency array, and 0.5 m for the high-frequency array. The frequency range covered by the array is approximately 50 Hz to 1.5 kHz, which is higher than the frequency range of the Swallow floats. The depth of the middle hydrophone was 408 m for both deployments.

2.2. HORIZONTAL DIRECTIONALITY OF AMBIENT NOISE

The experiments were carried out three times, at periods close to the Swallow float deployments (Annex A). The first two tows were near the nominal position of the trial; the last tow was approximately 95 km south of the site. The precise locations are given in Annex A.

For these experiments, the horizontal array was towed by NRV *Alliance* following a polygonal track according to a well-established procedure. The experimental procedure is explained in [1]. The main product of the data processing is an ambient noise rose, i.e.

a polar plot of the ambient noise spectrum level as a function of geographical direction for selected frequencies.

The horizontal array was configured for 128 hydrophones at a 2 m spacing, but only 64 phones were used due to software constraints. The data were processed on board ship for the following frequencies: 50, 150, 300 and 330 Hz.

Figure 2 shows an ambient noise rose obtained from towed array data collected in an area close to the nominal position of the float deployments, on 3 June 1992. The frequency is 50 Hz, that is 25 Hz higher than the maximum frequency of the MPL Swallow float data. The acoustic field at 50 Hz is strongly directional, with higher levels from the south, indicating that the noise sources are predominantly to the south of the experimental area.

It will be demonstrated that the direction of the average acoustic intensity below 25 Hz, as measured with the MPL Swallow floats, was in the south to north direction. Therefore, the MPL Swallow float noise data agree in directionality with the noise data collected with a towed array.

2.3. SWALLOW FLOAT EXPERIMENTS

The Swallow float experiment was carried out twice during the sea trial. The deployment times and locations for the SACLANTCEN and MPL Swallow floats are given in Annex A.

For each of the two deployments, three MPL floats (#8, 9 and 10) were tethered at the bottom in a triangular configuration, 6.5 km apart (Fig. E1). For the first deployment, the remaining 8 floats were deployed at a nominal depth of 1800 m in a horizontal array pattern inside the area of the triangle. For the second deployment they were deployed in a vertical array pattern at the centre of the triangle. The SACLANTCEN Swallow floats were deployed at 1000 m depth each time, also in the centre of the triangle.

During the second float deployment, a VLF sound source emitting a 20 Hz CW tone was deployed from NRV *Alliance*. The projector was towed in a linear trajectory in a north-south direction (Annex C), and was occasionally activated for 15 min periods. The projector tow was carried out in order to study propagation loss at this frequency and to check the angular precision of the MPL Swallow floats sensor system.

During both deployments, an aircraft from COMARAIRMED deployed a set of very low frequency (VLF) sonobuoys and conducted aerial shipping surveillance in a sector south of the experimental area (Annex D).

The four VLF passive sonobuoys were deployed in pairs, one pair oriented in the north-south direction, and the other west-east. Data monitoring and recording were carried out on board the aircraft. The recording periods are given in Annex A.

The SACLANTCEN floats are considered independently of the MPL floats because of the differences in hardware. The SACLANTCEN floats have no geophones: each float contains one hydrophone only. The recording device, the sampling frequency, and communication frequencies, are also different.

The depth of the SACLANTCEN floats was set for 1000 m, and the floats settled at 1006 m. The data are recorded with an upper bandwidth of 50 Hz. The floats have a 7-day life, although they were recovered after 1-2 days only.

In the first deployment, only one SACLANTCEN float was deployed, and the hydrophone appeared to be out of order. The hydrophone was changed for the second deployment, and the two floats functioned well.

To help explain some of the features present in the MPL float data, a list of seismic events contemporaneous with the two Swallow float deployments was obtained from the Istituto Nazionale di Geofisica (Italy) and the National Observatory of Athens (Greece) (Annex E).

3

MPL Swallow float results

A preliminary analysis has been carried out on the acoustic and non-acoustic data of the MPL Swallow floats. A description of the floats is included. Details of the two deployments during the sea trial are given in Annex F.

3.1. MPL SWALLOW FLOAT GENERAL DESCRIPTION

An MPL Swallow float is a free-floating glass sphere containing four sensors: one hydrophone and three orthogonal geophones. A schematic view of a float is shown in Fig. 3. In addition to the acoustic sensors, each float has the following equipment:

- ballast for depth control (adjustable to ± 100 m) and a float release mechanism;
- transducer for acoustic communication and float localization (8 kHz pings);
- magnetic compass to give the direction of the horizontal geophones relative to magnetic north (towards which the y-geophone is oriented);
- radio beacon (frequency around 160 MHz) to aid float localization when on the ocean surface;
- hardware for automatic recording of up to 20 h of digitized data onto tape (sampling frequency of 50 Hz).

The data recording is automatic. Readings from the four acoustic sensors follow a 0.02 ms cycle, and the values are stored in a temporary buffer. The recording on tape starts after 44 s of data are accumulated in the buffer. One second of data collection is lost during the writing process. Therefore each record of data is 45-s long and consists of 44 s of real data and 1 s of invalid data (zeros). All floats can store 80 records of data per hour, for a maximum of 20 h per deployment.

The floats also feature an automatic gain control (AGC) system which allows a variable gain of 0 to 36 dB to be added to the signal. A calculation is made of the number of clipped points during the last 39 s of each 45-s record. If more than 0.5% of the data points are clipped, the gain will be automatically reduced by steps of 0.5 dB. If no clipping occurs, the gain will be incrementally raised in the same manner. The gain setting is recorded onto tape, as well as the compass heading. More information on the data format can be found in Annex A of [2].

The internal clocks of the floats can be synchronized before deployment to ensure a common time base for the data recording. As the floats need approximately 8 h to settle to a deep depth, data are not recorded in the first 8 h of deployment. For this reason, the first record number on tape is always 640. Table A6 gives the synchronization time for the two deployments during the sea trial, the time of the first record to be written on tape, and the time of the last possible record (some of the floats may not have recorded valid data until the very end, due to an early recovery or other reasons).

As the floats are free floating, flow noise is minimized. However, mechanical vibrations can affect the geophone data at certain frequencies, mostly between 0.5 and 2 Hz. Table 1 shows the main resonance frequencies potentially affecting the data, and the origin of the resonances. The natural rocking frequency is the most likely problem; because of the distance between the geophones and the center of mass of the float, the motion is effectively communicated to the velocity sensors. Motion of the cassette tape recorder causes float rocking which may continue into the following record when data are collected again. The most straight forward solution to this problem is to disregard the first three seconds of data during the analysis, as was done for the present data. The rocking of the float can also be triggered by loud acoustic signals, assuming enough energy is present at or close to the rocking frequency.

The two other resonance frequencies are due to the motion of either the expendable ballast or the ITC transducer which are both located below the float. The data are not usually analyzed below 0.5 Hz, and the resonance at 1.6/1.7 Hz has been occasionally observed during past experiments.

Table 1 *Main resonance frequencies of the Swallow floats.*

Origin	Frequency (Hz)
Natural rocking frequency	0.35/ 0.38
Expendable ballast	0.4 and 1.6/ 1.7
ITC transducer	0.35

Generally, the data are good down to 0.5 Hz, except for the few seconds after the recording to tape, or when resonance occurs. The reader is referred to [3] for a more complete description of Swallow floats in general, and for a mathematical analysis of the resonance frequencies.

3.2 BASIC CONCEPT

As has been mentioned above, the Swallow floats are equipped with four sensors: one hydrophone to take acoustic pressure data and three geophones to measure the three orthogonal components of acoustic particle velocity. The simultaneous collection of pressure and particle velocity data is a unique feature of the MPL float system.

Pressure $p(\mathbf{x},t)$ and particle velocity $\mathbf{v}(\mathbf{x}, t)$ are the two variables of the acoustic field. Whereas pressure is a non-directional variable, particle velocity is a vector in space. The properties of the fluid are given by density ρ_0 and the compressibility $\kappa = 1/(\rho_0 c^2)$

The acoustic field variables are function of time t and space $\mathbf{x}$, they oscillate with the frequency of the sound source. The fluid properties, however, are considered to change slowly with time and location depending on the variability of the physical properties of the fluid. The functional relation between the acoustic variables is given by the two basic acoustic field equations (see also [4]):

$$-\text{grad}\, p(\mathbf{x},t) = -\nabla \cdot p(\mathbf{x},t) = \rho_0 \frac{\partial \mathbf{v}(\mathbf{x},t)}{\partial t}$$

$$\text{div}\, \mathbf{v}(\mathbf{x},t) = \nabla \cdot \mathbf{v}(\mathbf{x},t) = -\frac{1}{\rho_0 c^2}\frac{\partial p(\mathbf{x},t)}{\partial t}$$

Using the basic equations an expression for the instantaneous quantities of acoustic energy density E (= energy per volume element) and acoustic intensity $\mathbf{I}$ (= power per unit area) can be derived:

$$E(\mathbf{x},t) = \frac{1}{2}\rho_0 v^2(\mathbf{x},t) + \frac{1}{2}\frac{1}{\rho_0 c^2}p^2(\mathbf{x},t) \qquad \text{and}$$

$$\mathbf{I}(\mathbf{x},t) = p(\mathbf{x},t)\cdot \mathbf{v}(\mathbf{x},t)$$

The energy of acoustic waves traveling through a fluid is of two forms, the kinetic energy of the moving particles and the potential energy inherent in a compressed fluid. Particle velocity and pressure are both functions of time and space, consequently the energy density is not constant throughout the fluid.

The instantaneous intensity is the product of pressure and velocity. It is a vector in the direction of the particle velocity, alternating with the frequency of the sound source.

In the context of the ambient noise measurement, the instantaneous quantities are of no great practical significance. They are referred to here because the Swallow floats can measure them which is not possible with other systems. In the analysis of ambient noise data, plane wave propagation is assumed with waves traveling in one single direction. The principle result of the Swallow float measurements is the time averaged acoustic intensity vector computed from pressure and velocity data. This is a measure of both, the magnitude and the direction of the acoustic propagation evaluated at a single point in space.

The time averages are to be taken over a time T corresponding to the period of one complete cycle or longer of the harmonic wave motion. The time averaged energy density is:

$$\overline{E}(\mathbf{x}) = \frac{1}{T}\int_0^T E(\mathbf{x},t)dt = \frac{1}{2}\rho_0 v^2(\mathbf{x}) = \frac{1}{2\rho_0 c^2}p^2(\mathbf{x})$$

The time averaged intensity is:

$$\overline{\mathbf{I}}(\mathbf{x}) = \frac{p^2}{\rho_0 \omega}\cdot \nabla\phi(\mathbf{x})$$

p an v are the rms values of pressure and velocity, and $\nabla\phi(\mathbf{x})$ is the propagation vector. The magnitude of the intensity in the plane wave field is:

$$|\mathbf{I}(\mathbf{x})| = \frac{p^2}{\rho_0 c} = \rho_0 c v^2 = pv$$

Pressure can be obtained from velocity by computing the magnitude of the velocity vector and scaling with $\rho_0 \cdot c$, i.e.:

$$p^2(\mathbf{x}) = (\rho_0 c)^2 \cdot \sum_{j=1}^{3} v_j^2(\mathbf{x})$$

In the data analysis, auto-spectra of pressure and particle velocity are computed. The corresponding auto-spectra are related as follows:

$$S_p(f) = (\rho_0 c)^2 \cdot \sum_{j=1}^{3} S_{vj}(f)$$

The indices p and v stay for pressure and velocity respectively. The pressure spectrum can be obtained either directly or using the above equation. The degree of similarity between the two results is an estimate for the quality of velocity data.

3.3. LOCALIZATION

The floats can be localized using the signals transmitted and received by the 8 kHz transducers which are below the floats. Each transducer periodically transmits a 10 ms acoustic pulse (carrier frequency 8 kHz). One such pulse is transmitted every record (i.e. every 45 s), the floats transmitting alternately in a 12-record cycle. Consequently, every float transmits a pulse every 9 min, and it is known which float transmits during any given record.

Once a float has transmitted, the following signals are recorded:
1. Surface reflected signal back to the transmitter;
2. Direct signal to the other floats (unavailable in the case of a bottom float listening to another bottom float;
3. Surface and bottom reflections.

An example of the first case is shown in Fig. 4 (Float 4 receiving signal from Float 4, second deployment). The delay between transmission and reception time has been converted to depth by multiplying it by half the sound speed of 1500 m/s (y axis). The time on the x axis is given in record number. The first arrival (depth 0 m) is due to a weak reflection from the glass sphere of the float. There is sometimes reverberation after the initial signal due to temperature-dependent resonance of the float glass shell. A louder arrival (1200 m) was received after the signal bounced on the sea surface, which is directly related to the float depth. Reverberations after the main arrival are due to sea surface scattering. Two weaker signals can be seen at approximately at 1800 and 3000 m depth: these signals correspond to a bottom reflected arrival, and a surface-bottom reflected arrival respectively. Another example is shown in Fig. 5 (Float 4 receiving signal from Float 4, first deployment). At the beginning of the recording period the float

was still descending to depth, as the surface reflected arrival indicates an increasing range to the surface, and the bottom reflected arrival indicates a decreasing range to the bottom.

The data from the surface reflected path for all floats are summarized in Figs. 6a–6b which show float depth as a function of time (record number) for both deployments. Occasionally the depth information is not included for the entire time of the experiment; the information in these cases is irrelevant as the floats were either descending, ascending, or being recovered. The small depth oscillations of the floats in time are probably due to an internal wave action (the vertical velocities associated with the oscillations are of the order of 1 cm/s or less). Higher alterations in depth have also been observed in the Pacific and Atlantic oceans [5], [6].

An example of the type of signal recovered when the transmitting and receiving floats are different is shown in Fig. 7 (Float 2 receiving signal from Float 0, second deployment) and Fig. 8 (Float 9 receiving signal from Float 10, second deployment). The propagation time has been converted into range by multiplying it by a sound speed of 1500 m/s (y axis). The time on the x axis is represented by record number. The earlier arrival in Fig. 7 represents the direct arrival from Float 2, indicating that the range between the two floats is increasing. The subsequent signals are the surface reflected arrival, bottom reflected arrival, and other multi-reflection arrivals (very weak). In Fig. 8, there is no direct path since the two floats are moored at the bottom, and the sound speed profile at this depth is upward refracting, therefore only the surface reflected path is visible is this figure. The range obtained this way has to be converted into an estimated slant range between the two floats. The range between two bottom floats should be constant, as they are moored. There is usually a slight linear variation in time due to clock drift which is float dependent. The clock drift is cancelled out by averaging any travel time with the travel time of the reciprocal acoustic path (for example, the travel time for the path 'Float 6 to Float 4' will be averaged with the time for the path 'Float 4 to Float 6').

To obtain a geographical plot of float positions as a function of time, a least-square fit algorithm is normally applied to the series of slant ranges [7]. For these experimental data, however, the positions of the individual mid-depth floats were estimated with the help of only two bottom floats, by applied geometry. The position error using this technique is estimated to be within 30 m. The final float tracks for both deployments are shown in Figs. 9a–9b. The period covered for each float is the same as in Figs. 7–8, therefore the tracks are sometimes shortened when data were not available for the entire period. The average drift velocity of the floats is of the order of 2.5 to 3.0 cm/s.

3.4. GAIN, COMPASS, BATTERY VOLTAGE

The header of each acoustic record contains non-acoustic information, including the AGC (Automatic Gain Control) setting, the compass heading of the float (magnetic heading of the y- geophone), and the battery voltage. Useful information on the quality of the acoustic data, or on potential equipment failures can be obtained from the analysis of these non-acoustic data.

Figures 10a–10j and 11a–11i show the non-acoustic data as a function of record number for each MPL Swallow float during the two deployments. Again, the record number can be translated into real time by using the start times of Table A6, and by counting 80 records per hour.

It can be seen in Figs. 10 and 11 that the battery voltage is relatively constant for all floats throughout the two deployments, with sometimes a small decrease towards the end of the period. The batteries worked well and did not need a recharge between deployments. The AGC gain and the compass heading can provide additional information. For example, when the floats are still descending, the heading usually varies relatively quickly, and the AGC gain is minimum due to the high flow noise. An example can be seen in Fig. 10b, where the float stabilizes at depth around record 1450.

Transients of acoustic or non-acoustic nature are also discernible. For example, in Fig. 10d, at record 1760 (approximately), the float rotates twice through 360°, and the AGC gain simultaneously registers zero. It can be hypothesized that the float was struck, and that the impact induced the rotation. The flow noise resulting from the motion overloaded some of the channels (the horizontal geophones in this case), and the AGC gain decreased to adapt to the higher noise level. The rotation could also be created by current shear. The origin of the noise, however, is more likely to be mechanical rather than acoustical in nature since nothing is observed on the hydrophone channel. Figures 11a–11i give an example of acoustic noise. In this case, at record 640 (beginning of the recording period), the projector was transmitting a loud 20 Hz continuous tone, and some of the channels overloaded. As the floats were already stabilized at depth, the magnetic heading of the floats was stable, and the AGC gain decreased steadily to adapt gradually to the projector signal. Note that several cycles of gain decrease/increase can be seen throughout the experimental period, as the projector is activated periodically for approximately 15 min. The total amount of channel overload and therefore the associated gain decrease, diminishes as the range between the projector and the floats increases.

The bottom floats are tethered, which affects both the stability of the heading and the flow noise level (and therefore the AGC gain). The heading is normally more stable overall, but some short-period vibrations can be seen, for example in Fig. 10i. These motions are due to the flow circulation around the tethered float. As the bottom floats are not completely free floating, the acoustic data can be contaminated by flow noise, and the AGC gain lowers to adapt to this situation. As shown in Fig. 10i, between records 1000 and 1600. The AGC gain stabilizes after record 1800, as for the heading of the float.

Technical problems can be identified, for example when the AGC gain in Figs. 10h and 11g (float 8, first and second deployment) indicates malfunctioning. In the first deployment, after stabilization of the float at depth (record 900), the gain increases to values mostly above 20 dB, which are very different from the gain values of the other bottom floats. In the second deployment, the gain remains around 36 dB for most of the period, indicating very low sensitivity channels, and the AGC gain had to increase to register acoustic noise. Analysis of the acoustic data over the first deployment showed that the sensors were functioning correctly up to record 920, when both sensors (hydrophone and z- geophone) started recording 0 volt values. As the compass heading stabilized at record 920, it is assumed that the failure occurred when the float moored itself at the bottom. As both acoustic sensors stopped functioning at the same time, the problem is more likely to be in the electronics, possibly damaged by impact with the bottom.

Tables 2 and 3 list the main events in the non-acoustic data during the two deployments. Record numbers are approximate. The settling time indicates that the preceding records may be contaminated by flow noise as the float is still descending to depth. The release time also indicates potential flow noise contamination for subsequent records. For the second deployment, the settling and release times are not given as the acoustic data were

taken after the floats settled to depth. No distinction is made at this point between acoustic and non-acoustic sources for the loud events.

Table 2 *Events during the first deployment (time in approximate record number).*

Float #	Settling time	Release time	Loud events	Comments
0	–	900	–	
1	1440	–	1950, 2100	
2	–	–	1300, 2050	
4	1300	–	1800	
5	–	1150	–	
6	1450+	–	1700, 1900	Loud event at 1500? (the float could still be settling down)
7	1300+	–	–	
8	900+	–	–	No valid acoustic data after mooring
9	950	–	–	Tether noise at beginning, but data seem clean after 1800 (gain stabilizes).
10	1000+	1600	–	Tether noise seems low from 1000 to 1600

Table 3 *Events during the second deployment (time in approximate record number).*

Float #	Loud events	Comments
0	700, 1650, 2050	
1	2150	Wide cycles in heading (stronger current shear?)
2	–	
4	1550	The compass apparently failed around record 1550. The hydrophone was not functioning during the deployment.
5	–	
6	700, 1050, 1550	
8	1170, 1725	No valid acoustic data
9	1500	
10	–	Erratic heading due to multiple crossings around 360°

3.5. ACOUSTIC DATA

This section will cover some aspects of the acoustic data collected with the MPL Swallow floats during the two deployments the sea trial. The full data set was sampled to demonstrate that the acoustic data are consistent between different floats and different deployments, comparable to previous data collected with the same floats in other locations, and reasonable for the area and environmental conditions at the time of the experiments. The sample in addition helps in identifying particular acoustic and non-acoustic events recorded during the experiments.

In order to be consistent with the previous data collected with the same floats, an effort was made to use the same formats and presentation as for previous MPL reports or external publications.

3.5.1. Data overview

Figures 12a–12j (first deployment) and Figs. 13a–13i (second deployment) show the periods for which the data are overloaded on any of the four acoustic channels. The figures present the number of clipped points (or data points equal to the maximum value allowed by the A/D converter) throughout the time series, for all four acoustic sensors. All data for periods of high clipping should be analyzed with care.

A sample of the raw time series is shown in Figs. 14a–14d, for each of the four acoustic sensors (hydrophone and three geophones) of Float 2 during the first deployment. The units are in volts, corrected for the AGC gain. The time series of Figs. 14a–14d are representative of deep mid-ocean data collected with Swallow floats: both short spikes and longer transients are often observed with other features which are discussed later.

Spectral analysis of the data is carried out on a record basis. The first 3 s of each 45-s record are disregarded as they may be contaminated by tape recorder noise. The last second is also disregarded as it is the period during which the buffer data are recorded on tape, when acoustic data are not collected. The remaining time sequence is separated into seven sections of 512 points (10.24 s) with an overlap of 50% between sections. A Fast Fourier Transform is applied to each section, and the seven spectra are averaged into one final spectrum for the record. Spectra can be averaged over several records for longer time averages. The calculation is explained in more detail in [8].

As the sampling frequency is 50 Hz, the spectra are calculated for the frequency range of 0 to 25 Hz (the data below 0.5 Hz are contaminated by self-noise, as explained in subsect. 3.4.2). As the hydrophone data are converted from V to μPa, the hydrophone spectra are in dB// 1 $\mu Pa^2/Hz$. An example is shown in Fig. 15a, where the hydrophone spectrum is the dashed line (the average period is 2.5 h in this case). An equivalent spectrum can be calculated with the three orthogonal geophones. (By using the conversion factor of $\rho_0 c$, the equivalent geophone spectrum has the same units as the hydrophone spectrum). If the medium is spatially homogeneous (as it typically is at mid-depth of deep water) the two spectra are equivalent and the mean kinetic energy density per frequency is equal to the mean potential energy density per frequency [3].

We can hypothesize that above 5 Hz, the noise spectrum level is dominated by shipping noise. In Fig. 15a the background noise level between 10 and 25 Hz is approximately flat (except for the individual shipping lines) and around 85 dB for both deployments, which corresponds to a reasonable noise level for an area of heavy shipping [9-10]. Several discrete shipping lines can also be seen above 5 Hz and the line levels will vary according to local traffic.

The spectrum is fairly flat above 15 Hz, at approximately 87 dB. The ambient noise rose from Fig. 2 gives an average level in the south direction of 68 dB re μPa/Hz deg. The high levels cover an area of approximately 130°, therefore the average noise level in the south quadrant is 91 dB + 10log(130°) = 89 dB re μPa/Hz. The MPL Swallow floats and the towed array in this case are within 2 dB in agreement. Considering the small differences in frequency, sensor depth and date, the difference in level is very small.

Below 5 Hz, the noise level is dominated by wind and wave–wave interaction effects. During the second deployment, the winds increased from light to 17 kn (9 m/s) between 21:00 (7 June) and 8:00 (8 June). Figures 15a–15g present a 2.5-h average of the spectra for the entire period of the second deployment, and the effect of the increasing wind speed can be observed in the levels below 5 Hz, which gradually increase (the hydrophone data show the increase well, the geophone data unfortunately is contaminated by mechanical events). Wind correlation is discussed in [4].

Figures 16-18 (a and b) and 19 show examples of the type of information obtained from time-spectral analysis of hydrophone and geophone data for some of the floats during the first and second deployment of the sea trial. The figures show a) the gray scale plot of the hydrophone spectra for the duration of the deployment and b) the gray scale plot of the equivalent geophone spectra for the same period. The spectrum level scale in dB is on the right-hand side of the figures. The spectra were averaged over 3 min, the resolution of the plots therefore is 0.098 Hz on the horizontal axis per 3 min on the vertical axis.

To quantify more precisely the similarity of the spectra, a 2.5 h (or 200 records) average of the spectra was performed for each float during the second deployment (the first deployment data were used for Float 7 which was deployed only once, and for Float 4 which had a defective hydrophone in the second deployment). The absolute time of the period varies for each float, attempting to avoid those times when the geophones were contaminated by non-acoustic events (being non-acoustic in nature, these events also occur at different times for each float). The averages are shown in Figs. 20a-29a. The geophone equivalent spectra are the solid lines, and the hydrophone spectra are the dashed lines. Figures 20b-26b show the ratio (in dB) between the two spectra.

Figures 27-29 are for the bottom floats (no horizontal geophones), therefore the spectra ratios are not available for these floats. A positive ratio indicates that the geophone levels were higher than the hydrophone levels.

The spectra and spectral ratios of Figs. 20-29 (a and b) were compared with those of two previous Swallow float experiments: the August 1990 Native 1 experiment (Atlantic Ocean), and the July 1989 experiment (Pacific Ocean). The average levels above 10 Hz were approximately 75 dB in August 1990 and 80 dB in July 1989. The averaged levels of this sea trial are closer to 85 dB, which may be contributed to higher shipping density. The level in the noise around 5 Hz however, is similar to those of the earlier experiments.

Figures 20c-26c show the three orthogonal geophone spectra for each of the mid-water floats in dB// 1 (μm/s)/Hz (the conversion factor $\rho_0 c$ was not used). These figures allow comparison of relative responses of individual geophones. Both horizontal geophones have similar responses, although the spectra of the vertical geophones tend to be 5-10 dB lower than those of the horizontal geophones. The weaker signal on the vertical geophones can be explained by mid ocean acoustic propagation. Due to the nature of the sound speed profile, the acoustic energy is trapped in the sound channel and propagates at shallow angles, causing a stronger response on the horizontal geophones. This is typical of data collected with Swallow floats during previous experiments. Data for the z-geophone only are given for the bottom floats (Figs. 27b-29b). The levels on the z-geophones are 10 dB lower for the bottom floats than for the mid-water floats.

The sound field directionality can be investigated by using the vectorial capability of the Swallow floats. Combining hydrophone and geophones signals, we can calculate the

magnitude and the direction of the acoustic intensity (see section 3.2) for discrete frequencies between 0.5 and 25 Hz.

Two examples of intensity vector plots are shown in Fig. 30 (first deployment) and 31 (second deployment). The resultant intensity vectors are frequency dependent, and are plotted here for each frequency bin of the spectral analysis (approximately every 0.1 Hz). The magnitude of the intensity, in dB// 1 $\mu W/m^2/Hz$, is obtained by measuring each vector along the vertical scale, starting at -80 dB (a conversion to dB // 1 $\mu Pa^2/Hz$ can be obtained by adding 122 dB). Directionality is given in degrees (compass on the right-hand corner).

The intensity vectors point in the direction opposite to the source. If there is more than one source, the vectors will point in some direction opposite to the source directions. Figures 30 and 31 show that during both deployments the prevailing direction of very low frequency acoustic energy is south-north. This is consistent with the closest shipping lane directly south of the experimental site. It will be shown later that some vectors at specific frequencies are directly associated with local shipping.

3.5.2. Non-acoustic noise of mechanical or other origin

Several types of non-acoustic noise can affect the Swallow float data caused by the hardware located in the float (self-noise or tape-recorder noise), or by external factors (float motion due to non-acoustic factors).

The grey scale plots shown previously are particularly useful in detecting non-acoustic noise. As a non-acoustic event is unlikely to affect the hydrophone and the geophones in the same manner, these periods can be recognized as the periods for which the hydrophone spectra and the geophone derived spectra are non-identical. For example, in Fig. 17a–17b the hydrophone spectrum appears normal, but the geophone derived spectrum around record 2050 is extremely noisy, and therefore at least one of the geophones is recording high particle velocities which are probably not of an acoustic nature.

Section 3.1 has already presented the different resonance frequencies which could affect the Swallow float data. Previous experiments in other locations have demonstrated that the main resonance frequencies observed are 0.35 Hz and 1.7 Hz [6]. Figs. 20b-26b show similar resonance frequencies.

Resonance frequencies are excited mainly by the operation of the tape recorder. When the data from the temporary buffer is recorded on tape, the tape recorder induces float oscillation that eventually dampens out. This effect is seen in the time series of the x- and y- geophones in Figs. 14b–14c, at the beginning of each record. Because of this known effects, the first three seconds of data of each record are discarded before the spectral calculations. In previous experiments, this effect was reduced by additional post-processing of the data: as the oscillation pattern is similar from one record to the next of any given float, the first few seconds of a few records can be averaged to determine the temporal pattern of the oscillation, which is then removed from subsequent records. This post-processing was not done for the present data, therefore even if three seconds of data were always rejected for all records, some tape recorder contamination can still be seen

for some floats. Figure 16b shows the gray plot for the geophone of Float 7, first deployment. The 1.7 Hz line is evident on this plot.

The very marked non-acoustic effect in Fig. 17a–17b around record 2050 has a different origin. Such an effect has been noted in previous experiments, but not to the extent observed during this sea trial. The loud events are characterized by:

1) a strong oscillation in the time series of the horizontal geophones (Fig. 14c, record 1553) which is slowly dampened in time and which is normally associated with large amounts of clipping;
2) a very high geophone noise level below 5-10 Hz (Fig. 32);
3) a normal hydrophone noise level (Fig. 32) with no clipping in the hydrophone time series (Fig. 14a);
4) no apparent directionality in the intensity vectors (Fig. 33);
5) occasional resonance frequencies every 0.45 Hz in the geophone spectra (Fig. 34).

The above items seem to indicate that the float received a physical shock which started a rocking motion. The motion is sensed primarily by the horizontal geophones, although in cases it also affects the vertical geophone (to a lesser extent). The most probable cause would be an encounter by the float with nekton [6] or fish. Nekton would be attracted either by the bright yellow color of the floats, or by the pinging of the localization transducer. A similar effect has been observed on one occasion during a deployment in the Pacific Ocean, and several times during a deployment in the Atlantic Ocean. In the latter case, the effect was more frequent for the shallower floats than for the deeper floats, which would corroborate the hypothesis of nekton as nekton is more dense in shallower water. In the case of the Mediterranean Sea, the event happened frequently during the second deployment, with no correlation with float depth. A higher density of nekton in the Mediterranean area may be a factor. The absence of correlation with depth could be due to the much clearer water in the Ionian sea, and the deeper distribution of nekton.

Tether lines cause strumming which affects the bottom float data. Figure 19a shows a broad line around 5 Hz at the beginning of the deployment, and reappearing occasionally. The vertical geophone is also affected by strumming for the time-averaged section around record 700 (Fig. 35). Frequent strumming complicates the analysis of bottom float data.

The main non-acoustic events for all floats during both deployments are listed in Table 4. The main criteria for selecting these periods was: a high-level noise on the geophone and no or low noise on the hydrophone.

Table 4 *List of main non-acoustic events for each float.*

	Float number	Records affected
First deployment	0	880
	1	1450, 2000, 2010, 2100-2170
	2	1280-1310, 1580-1600, 1680, 1920, 1970, 2040-2060, 2120
	4	1760-1800
	5	–
	6	1450-1530, 1700, 1910-1920, 1980-2000, 1330
	7	–
Second deployment	0	1400-1440, 1630-1670, 1735-1745, 2030-2060
	1	850-865, 950-975, 1035-1090, 1360-1370, 1390-1400, 1880-1890, 2210-2215
	2	1645-1655, 1715-1725, 2060-2065, 2105-2125
	4	1545-1555, 1590-1620, 1670-1685, 1730-1745, 1990-2020, 2140-2170
	5	1040-1050, 1415-1430, 1668-1672, 1805-1815, 1890-1905
	6	1016-1030, 1045-1065, 1385-1440, 1550-1580

3.5.3. Acoustic noise

The following acoustic sources were recorded by the MPL Swallow floats during the experiment and could be identified: the 20 Hz CW projector tone, several ships including NRV *Alliance*, minor seismic events some of which were monitored by land stations in Italy and Greece.

The best located source was the projector towed by NRV *Alliance*. The ship's position was monitored throughout the tow, and the position of the projector can be extrapolated from that. The projector was activated a few minutes before the floats started recording data (i.e. after their initial 8 h period of descent to depth without any data recording). The initial AGC gain for the floats is set to 14 dB, therefore at the beginning of the recording, all floats were saturated by the loud projector tone. Figure 36 shows the number of clipped points for all acoustic sensors and the AGC gain as a function of record number for float 5. The number of clipped points being higher than 0.05% at the first readings, the AGC gain goes down in steps of 0.5 dB. The data should not be used for the initial time period when the percentage of clipped points is too high. It can also be observed that the number of clipped points is higher for the y- geophone than for the x- geophone, which is due to the orientation of the float. The magnetic heading of float 5 is around 0° during this period, indicating that the y- geophone is in line with the acoustic propagation from the projector directly south of the float field. The x- geophone, perpendicular to the flow, has a minimal response.

Figures 37a-37e) show the intensity plots obtained by all functioning mid-water floats for a three-minute (four-record) period during the first tone emission during the second

deployment. The time was selected to avoid the period of high clipping, i.e. a few records after record 640 (beginning of the recording). The projector was at approximately 20 n. mi. south of the Swallow float field at that time. The intensity vectors should point in the direction opposite to the source, which was always south of the float field. There are some large discrepancies in the direction obtained from the different floats, the angle reading from 0° to 23°, which may be due partly to the calibration curves used for the hydrophones and geophones. The calibration curves of Float 6 are applied for all floats during the processing, and the angle error is minimum for Float 6. The use of correct calibration curves for each float may reduce the error on the angle. However, large errors such as for Float 5, are probably due to small differences between the two horizontal geophones within any particular float. If the x- geophone has a slightly different response than the y- geophone, the angle accuracy would diminish. One solution to this problem is to take the angle measurements over a longer period. If the float rotates during the measurement period, changing the location of the source relative to the x- and y- sensors, the error would decrease. In Fig. 37, the best angles are achieved by Floats 0, 1 and 6, which rotated through 17°, 4° and 32° respectively during the measurement period. The worst estimates are made by Floats 2 and 5, which rotated by less than 1.5° during the measurement.

Ships can emit several frequency-related lines simultaneously, and independent intensity vectors can be used for tracking the source. For example, Fig. 38a shows a three-minute average spectrum taken during the second deployment, and Fig. 38b shows the associated intensity vector plot. It is assumed that at least two ships were in the area close to the float field during this particular period. The assumption is based on two series of strong harmonically related lines. The first series of lines at 6.6, 9.9 and 13.2 Hz is oriented at 22°, indicating a source at 202°. The second series at 5.3, 7.0, 8.9 and 10.6 Hz is closely related and indicates a source at 320°. Of course, if two ships transmitting the same harmonic lines were in the area, the floats would show the resulting field from the addition of the two sources. However, the presence of 3 or 4 strong harmonic lines all pointing in the same direction indicates that only one ship is related to these particular lines. Figure 18 also shows well the different harmonic lines around record 1708.

A third source of interest is a low intensity seismic event which was monitored by land stations in Greece during the first deployment. This seismic event is the first shown in Table E1, Annex E, with an epicentre south of Crete (Greece). The direction from the estimated epicentre to the float field is 122°. Figures 39 and 40 show the spectrum level and the intensity vector plots averaged over four records before and during the event. The spectrum levels during the event are affected by significant clipping. The observed effect is a large increase in the spectrum levels below 10 or 15 Hz, and a reorientation of the intensity vectors in the same frequency band. The intensity vectors have a direction of 300°, which is almost exactly 180° from the direction of the epicentre. Therefore a large amount of low-frequency energy travelled from the epicentre, probably in the sound channel, and was registered by all the floats deployed in the area.

The other seismic events listed in Table E1 did not affect the floats. The epicentres were more distant and inland. The underwater propagation path did not exist for these, or at least not in a direct manner as for the Crete earthquake. However, during the first deployment (and to a lesser extent during the second deployment), the floats registered a large number of secondary events with similar characteristics to that of the Crete earthquake. Also, the events were generally registered on several floats simultaneously, indicating that the sources should be acoustic in nature. The majority of the secondary sources are from the south-east quadrant. In this direction, south of Crete, lies a subduction front area, or area normally rich in seismic activity. It is believed that the area

around the Island of Crete was seismically active during the first deployment, and that the events were caused by this activity.

Table 5 *List of main acoustic events.*

	Records affected
First deployment	656-660, 676, 736, 744-752, 808, 828, 852, 908, 928, 968-972, 984, 1000-1004, 1032-1036, 1100, 1144-1148, 1192, 1280, 1408, 1428, 1448, 1456, 1488, 1512, 1556, 1692, 1708-1712, 1728, 1740-1752, 1776, 1788, 1812, 1824, 1840, 1924, 1948, 1964, 2156-2160, 2232
Second deployment	752, 820-828, 1064, 1096, 1168, 1252, 1364-1372, 1480, 1604, 1672, 1680, 1732, 1912, 1968, 2000

The main acoustic events during both deployments are listed in Table 5. To qualify, an event had to be registered by several floats at once, the spectrum levels had to increase in the 0-5 Hz band, and there had to be some directionality in the vectors for that frequency band. A 4-record average was made before the check.

4 Conclusions

During a sea trial in the Ionian Sea in June 1992, ambient noise data were collected. The experiment was specifically designed to provide information in the very low frequency range, i.e. 0.5 to 50 Hz. The principal instrumentation was an advanced sensor system provided by the Marine Physical Laboratory, Scripps Institution of Oceanography which consisted of free floating glass spheres also called Swallow floats. The spheres were equipped with a hydrophone and three geophone sensors to measure pressure and particle velocity of the underwater acoustic wave field.

Other ambient noise data in the higher frequency range was collected with different equipment: two independent SACLANTCEN Swallow floats, vertical and horizontal line array and two groups of air-deployed VLF sonobuoys. A VLF transmission of a sinusoidal signal at 20 Hz was made to measure the propagation loss at this frequency for various ranges. This memorandum summarizes the information (both acoustic and non-acoustic) from the sea trial.

The analysis of the VLF noise data shows that the data are of good to excellent quality. If the data from the four acoustic sensors of the floats are analyzed together, they give an estimate of the three-dimensional acoustic field, i.e. the magnitude and direction of the ambient noise. Spectral levels of ambient noise have been computed. They are similar to those previously collected in the Atlantic and the Pacific, however, they seem to be higher in level. A detailed analysis of the spectral levels has not been made.

It was found that the float data were also in good agreement with ambient noise directionality data obtained with a towed array in the higher frequency range. It can be concluded that the present set of data is well suited for further analysis in accordance with the scientific objectives of the intended research.

Acknowledgments: The authors would like to thank the crew of NRV *Alliance*, SACLANTCEN and MPL scientific and technical staff for their contributions to the success of this experiment, and the Istituto Nazionale di Geofisica, Italy and the National Observatory of Athens (Seismological Institute), Greece for the provision of seismological data.

References

[1] Wagstaff, R.A. Onboard acoustic data-processing for the statistical analysis of array beam-noise, SACLANTCEN SM-144. La Spezia, Italy, SACLANT Undersea Research Centre, 1980.

[2] D'Spain, G.L. Energetics of the ocean's infrasonic sound field, Ph. D. thesis. San Diego, University of California, 1990.

[3] D'Spain, G.L., Hodgkiss, W.S., and Edmonds, G.L. The simultaneous measurement of infrasonic acoustic particle velocity and acoustic pressure in the ocean by freely drifting Swallow floats. *IEEE Journal of Oceanic Engineering*, 16, 1991: 195-207.

[4] Desharnais, F. and D'Spain, G.L. Acoustic intensity measurements with Swallow floats. *Canadian Acoustics*, 22, 1994: 159-160.

[5] D'Spain, G.L., Culver, R.L., Hodgkiss, W.S., and Edmonds, G.L. Freely drifting Swallow float array: August 1988 trip report, MPL Tech. Mem. 420. San Diego, CA, Marine Physical Laboratory, Scripps Institution of Oceanography, 1990.

[6] D'Spain, G.L., Hodgkiss, W.S., and Edmonds, G.L. Freely drifting Swallow float array: August 1990 NATIVE 1 experiment (First deployment), MPL Tech. Mem. 426. San Diego, CA, Marine Physical Laboratory, Scripps Institution of Oceanography, 1991.

[7] Culver, R.L. Localizing and beamforming freely-drifting VLF acoustic sensors, Ph. D. thesis. San Diego, CA, University of California, 1988.

[8] Desharnais, F. Analysis of Swallow float data at SACLANTCEN - Software notes for future use and developments, SACLANTCEN SM-296. La Spezia, Italy, SACLANT Undersea Research Centre, 1996.

[9] Ross, D. Mechanics of underwater noise. New York, NY, Pergamon, 1976.

[10] Urick, R. Principles of Underwater Sound, 3rd ed. New York, McGraw-Hill, 1983.

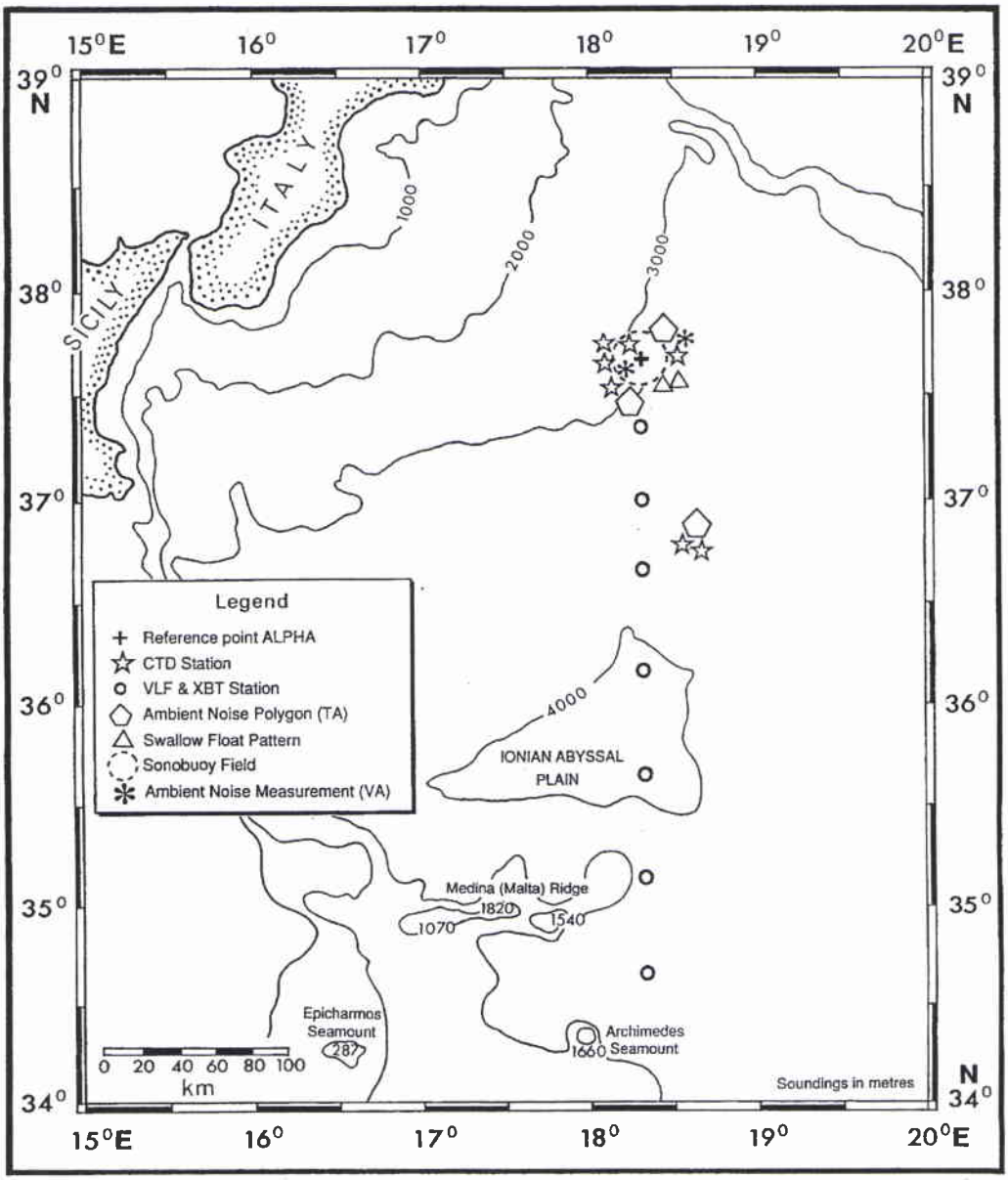

Figure 1 *Measurement site and area.*

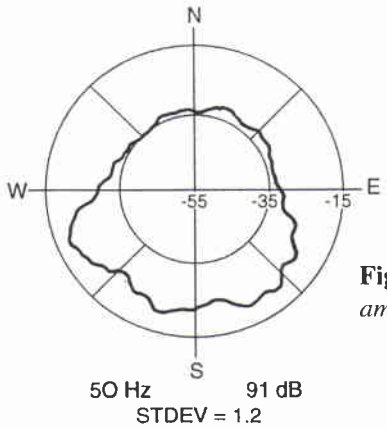

Figure 2 *Horizontal directionality of the ambient noise field - 50 Hz.*

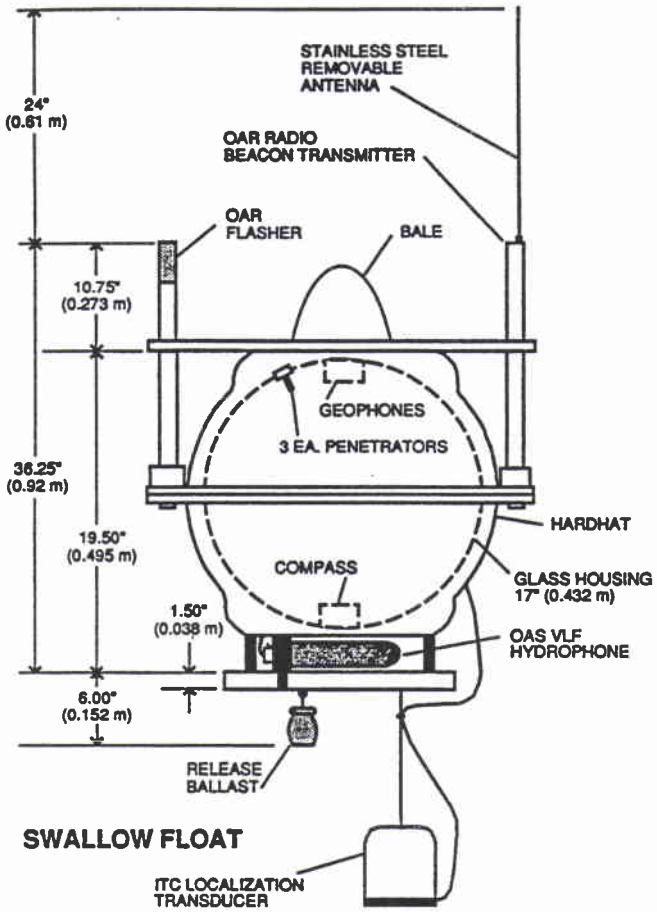

Figure 3 *Swallow float design.*

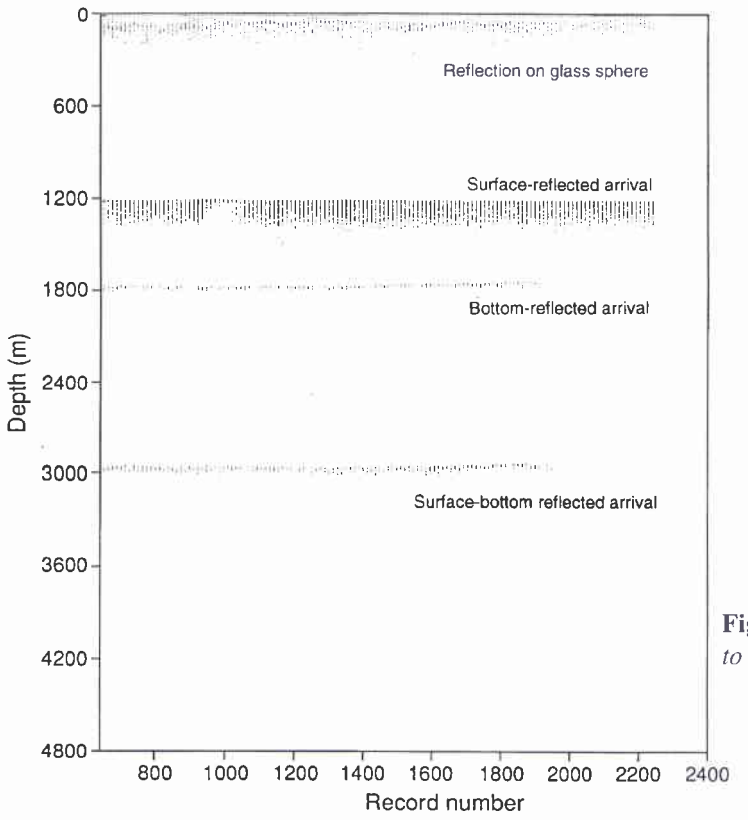

Figure 4 *ITC data: Float 4 listening to itself, second deployment.*

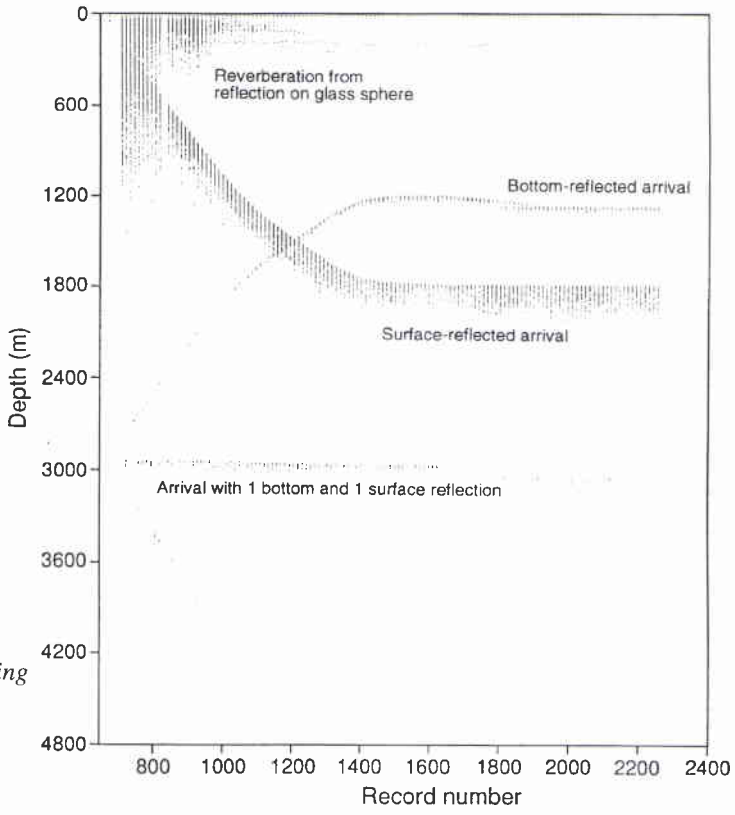

Figure 5 *ITC data: Float 4 listening to itself, first deployment.*

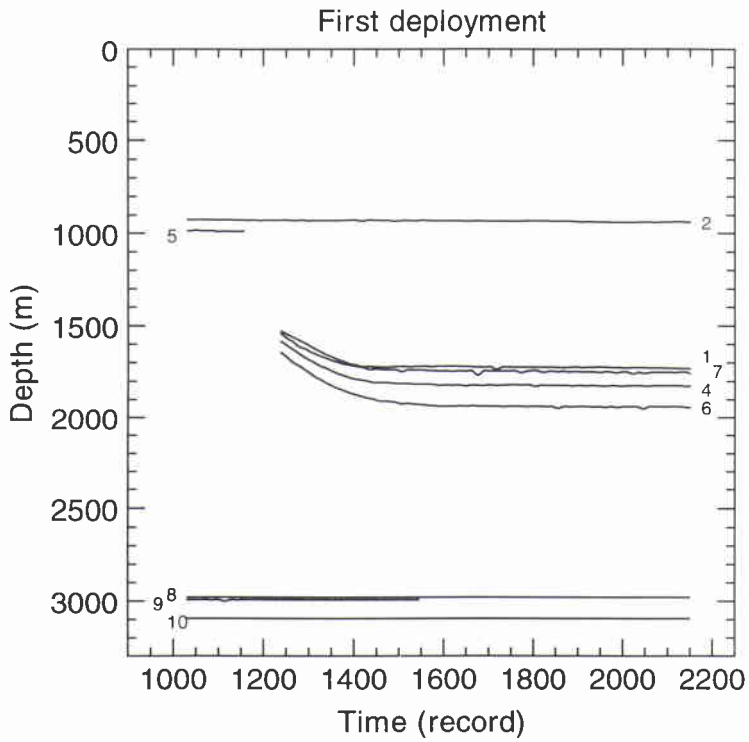

Figure 6a *Float depth as a function of time (record number): (a) first deployment. Numbers indicate float numbers.*

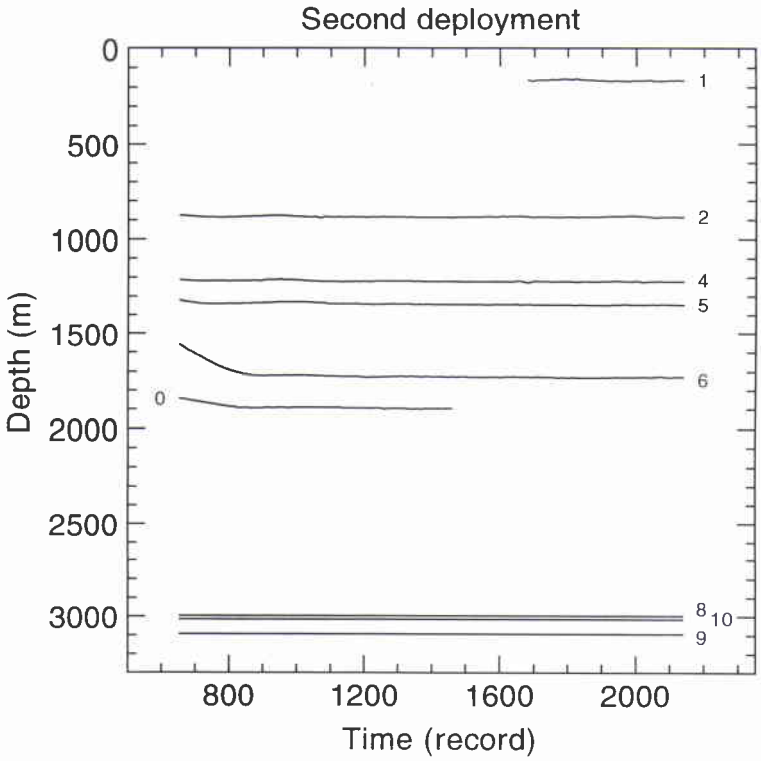

Figure 6b *Float depth as a function of time (record number): (b) second deployment. Numbers indicate float numbers.*

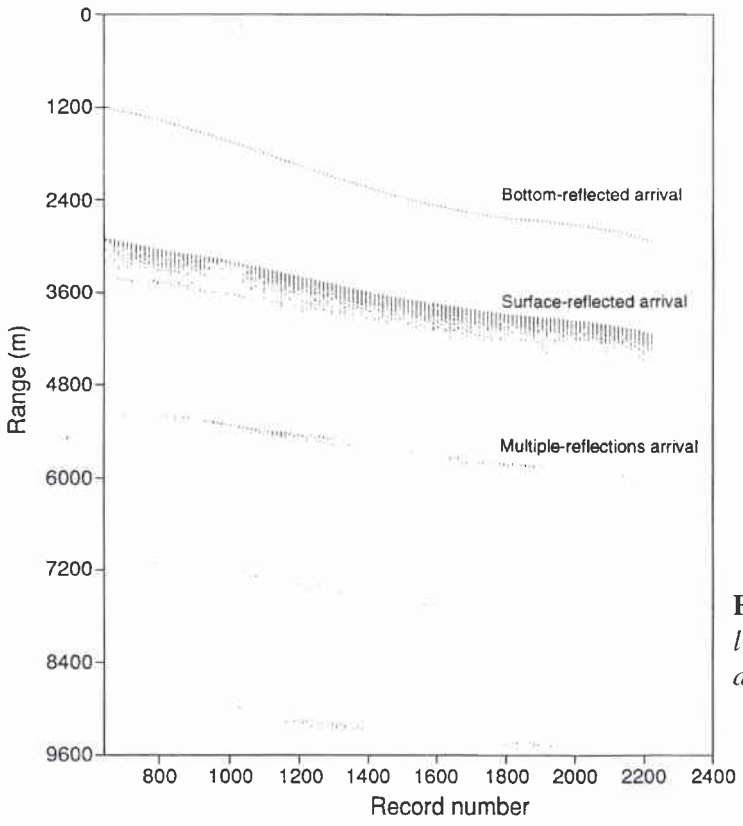

Figure 7 *ITC data: Float 2 listening to Float 0, second deployment.*

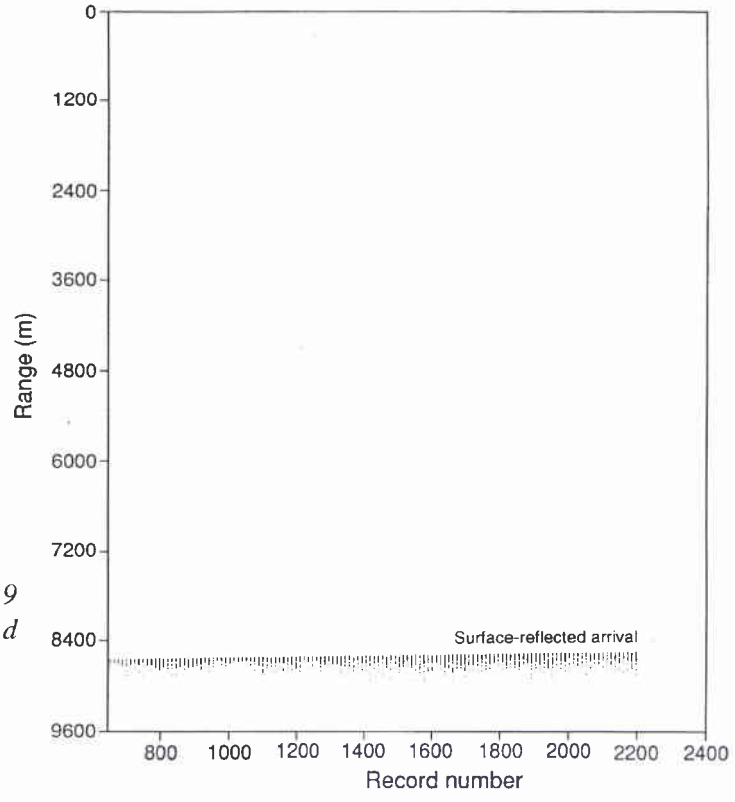

Figure 8 *ITC data: Float 9 listening to Float 10, second deployment.*

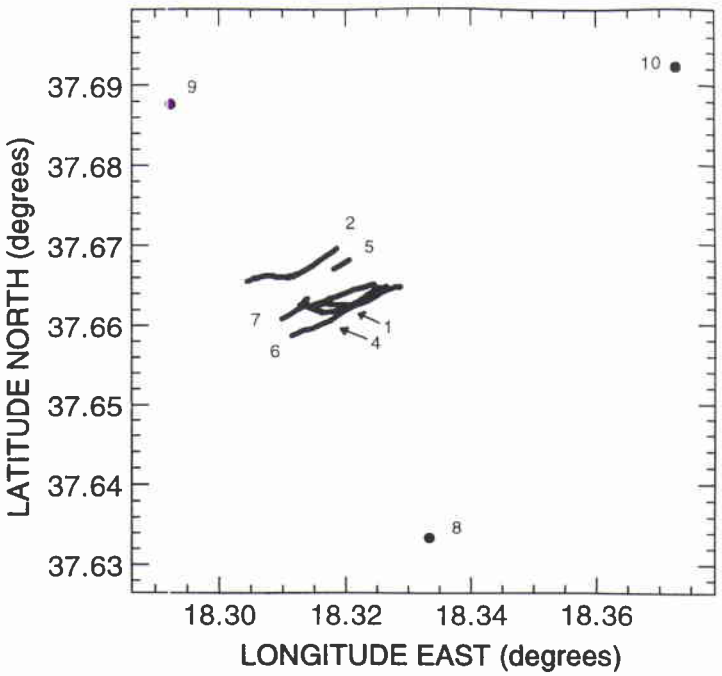

Figure 9a *Float tracks: (a) first deployment. (Floats 8, 9 and 10 are moored at the bottom).*

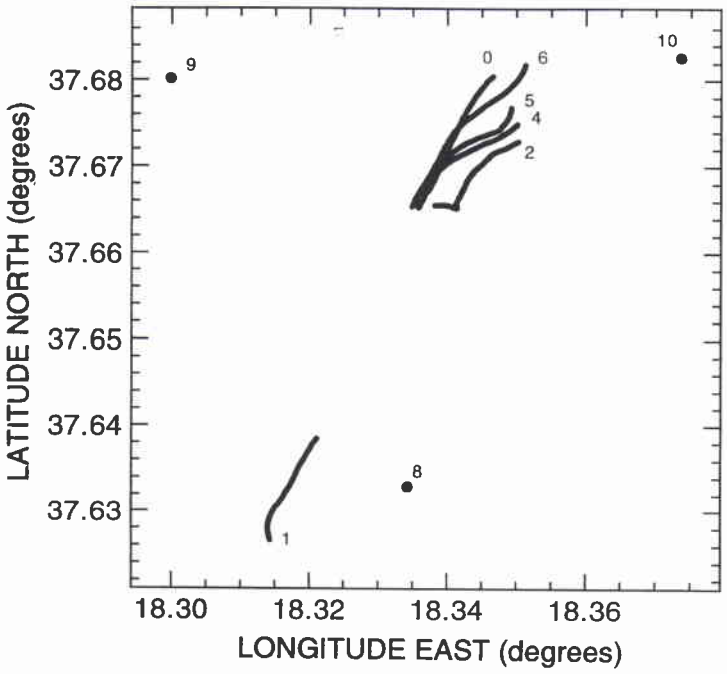

Figure 9b *Float tracks: (b) second deployment. . (Floats 8, 9 and 10 are moored at the bottom).*

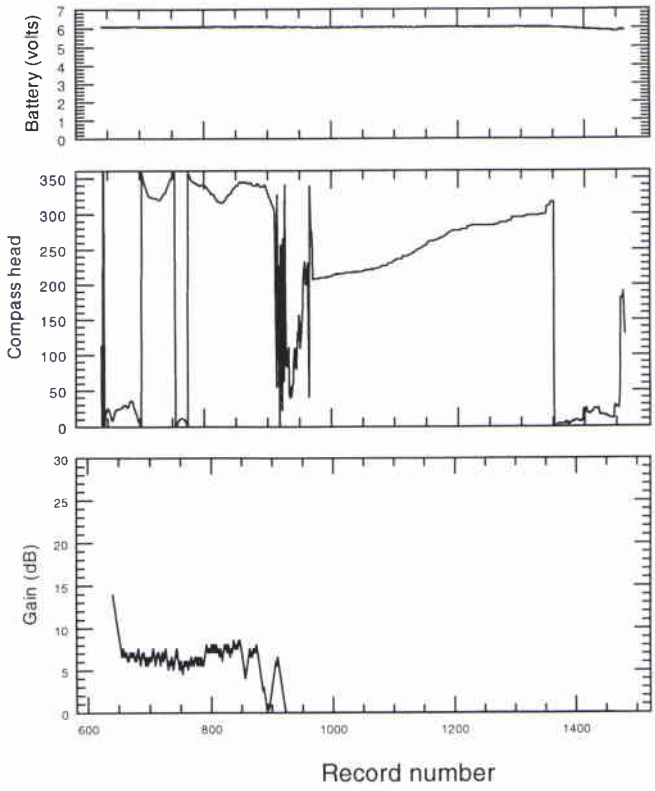

Figure 10a *Battery voltage (V), compass heading (magnetic degrees) and AGC gain (dB). First deployment, Float 0.*

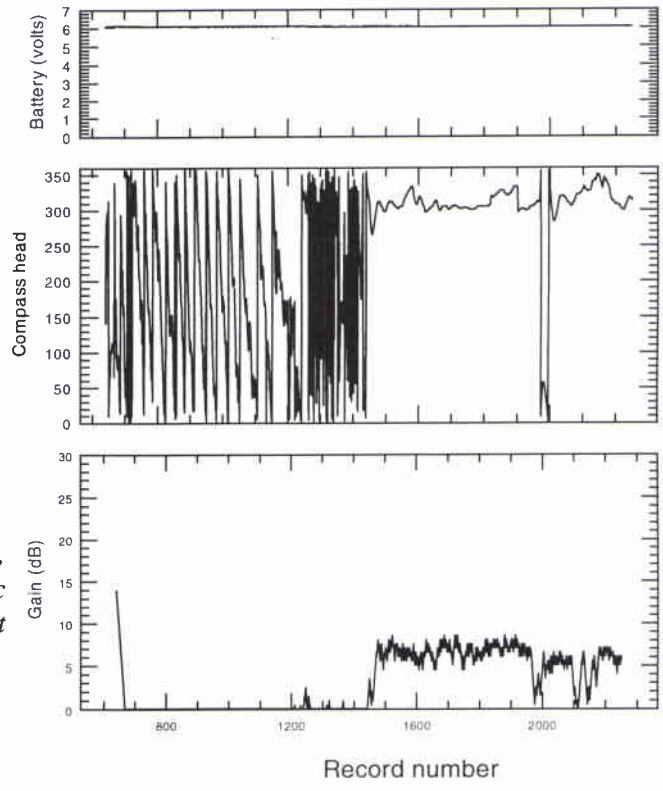

Figure 10b *Battery voltage (V), compass heading (magnetic degrees) and AGC gain (dB). First deployment, Float 1.*

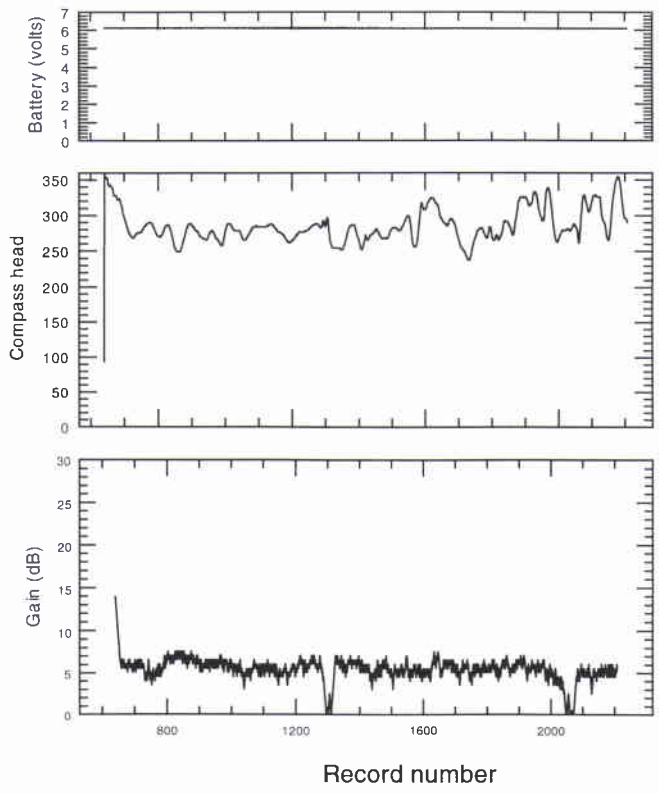

Figure 10c *Battery voltage (V), compass heading (magnetic degrees) and AGC gain (dB). First deployment, Float 2.*

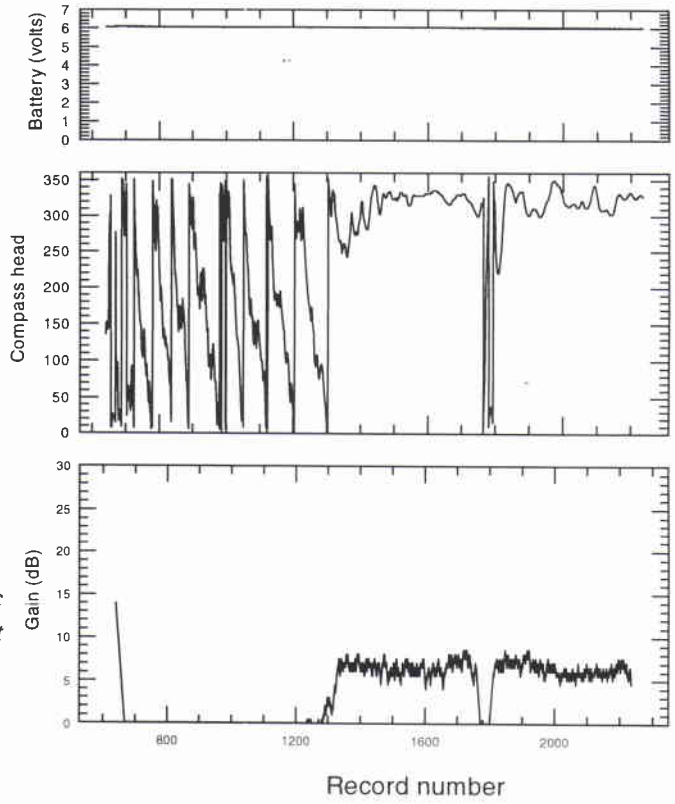

Figure 10d *Battery voltage (V), compass heading (magnetic degrees) and AGC gain (dB). First deployment, Float 4*

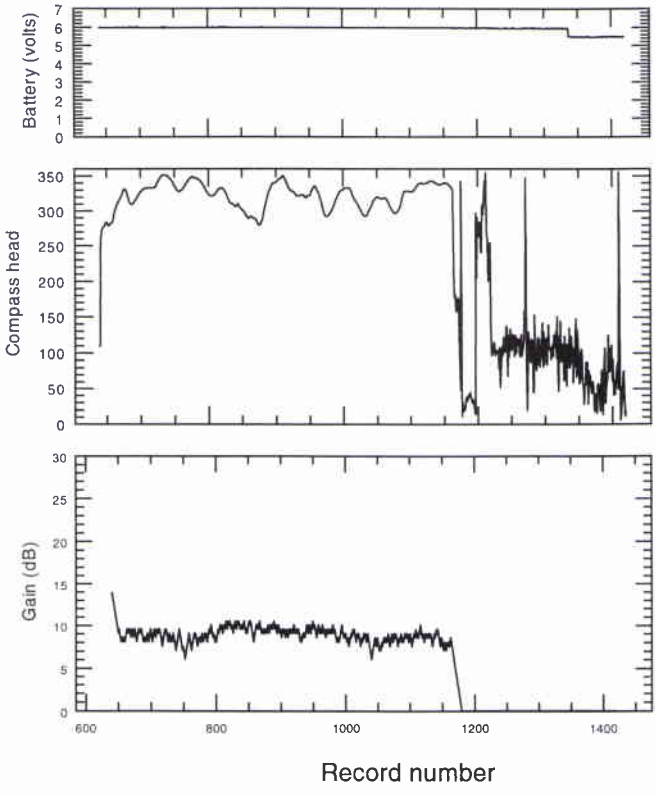

Figure 10e *Battery voltage (V), compass heading (magnetic degrees) and AGC gain (dB). First deployment, Float 5.*

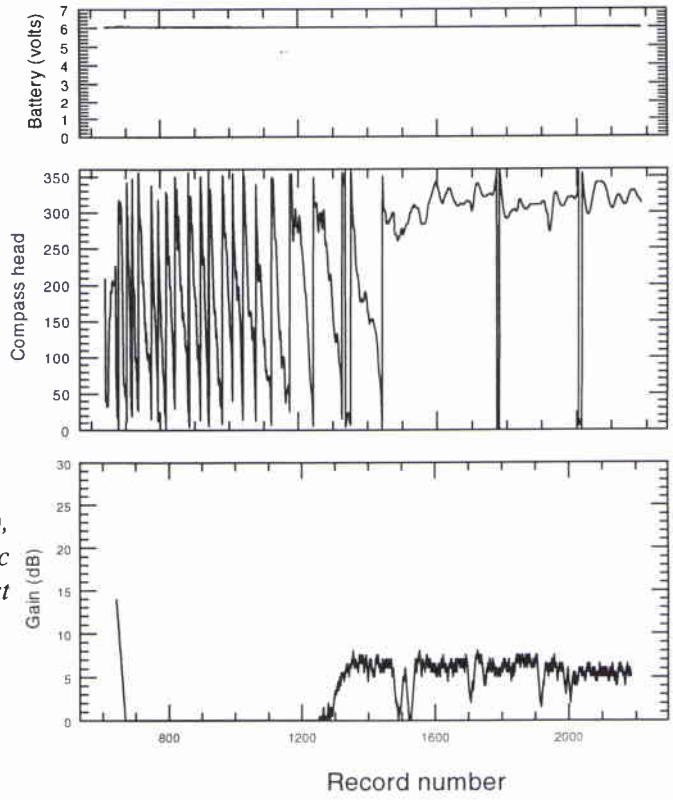

Figure 10f *Battery voltage (V), compass heading (magnetic degrees) and AGC gain (dB). First deployment, Float 6.*

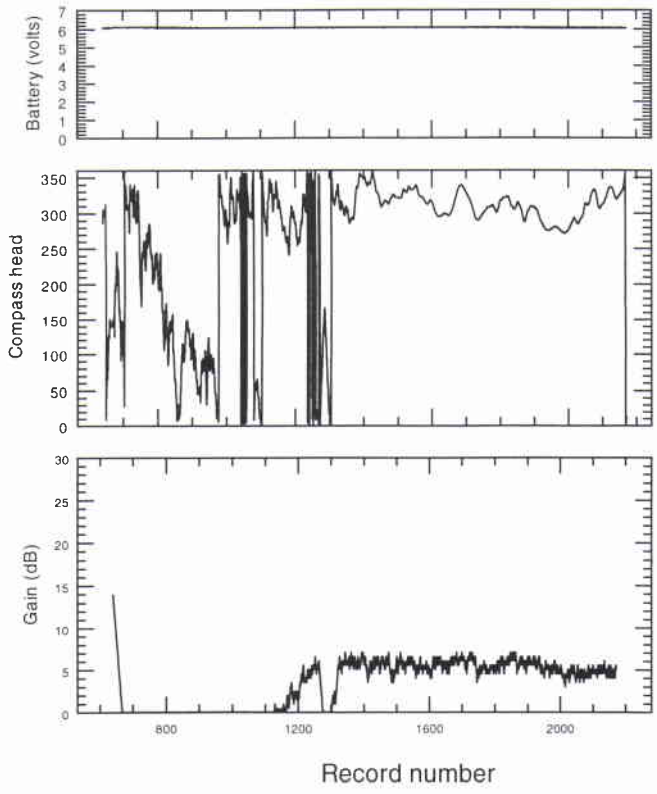

Figure 10g *Battery voltage (V), compass heading (magnetic degrees) and AGC gain (dB). First deployment, Float 7.*

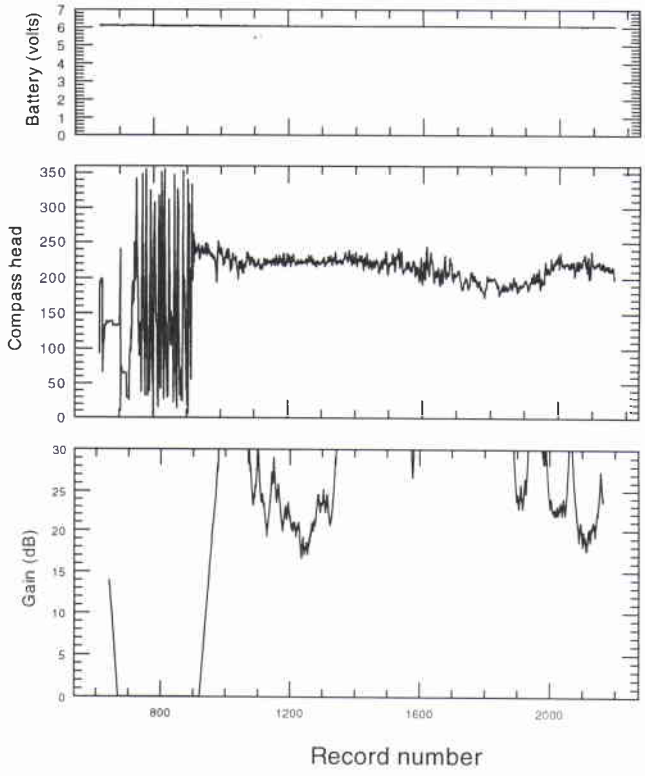

Figure 10h *Battery voltage (V), compass heading (magnetic degrees) and AGC gain (dB). First deployment, Float 8.*

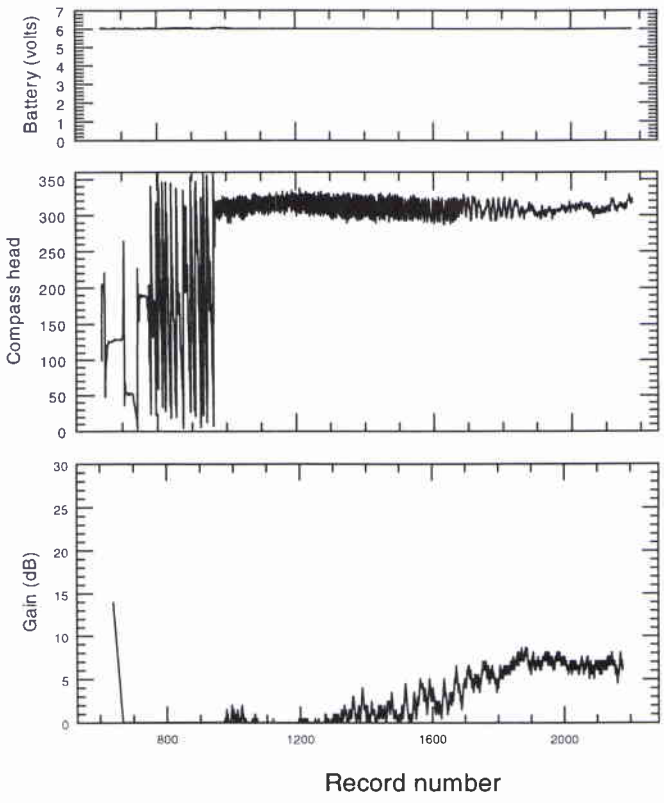

Figure 10i *Battery voltage (V), compass heading (magnetic degrees) and AGC gain (dB). First deployment, Float 9.*

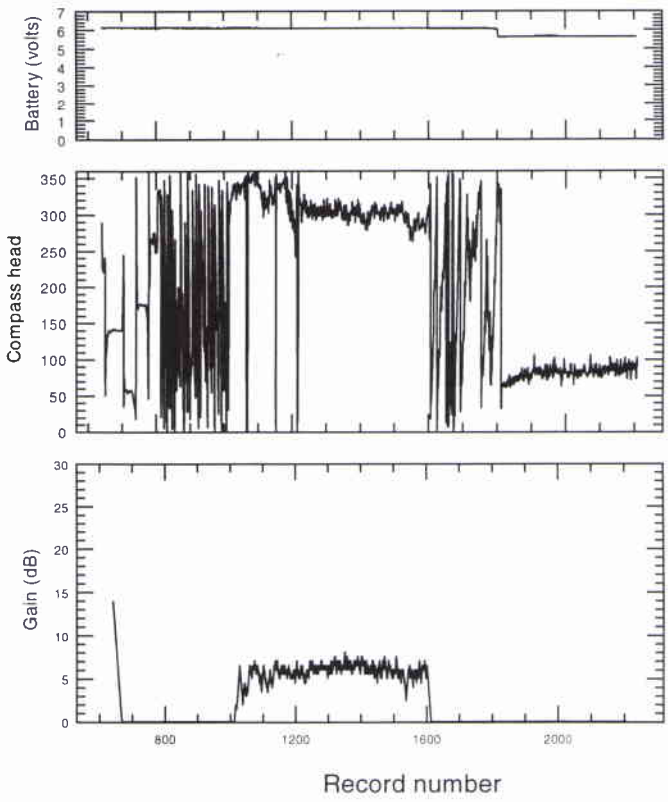

Figure 10j *Battery voltage (V), compass heading (magnetic degrees) and AGC gain (dB). First deployment, Float 10.*

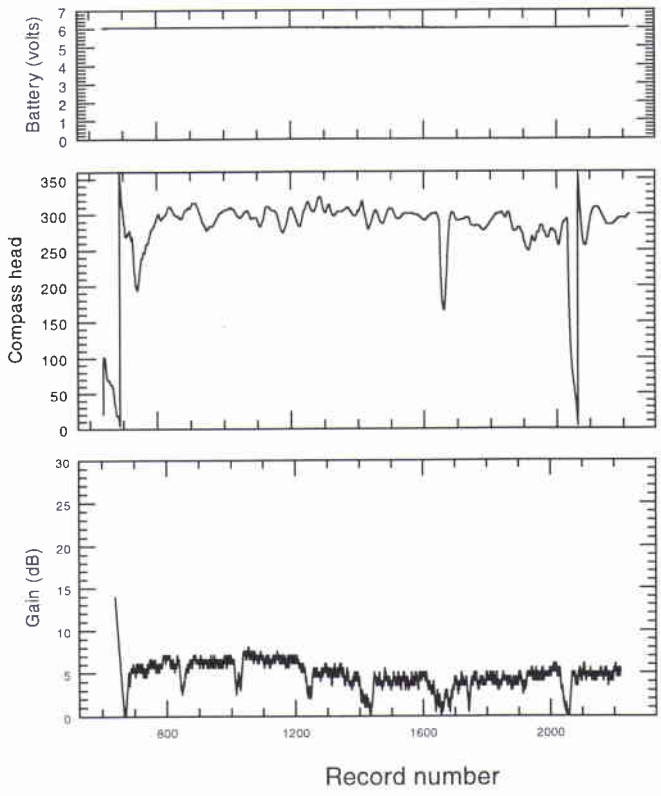

Figure 11a *Battery voltage (volts), compass heading (magnetic degrees) and AGC gain (dB). Second deployment, Float 0.*

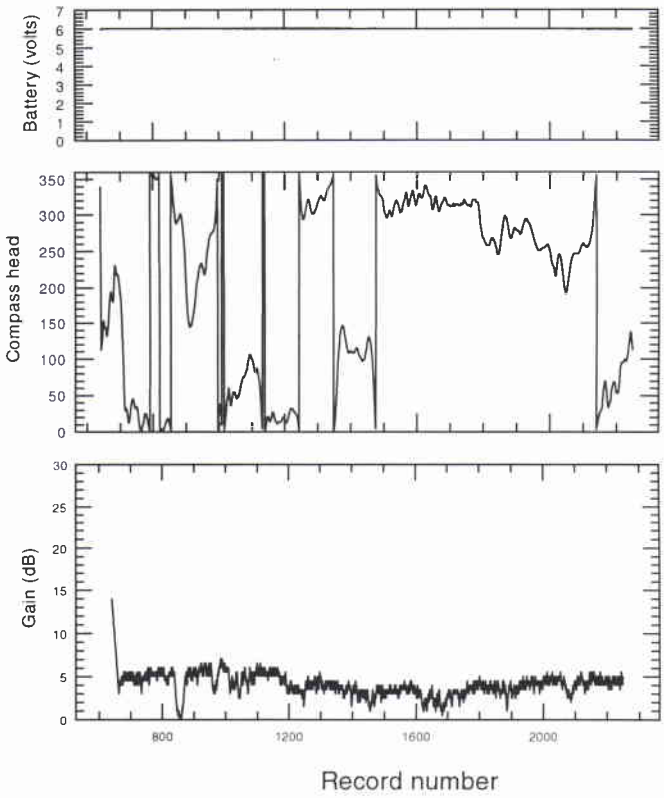

Figure 11b *Battery voltage (volts), compass heading (magnetic degrees) and AGC gain (dB). Second deployment, Float 1.*

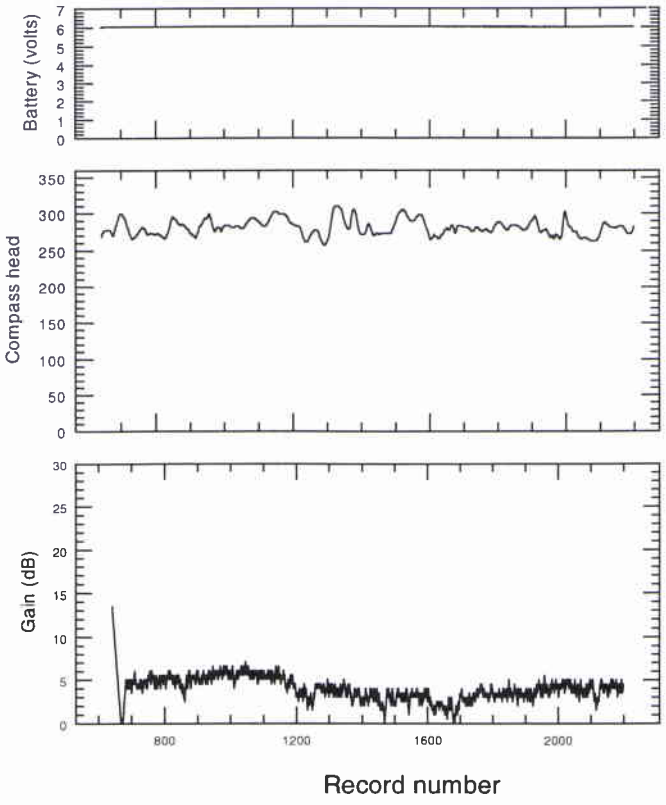

Figure 11c *Battery voltage (volts), compass heading (magnetic degrees) and AGC gain (dB). Second deployment, Float 2.*

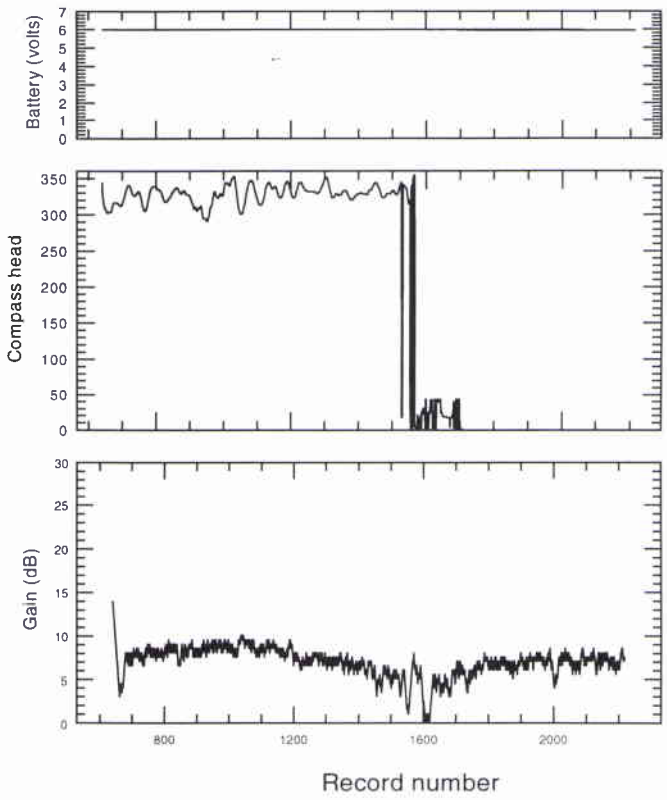

Figure 11d *Battery voltage (volts), compass heading (magnetic degrees) and AGC gain (dB). Second deployment, Float 4.*

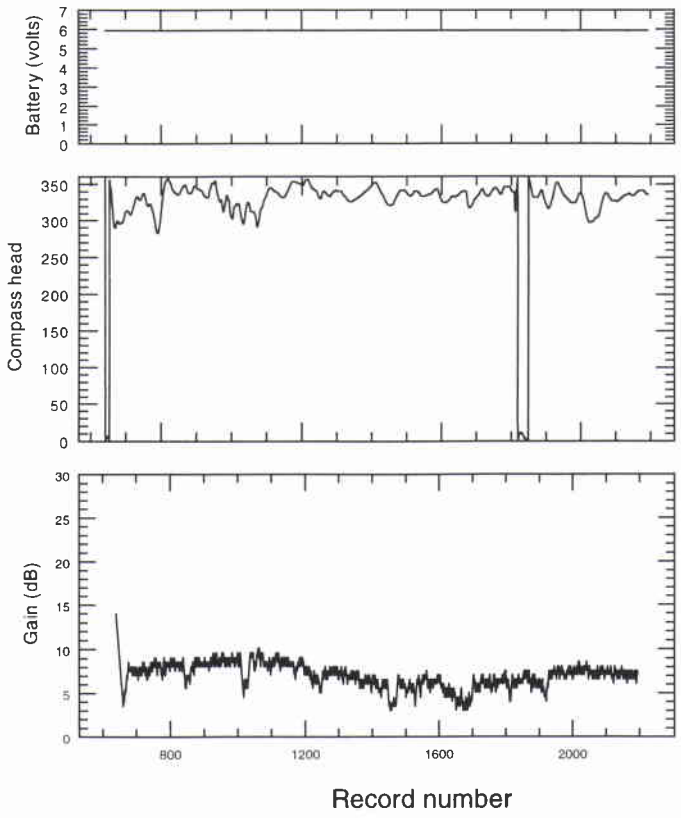

Figure 11e *Battery voltage (volts), compass heading (magnetic degrees) and AGC gain (dB). Second deployment, Float 5.*

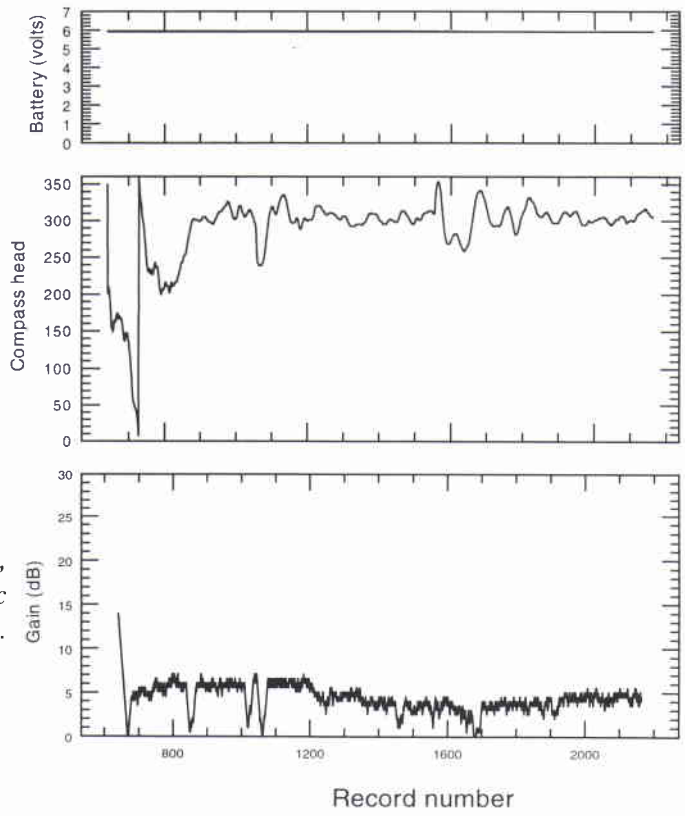

Figure 11f *Battery voltage (volts), compass heading (magnetic degrees) and AGC gain (dB). Second deployment, Float 6.*

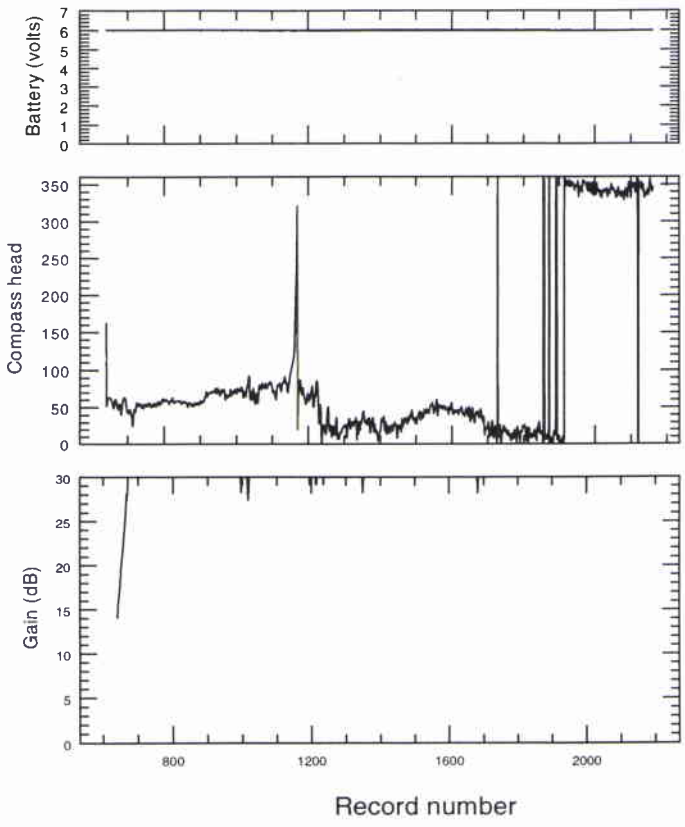

Figure 11g *Battery voltage (volts), compass heading (magnetic degrees) and AGC gain (dB). Second deployment, Float 8.*

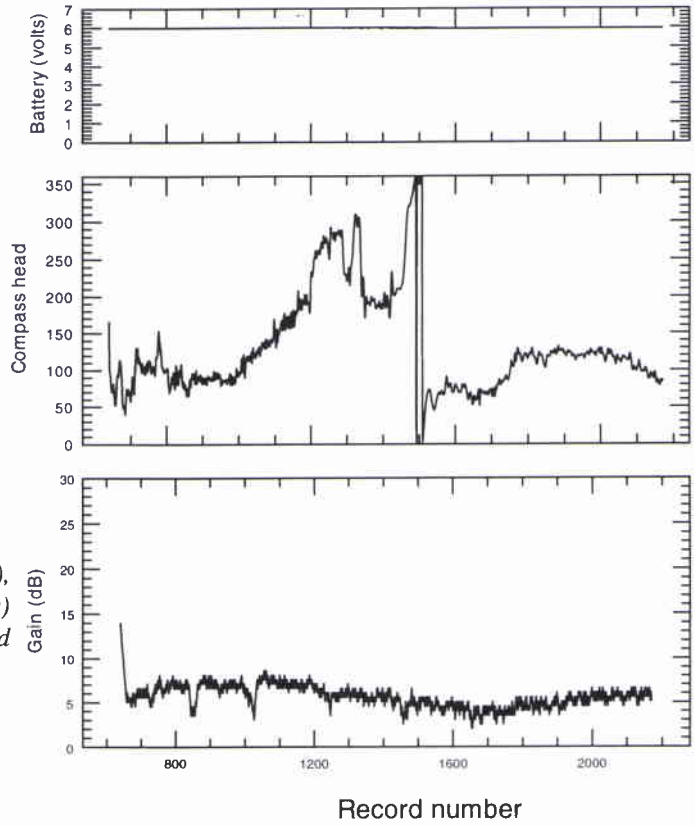

Figure 11h *Battery voltage (volts), compass heading (magnetic degrees) and AGC gain (dB). Second deployment, Float 9.*

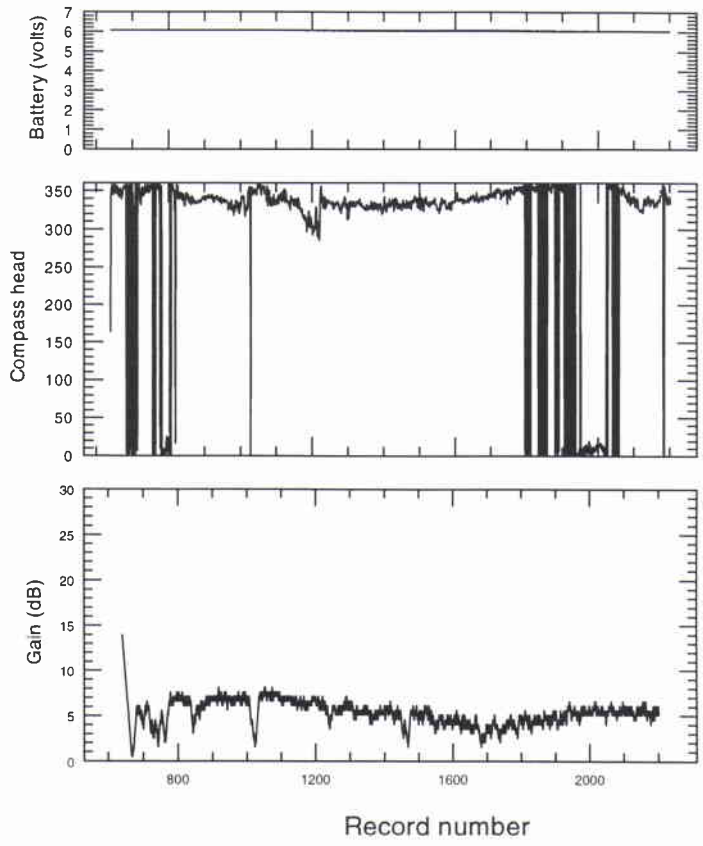

Figure 11i *Battery voltage (volts), compass heading (magnetic degrees) and AGC gain (dB). Second deployment, Float 10.*

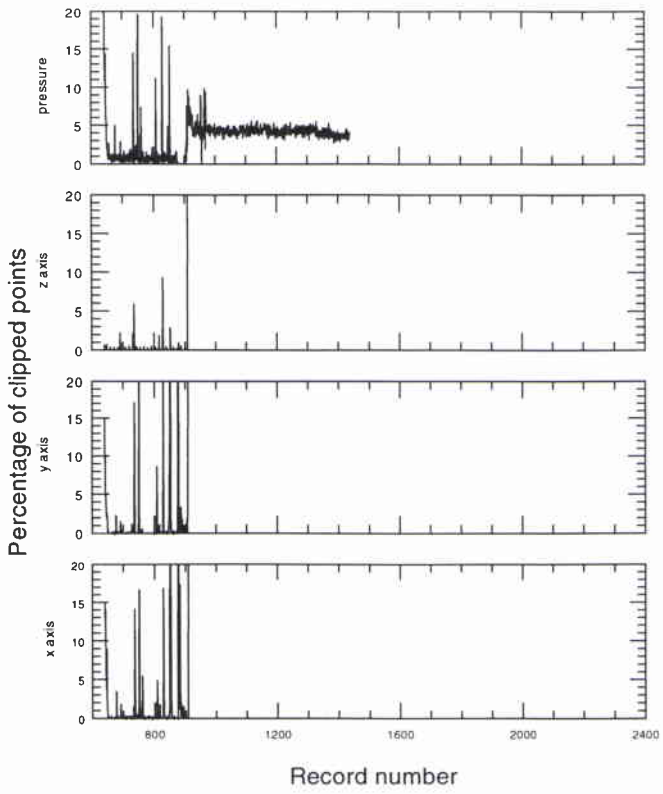

Figure 12a *Percentage of clipped points for all acoustic sensors. First deployment, Float 0.*

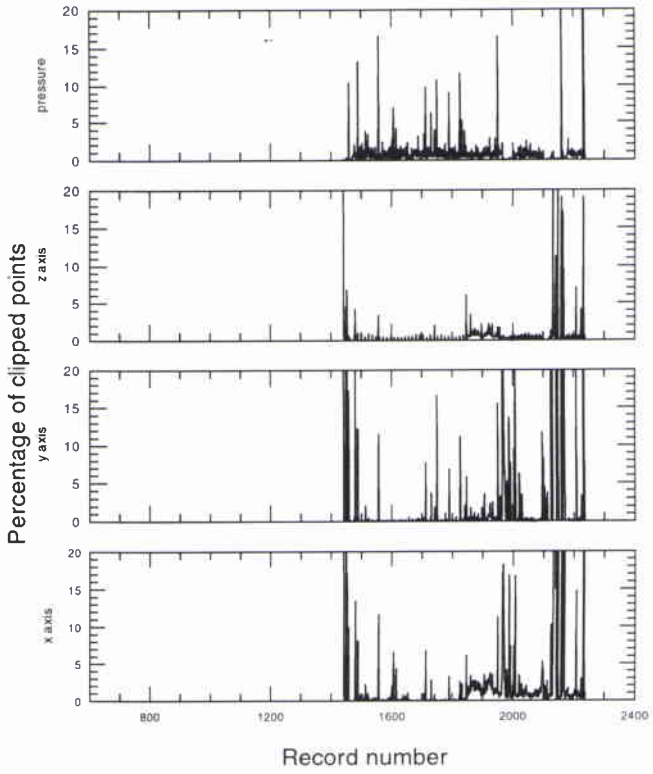

Figure 12b *Percentage of clipped points for all acoustic sensors. First deployment, Float 1.*

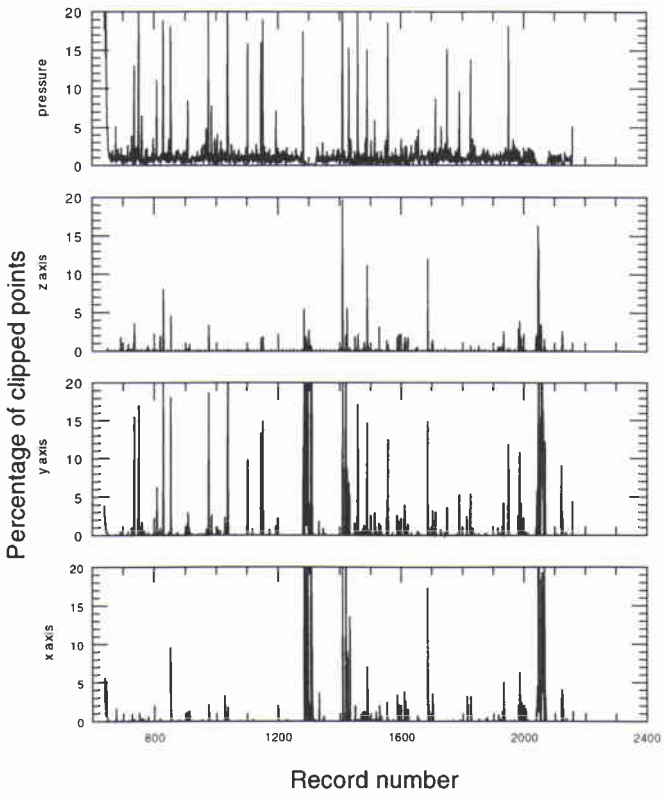

Figure 12c *Percentage of clipped points for all acoustic sensors. First deployment, Float 2.*

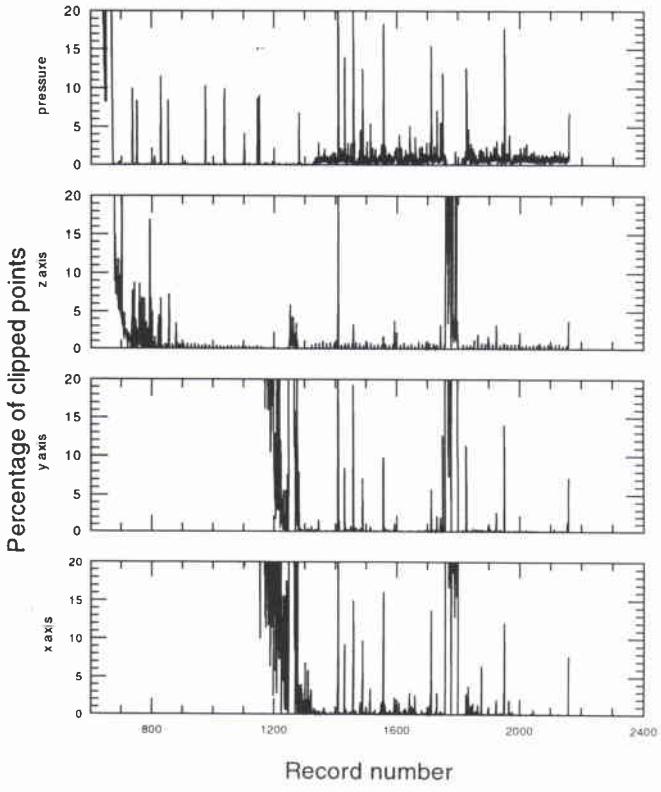

Figure 12d *Percentage of clipped points for all acoustic sensors. First deployment, Float 4.*

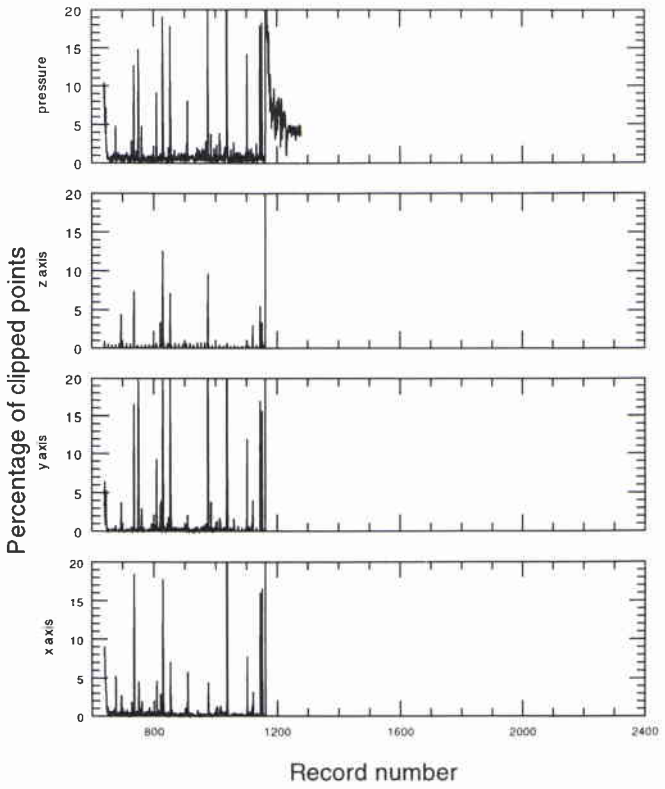

Figure 12e *Percentage of clipped points for all acoustic sensors. First deployment, Float 5.*

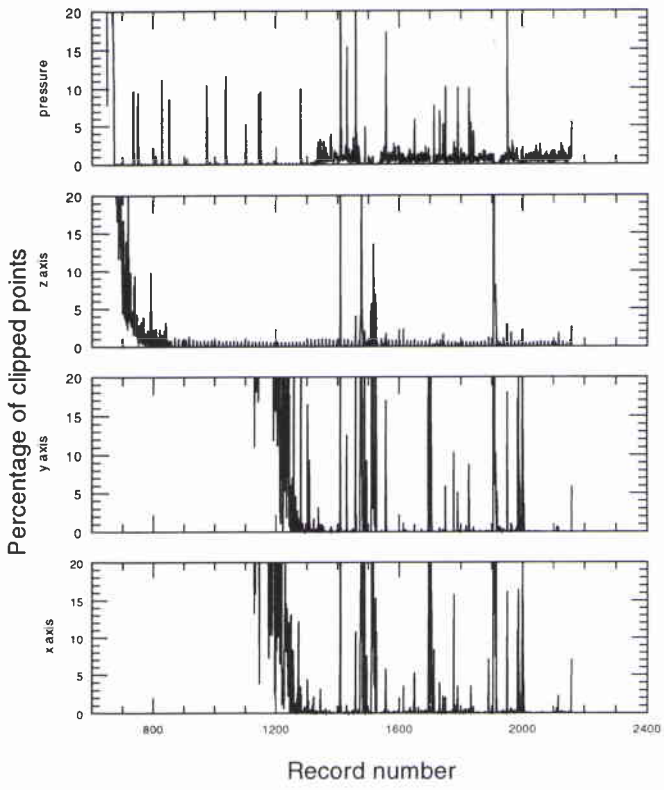

Figure 12f *Percentage of clipped points for all acoustic sensors. First deployment, Float 6.*

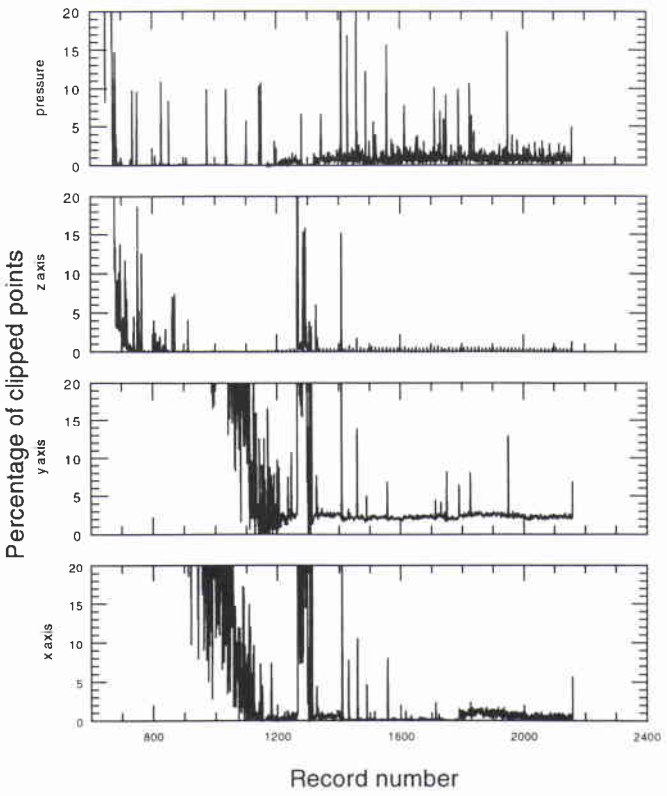

Figure 12g *Percentage of clipped points for all acoustic sensors. First deployment, Float 7.*

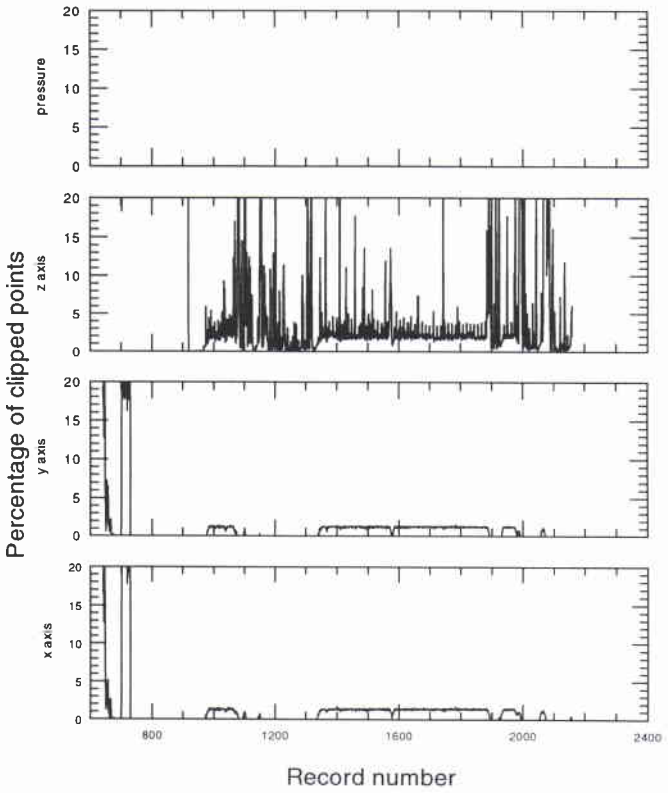

Figure 12h *Percentage of clipped points for all acoustic sensors. First deployment, Float 8.*

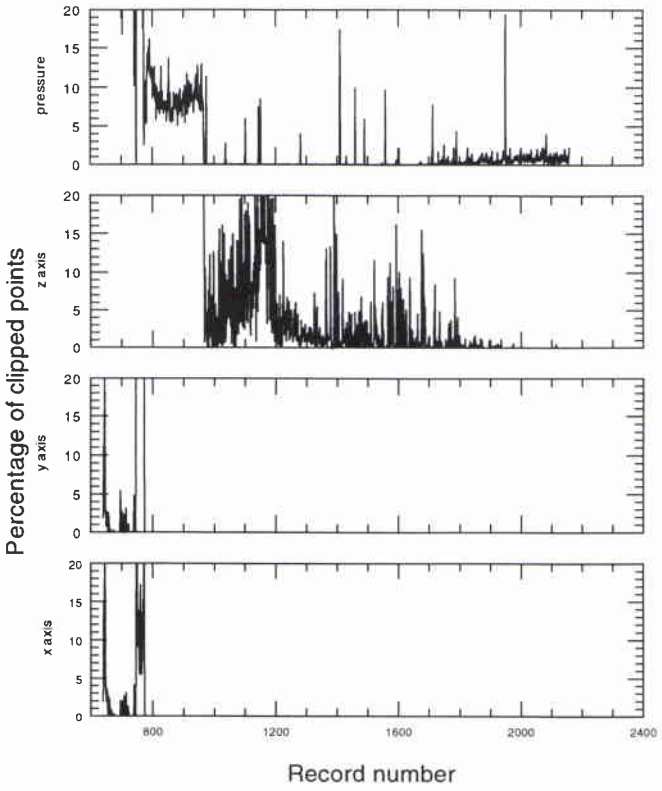

Figure 12i *Percentage of clipped points for all acoustic sensors. First deployment, Float 9.*

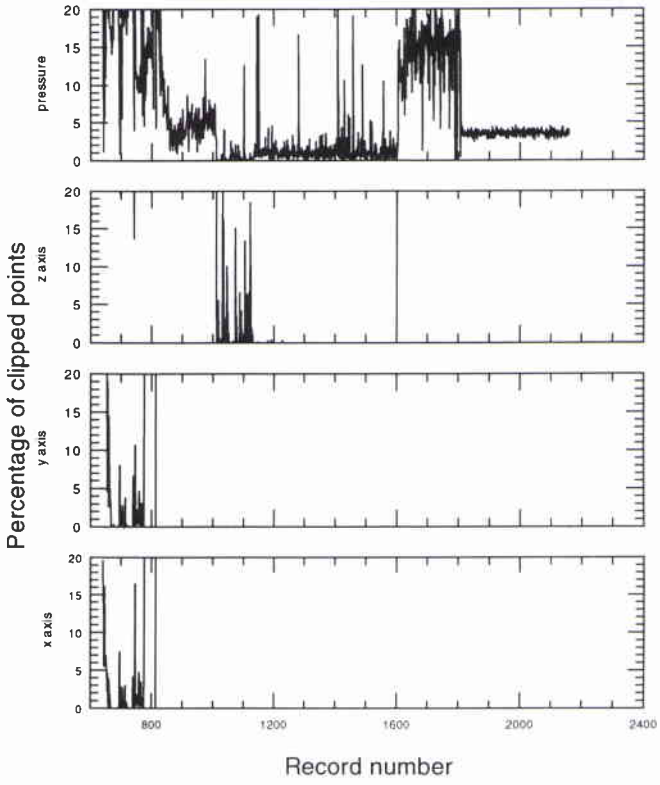

Figure 12j *Percentage of clipped points for all acoustic sensors. First deployment, Float 10.*

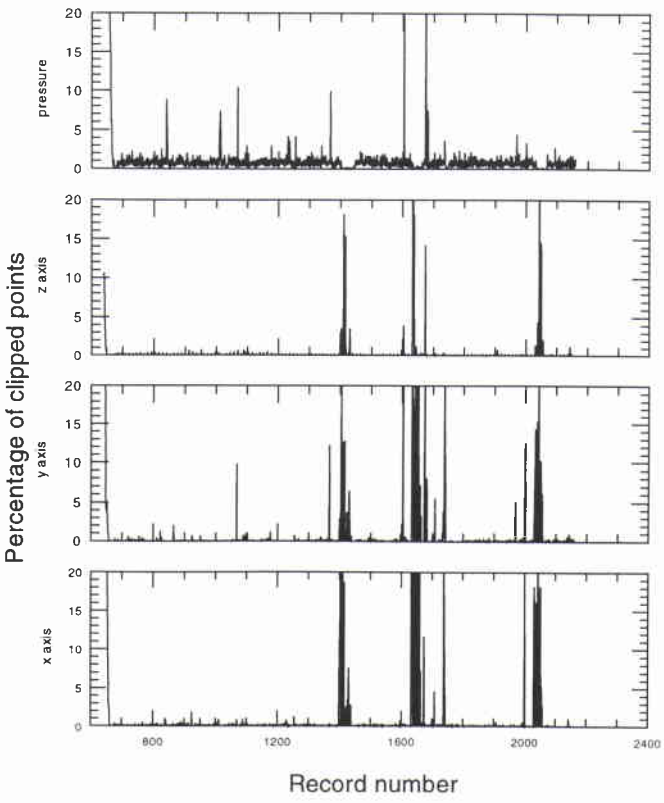

Figure 13a *Percentage of clipped points for all acoustic sensors. Second deployment, Float 0.*

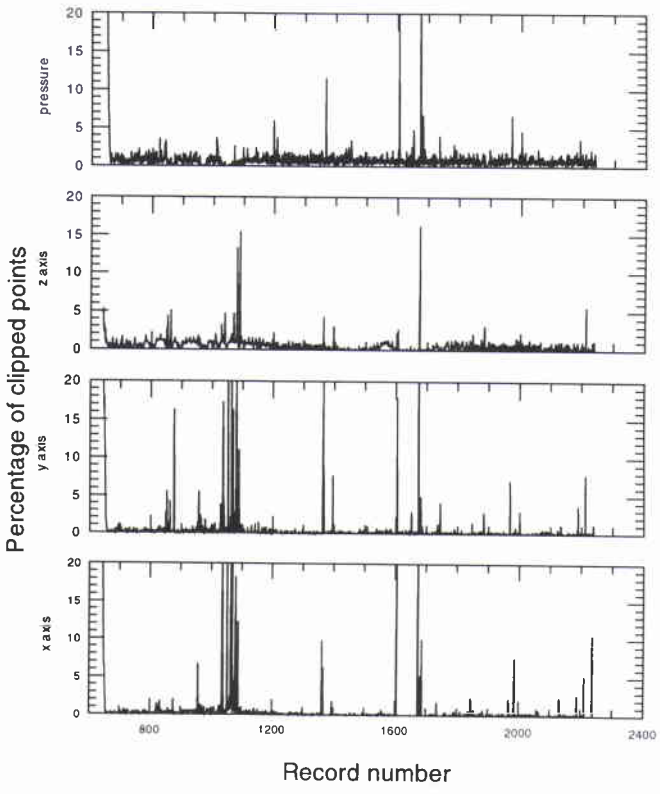

Figure 13b *Percentage of clipped points for all acoustic sensors. Second deployment, Float 1.*

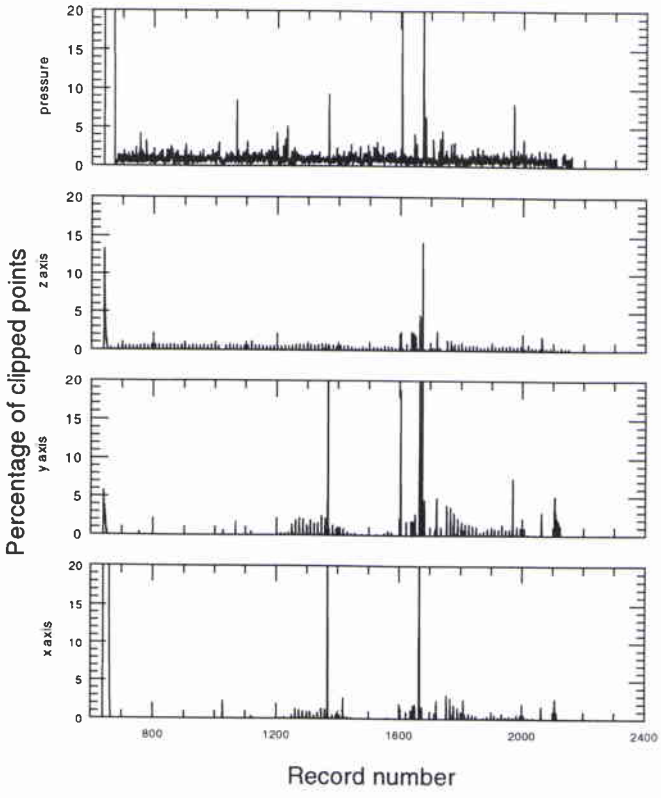

Figure 13c *Percentage of clipped points for all acoustic sensors. Second deployment, Float 2.*

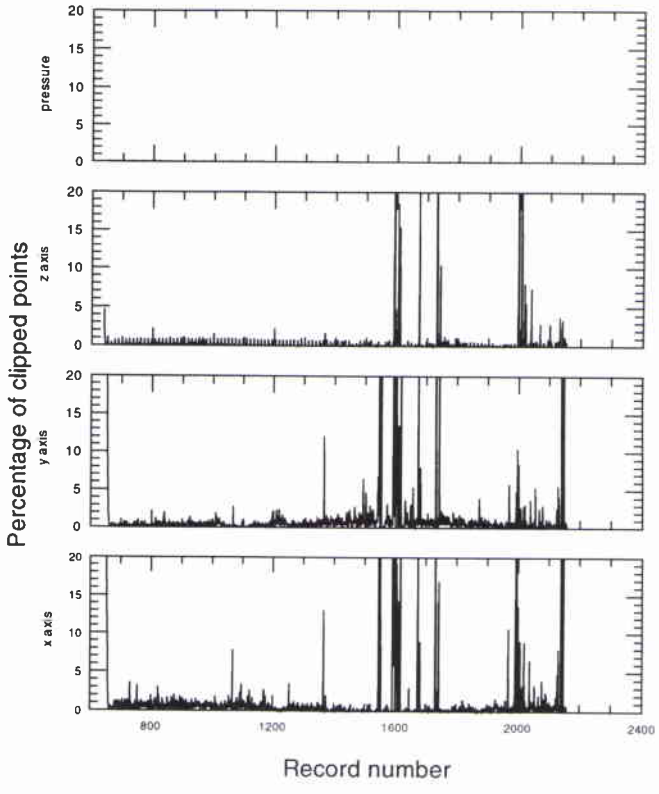

Figure 13d *Percentage of clipped points for all acoustic sensors. Second deployment, Float 4.*

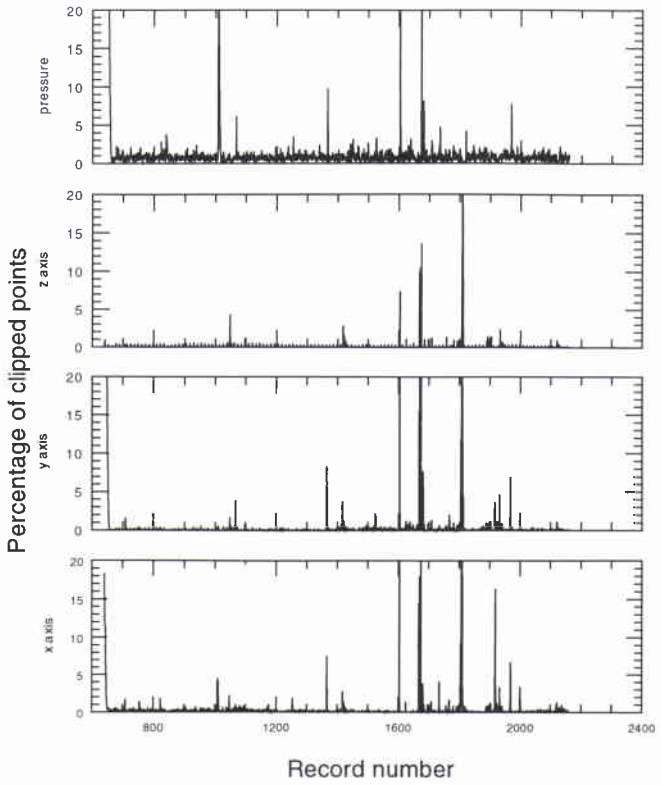

Figure 13e *Percentage of clipped points for all acoustic sensors. Second deployment, Float 5.*

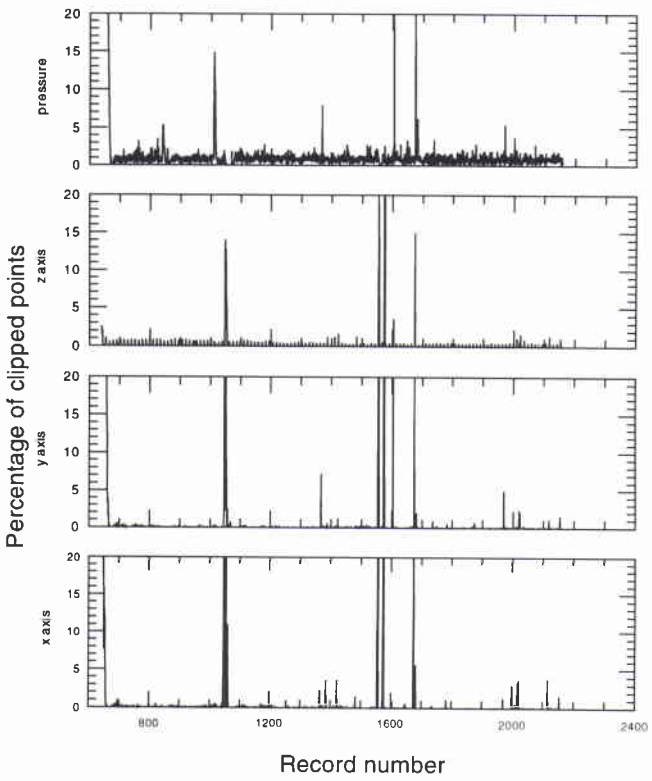

Figure 13f *Percentage of clipped points for all acoustic sensors. Second deployment, Float 6.*

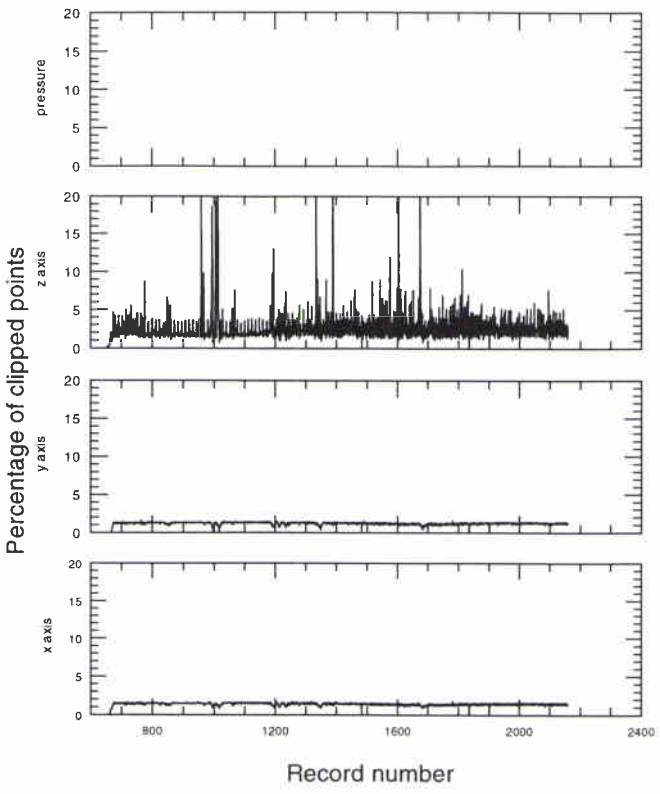

Figure 13g *Percentage of clipped points for all acoustic sensors. Second deployment, Float 8.*

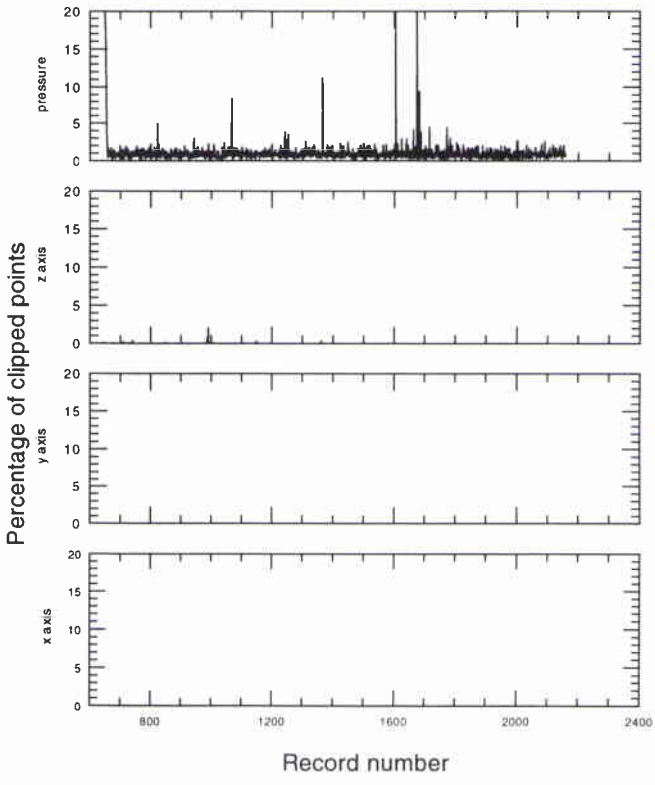

Figure 13h *Percentage of clipped points for all acoustic sensors. Second deployment, Float 9.*

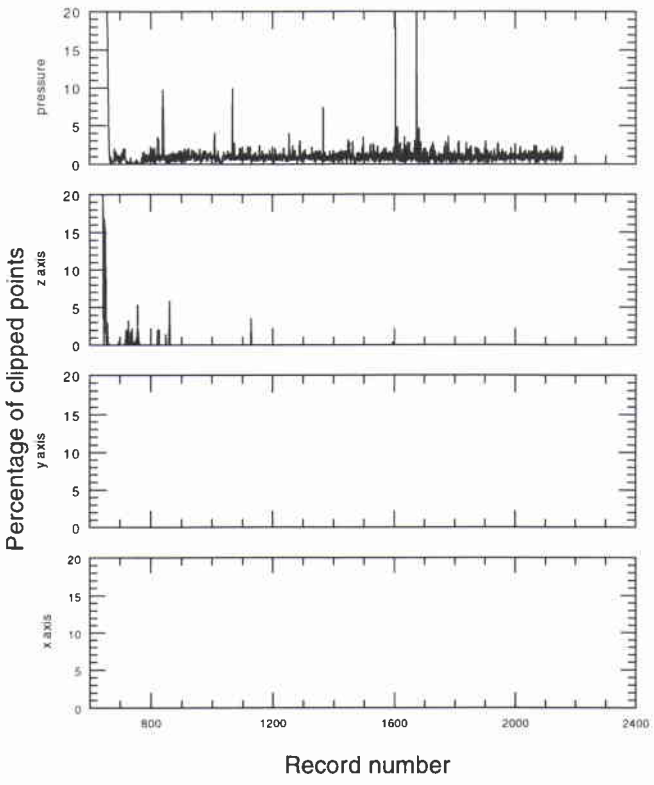

Figure 13i *Percentage of clipped points for all acoustic sensors. Second deployment, Float 10.*

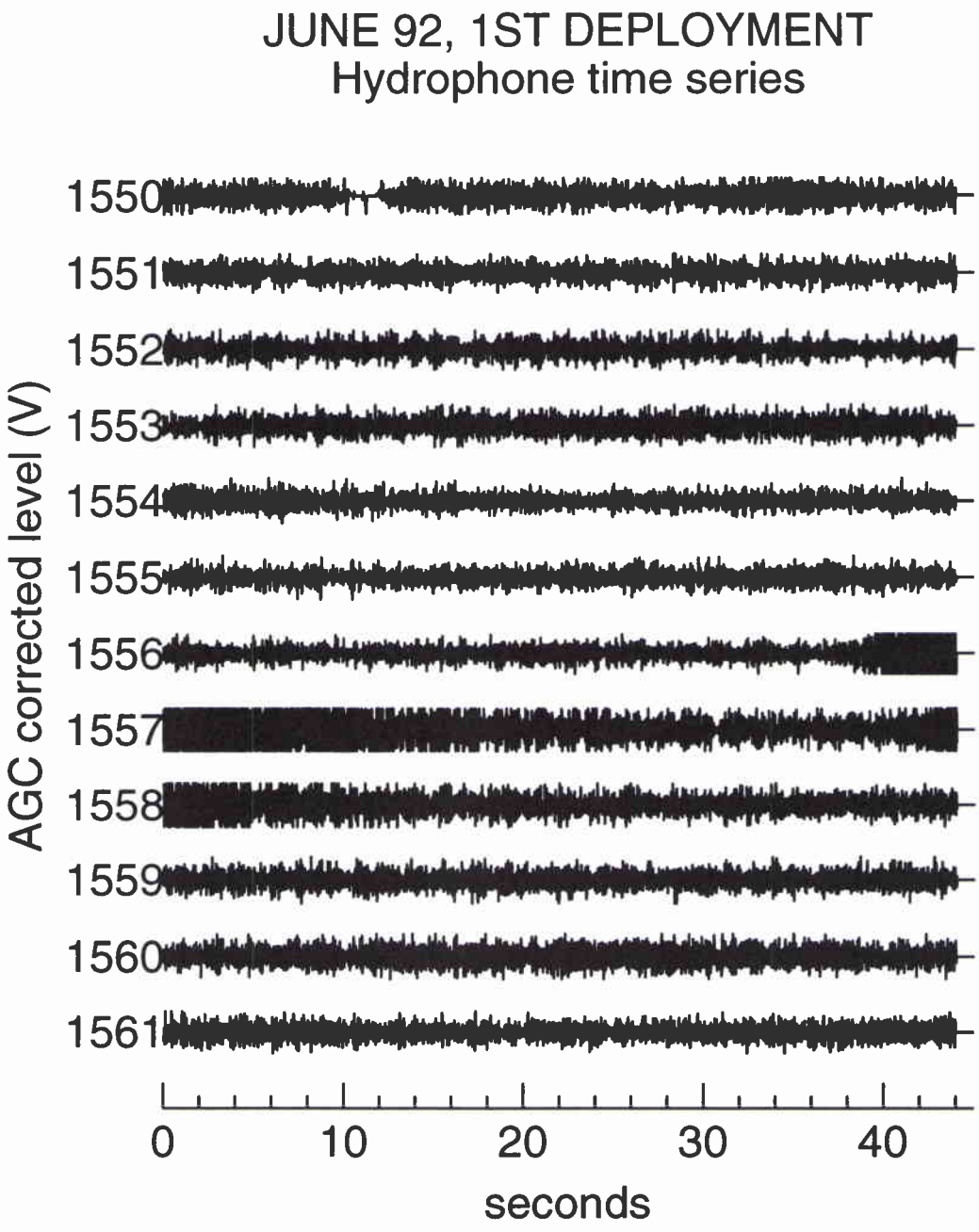

Figure 14a *Hydrophone time series, Float 2, first deployment. Record 1550 to 1561.*

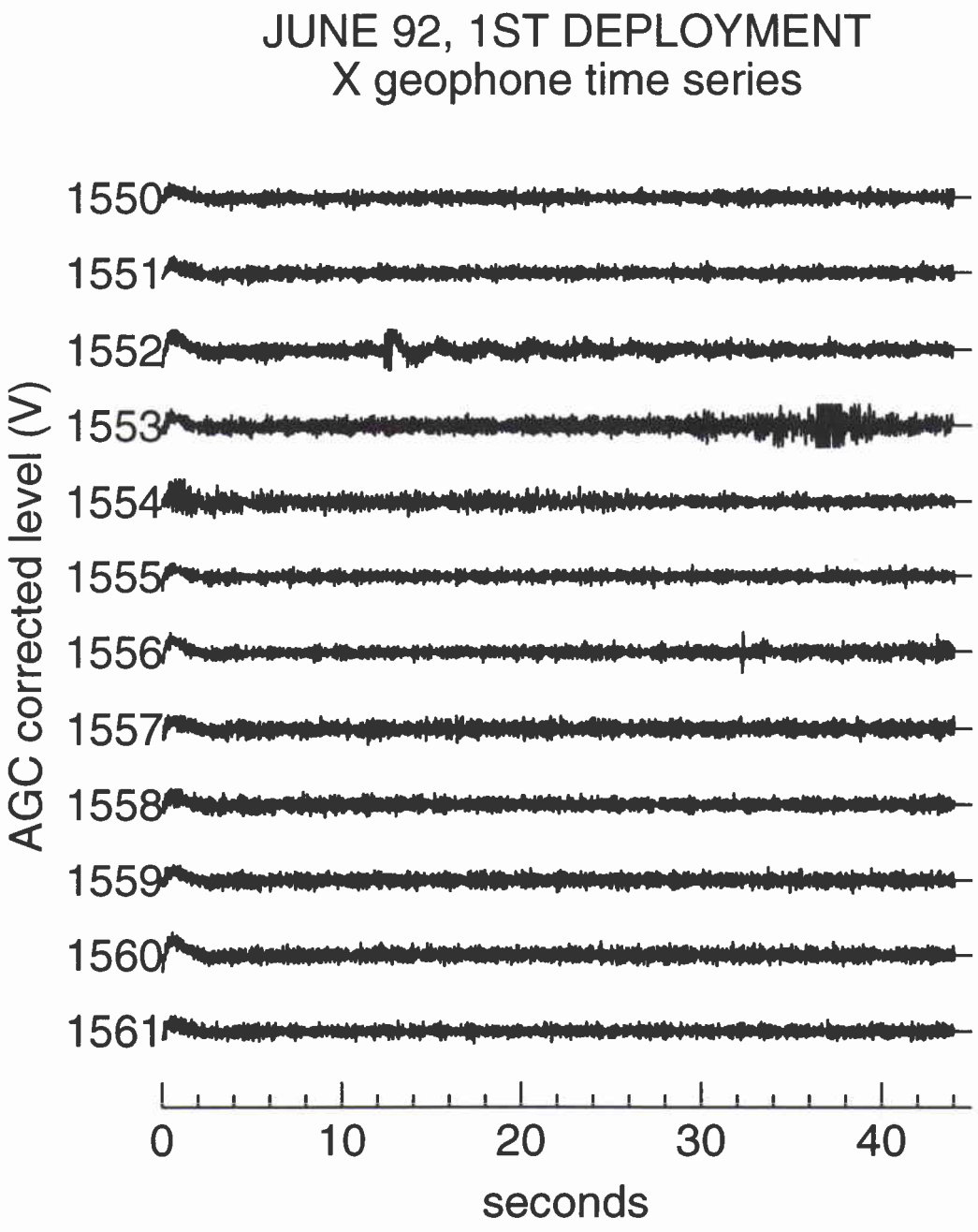

Figure 14b *x- geophone time series, Float 2, first deployment. Record 1550 to 1561.*

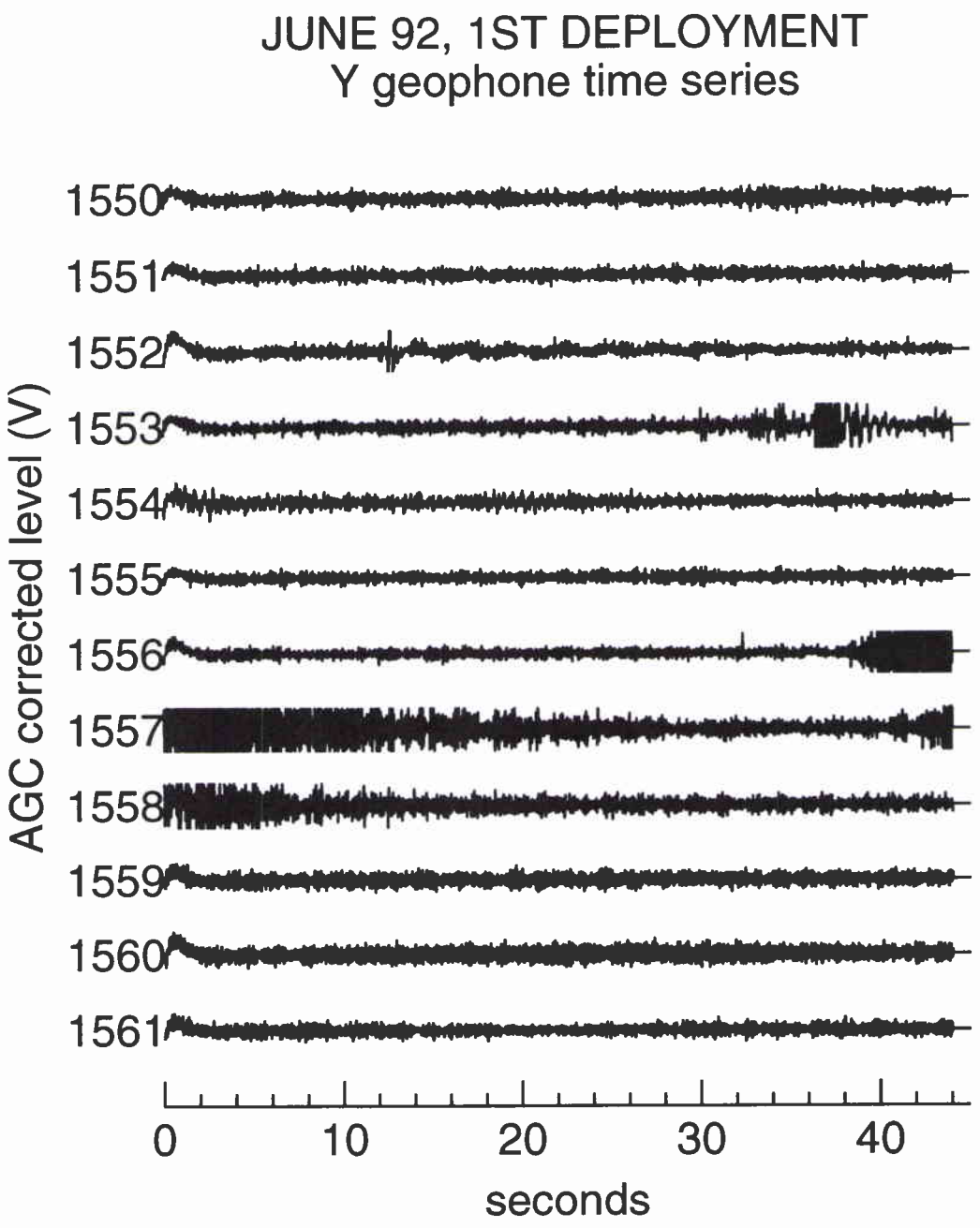

Figure 14c *y- geophone time series, Float 2, first deployment. Record 1550 to 1561.*

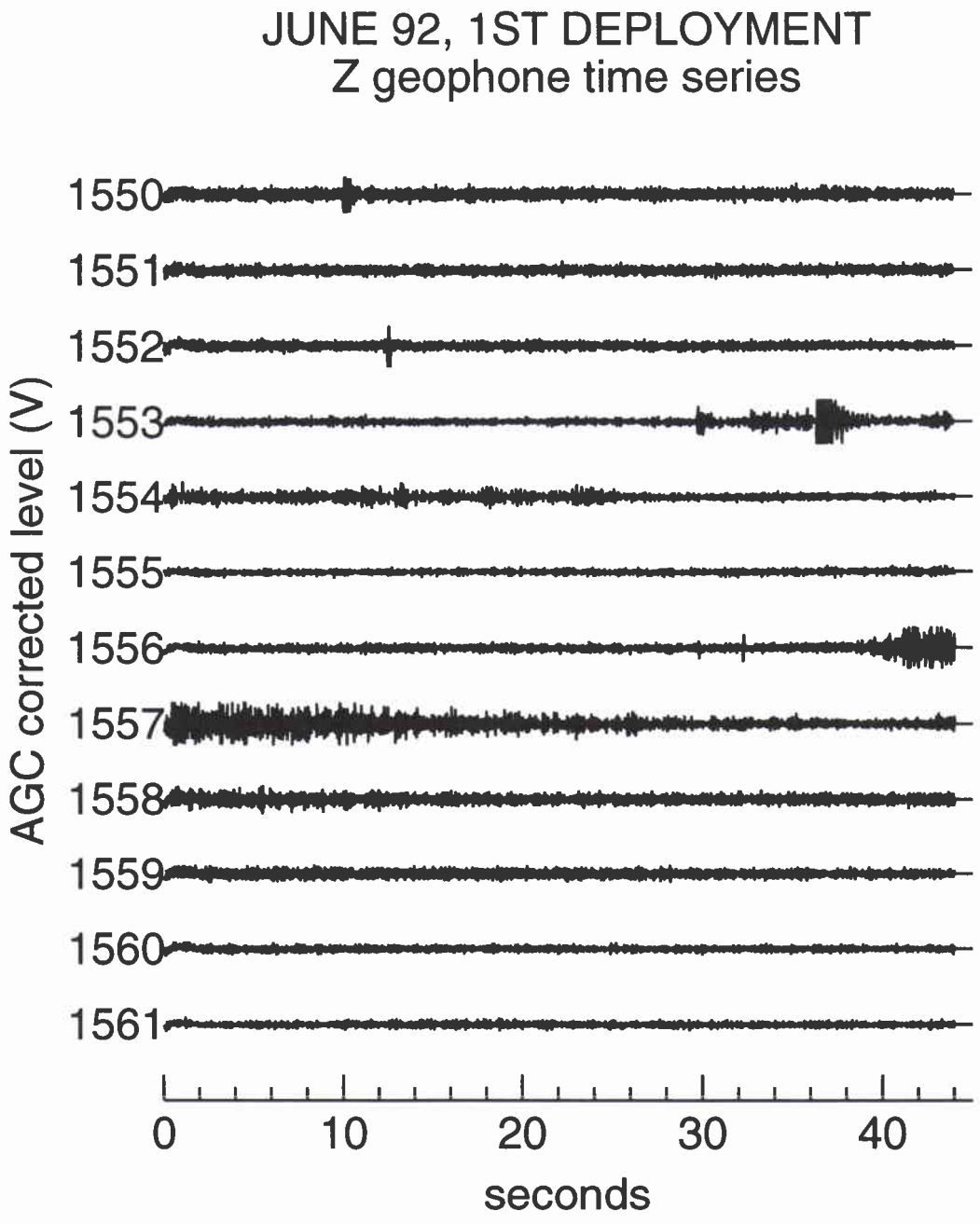

Figure 14d *z- geophone time series, Float 2, first deployment. Record 1550 to 1561.*

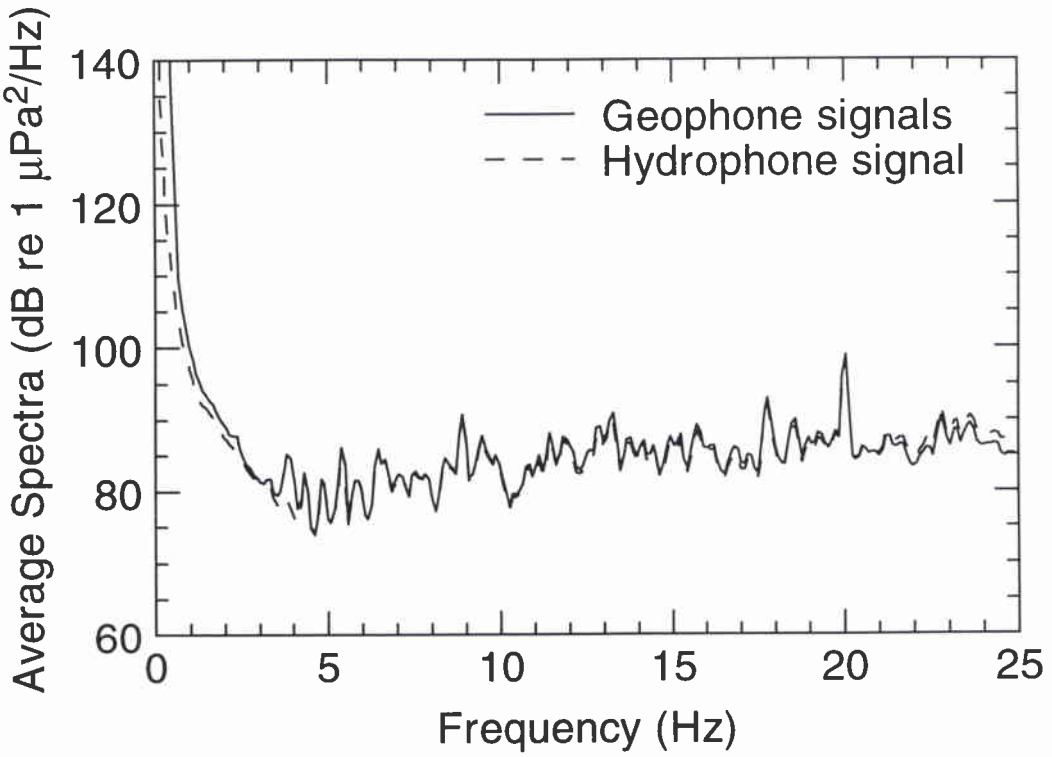

Figure 15a *Hydrophone spectrum and geophone equivalent spectrum, Float 6, second deployment. 2.5 h average from record 700 to 900.*

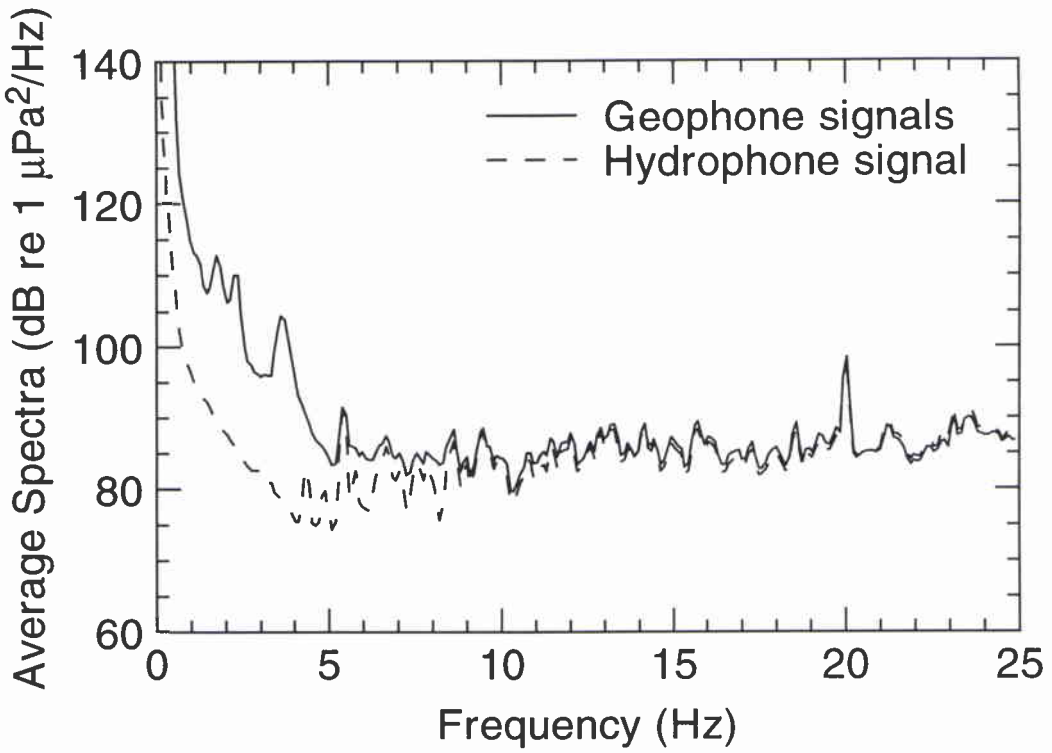

Figure 15b *Hydrophone spectrum and geophone equivalent spectrum, Float 6, second deployment. 2.5 h average from record 900 to 1100.*

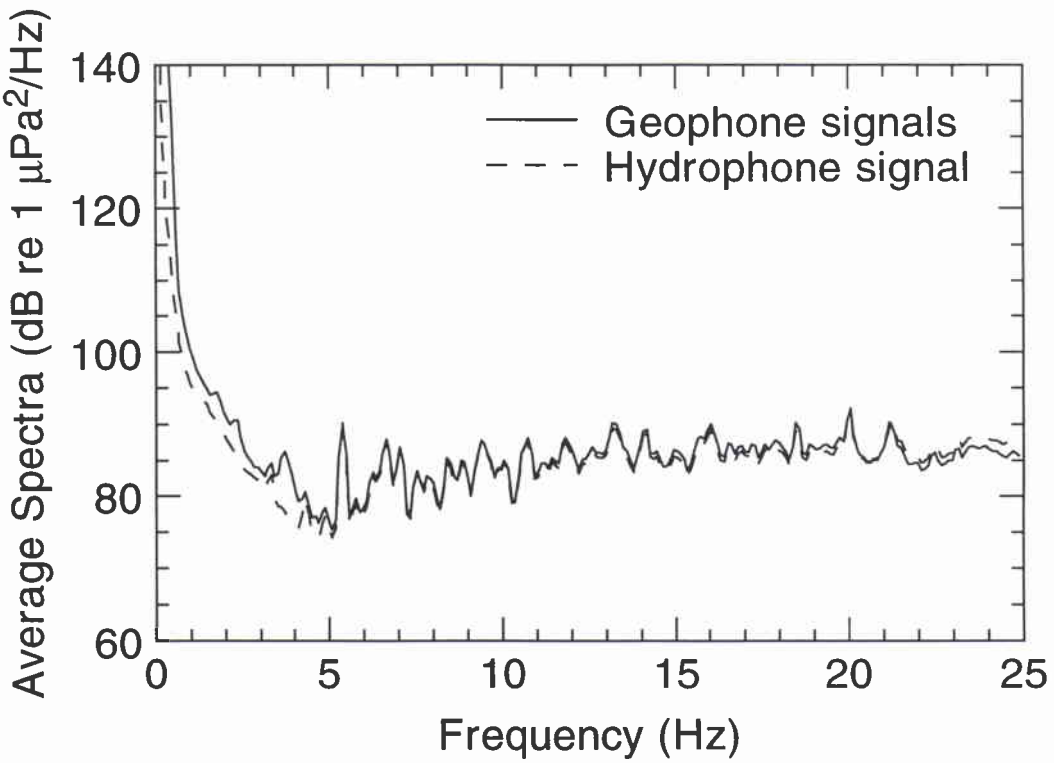

Figure 15c *Hydrophone spectrum and geophone equivalent spectrum, Float 6, second deployment. 2.5 h average from record 1100 to 1300.*

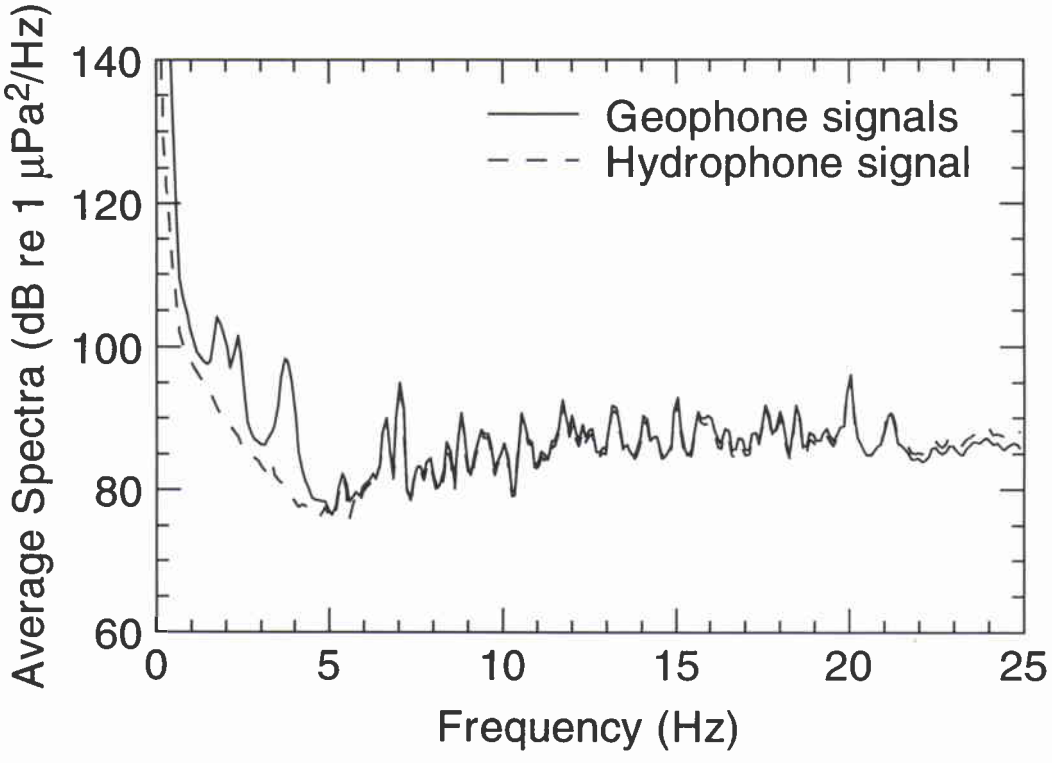

Figure 15d *Hydrophone spectrum and geophone equivalent spectrum, Float 6, second deployment. 2.5 h average from record 1300 to 1500.*

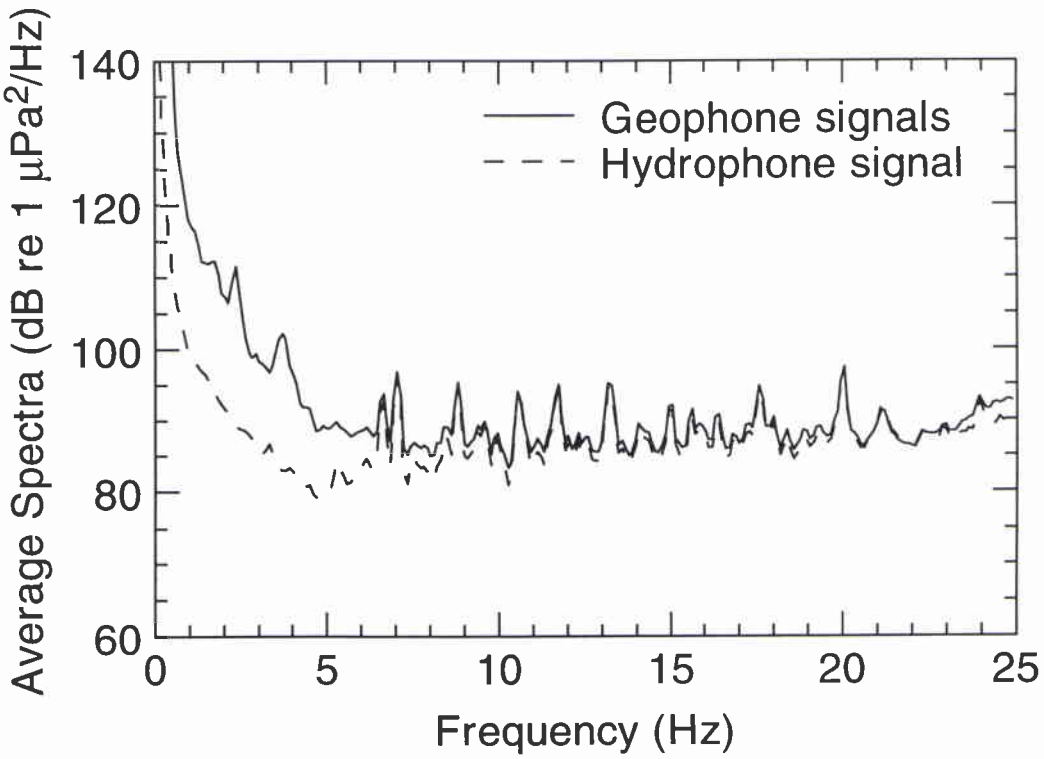

Figure 15e *Hydrophone spectrum and geophone equivalent spectrum, Float 6, second deployment. 2.5 h average from record 1500 to 1700.*

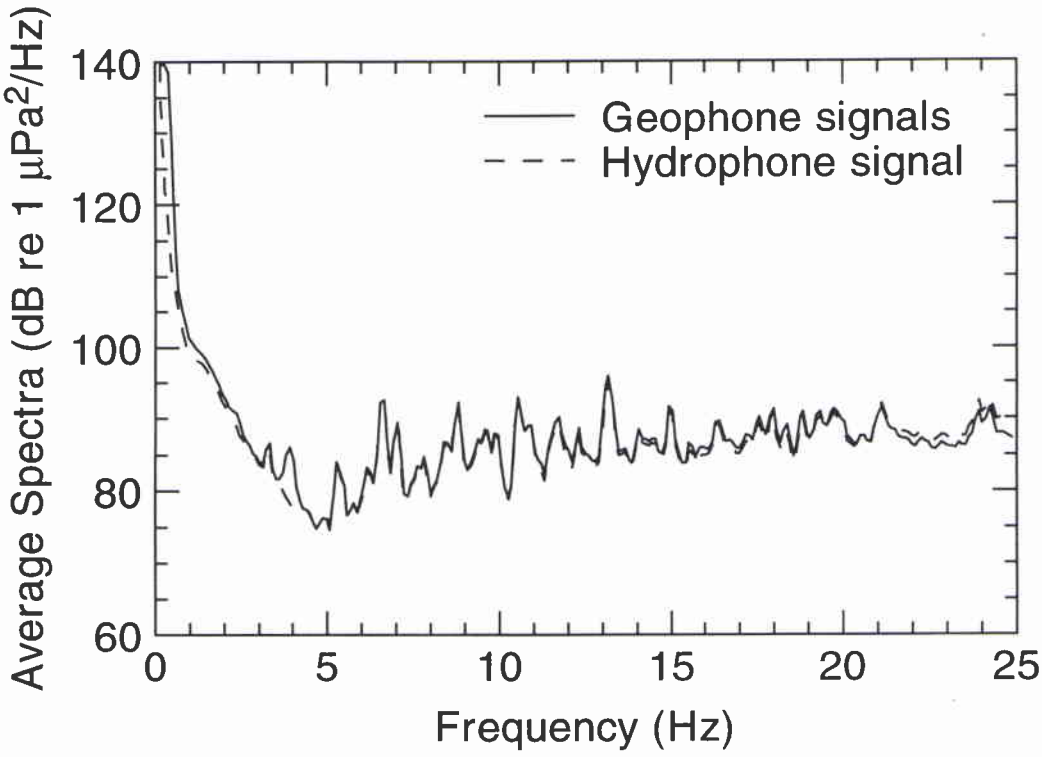

Figure 15f *Hydrophone spectrum and geophone equivalent spectrum, Float 6, second deployment. 2.5 h average from record 1700 to 1900.*

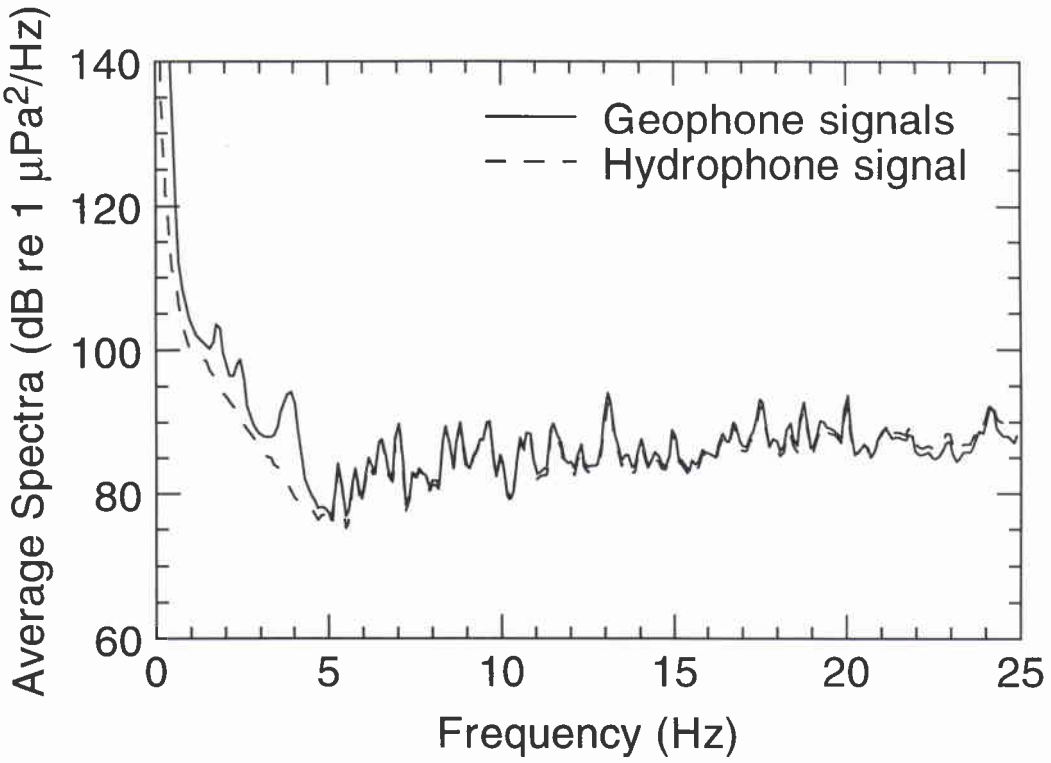

Figure 15g *Hydrophone spectrum and geophone equivalent spectrum, Float 6, second deployment. 2.5 h average from record 1900 to 2100.*

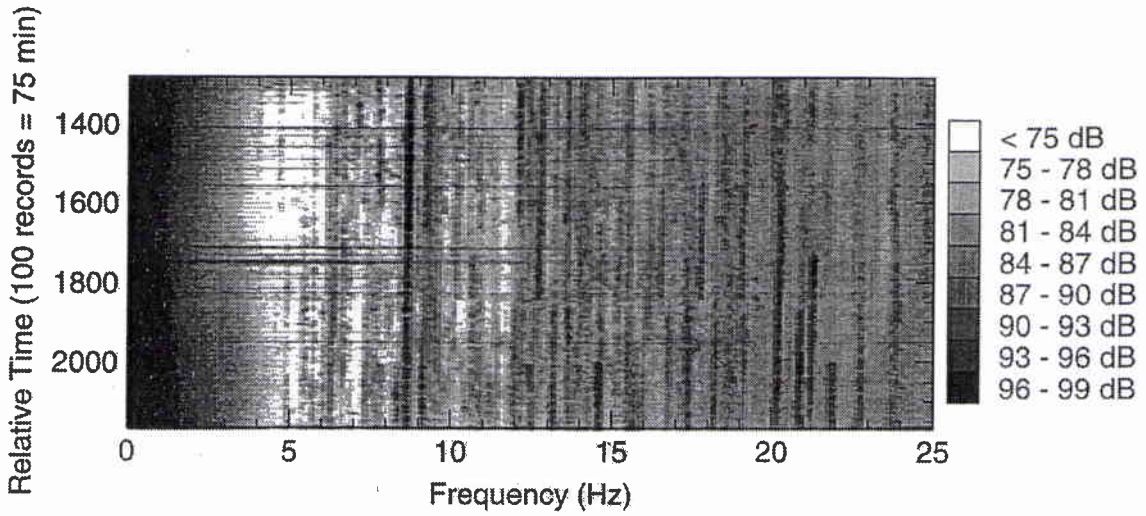

Figure 16a *Gray plot of spectrum level (dB// 1 $\mu Pa^2/Hz$) as a function of time (record number). Float 7, first deployment: hydrophone spectrum.*

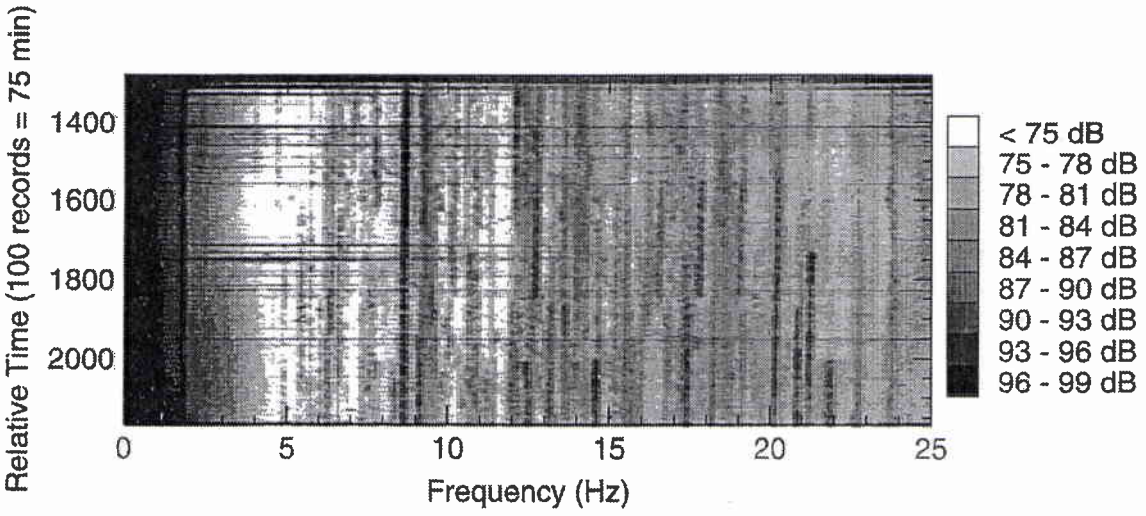

Figure 16b *Gray plot of spectrum level (dB// 1 $\mu Pa^2/Hz$) as a function of time (record number). Float 7, first deployment: geophone spectrum.*

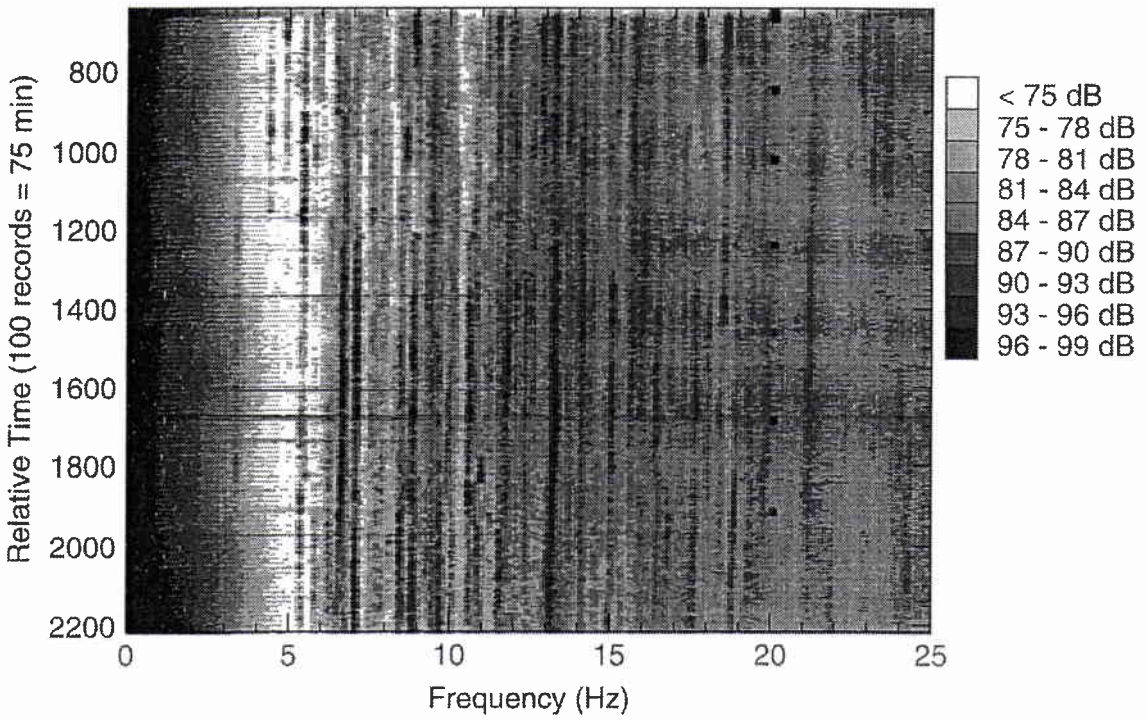

Figure 17a *Gray plot of spectrum level (dB// 1 μPa^2/Hz) as a function of time (record number). Float 0, second deployment: hydrophone spectrum.*

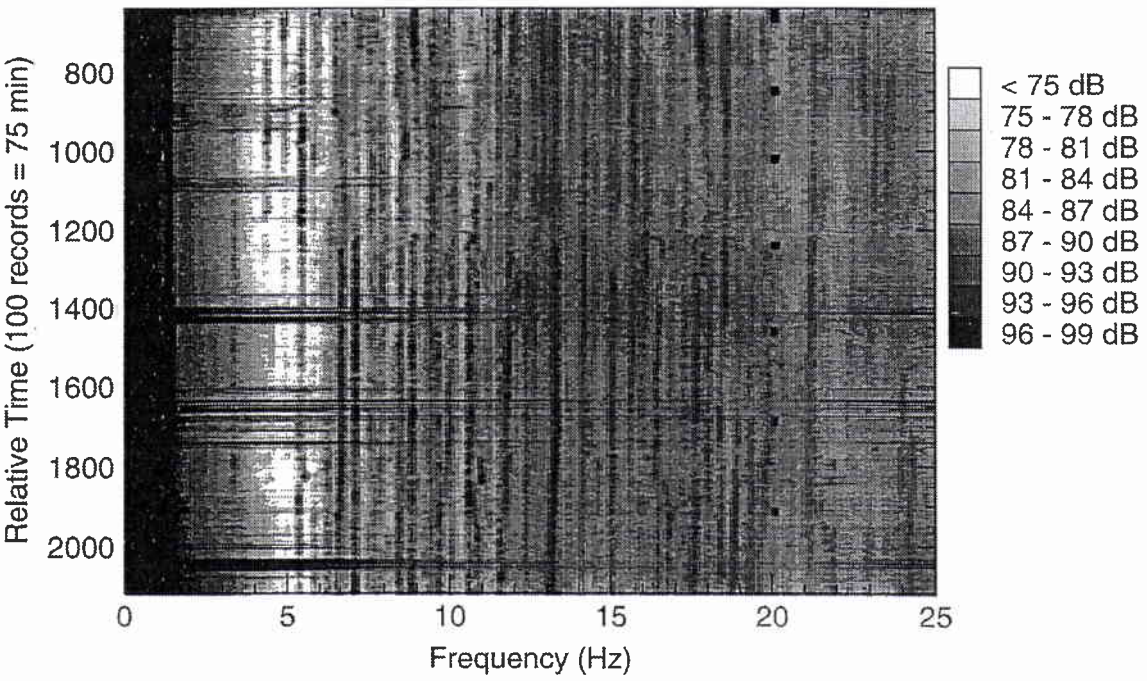

Figure 17b *Gray plot of spectrum level (dB// 1 μPa^2/Hz) as a function of time (record number). Float 0, second deployment: geophone spectrum.*

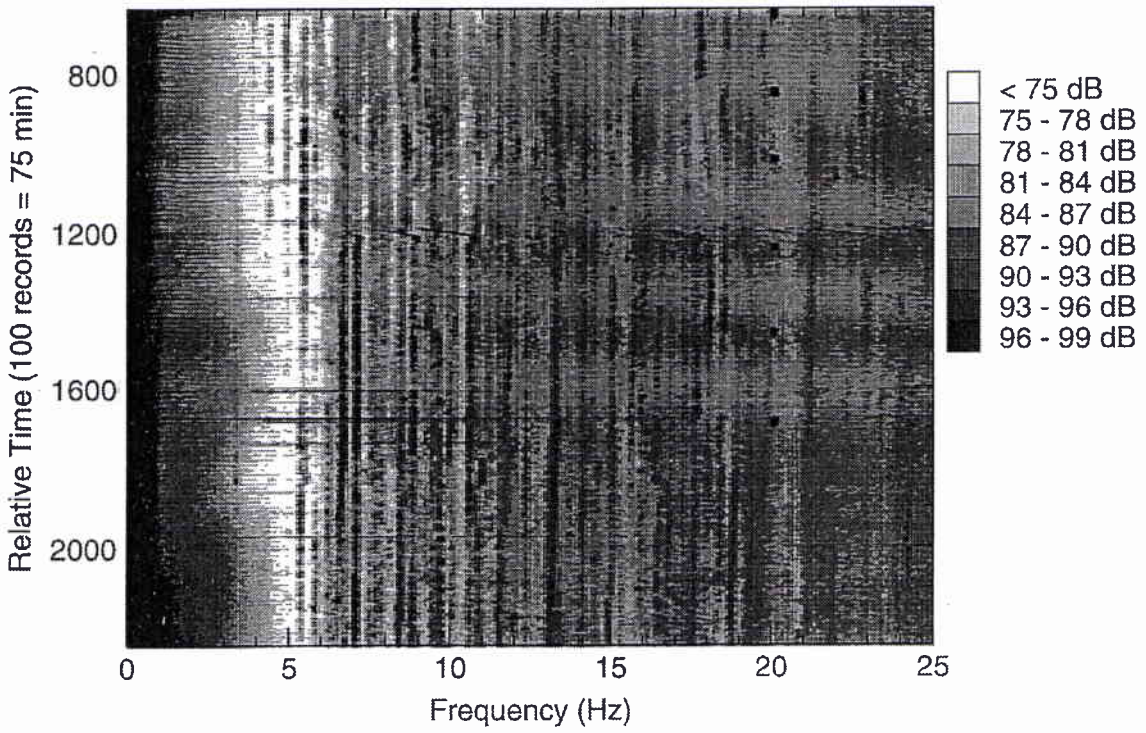

Figure 18a *Gray plot of spectrum level (dB// 1 μPa^2/Hz) as a function of time (record number). Float 1, second deployment: hydrophone spectrum.*

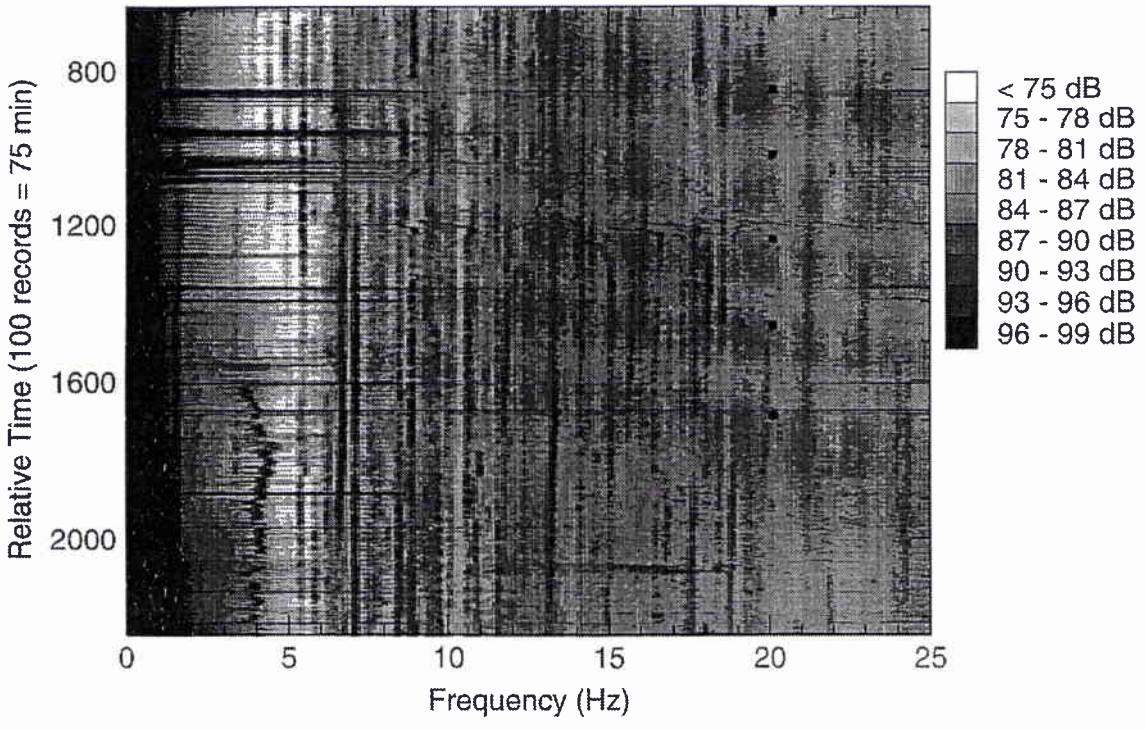

Figure 18b *Gray plot of spectrum level (dB// 1 μPa^2/Hz) as a function of time (record number). Float 1, second deployment: geophone spectrum.*

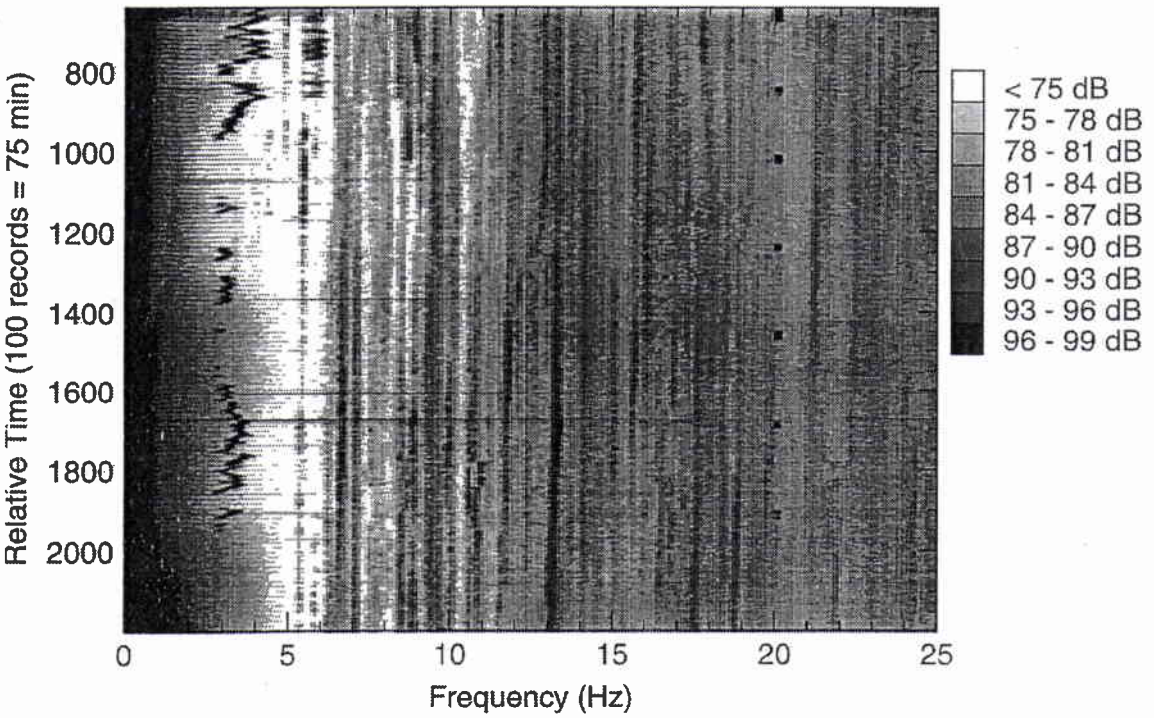

Figure 19 *Gray plot of spectrum level (dB// 1 μPa^2/Hz) as a function of time (record number). Float 10, second deployment: hydrophone spectrum.*

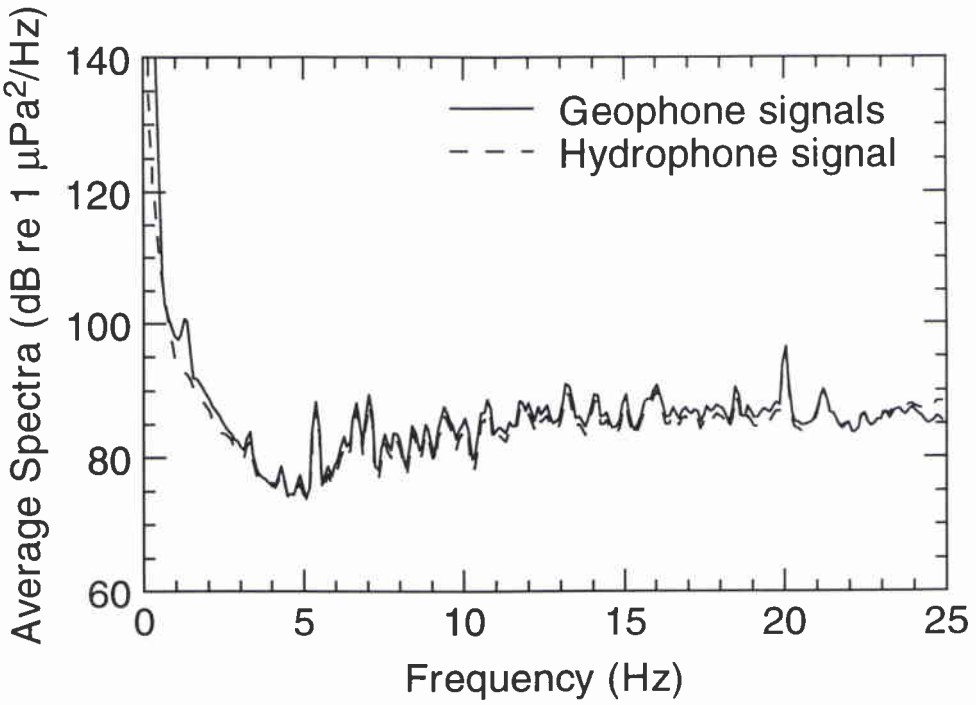

Figure 20a *Float 0, second deployment. 2.5 h time average, starting at record 1148. Average hydrophone spectrum (dashed line) and geophone equivalent spectrum (solid line).*

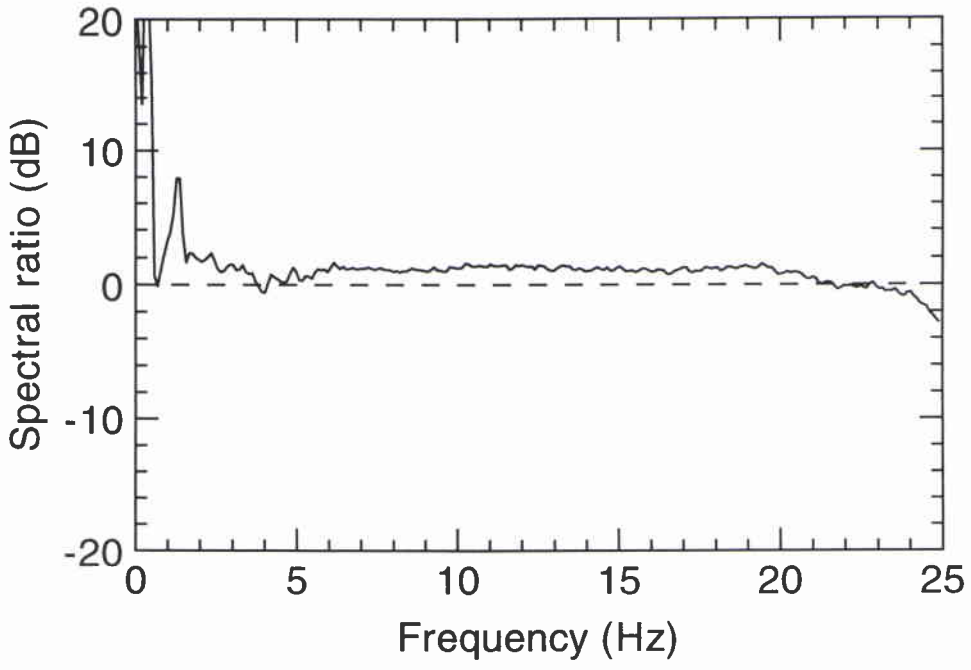

Figure 20b *Float 0, second deployment. 2.5 h time average, starting at record 1148. Ratio of averaged geophone to hydrophone spectra (dB).*

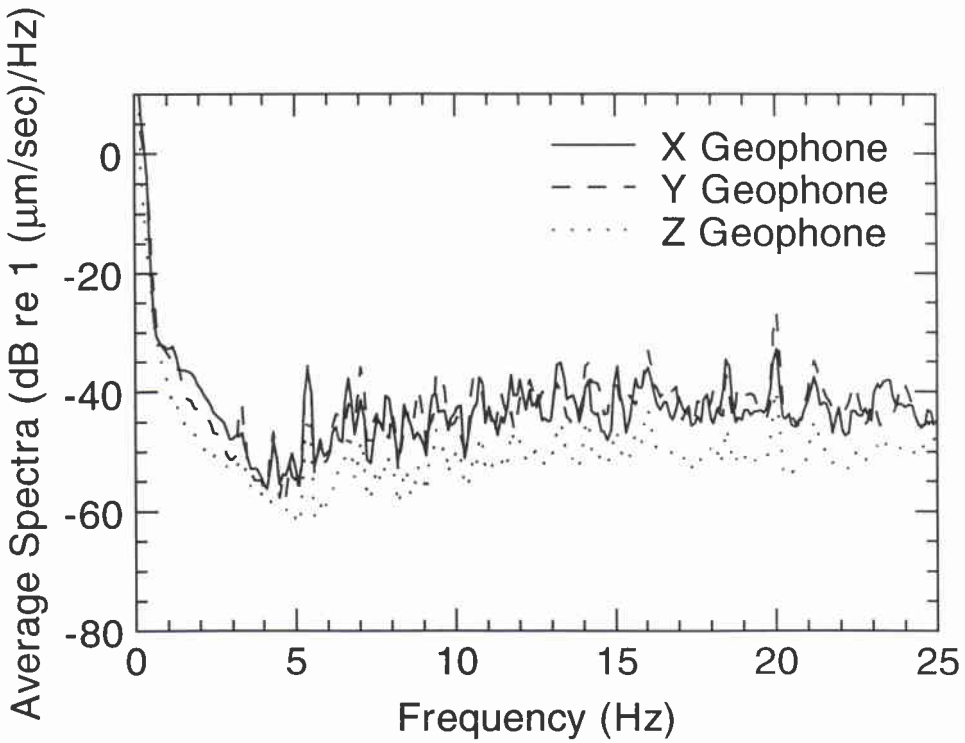

Figure 20c *Float 0, second deployment. 2.5 h time average, starting at record 1148. Average geophone spectra in dB re (1 µm/s)/Hz.*

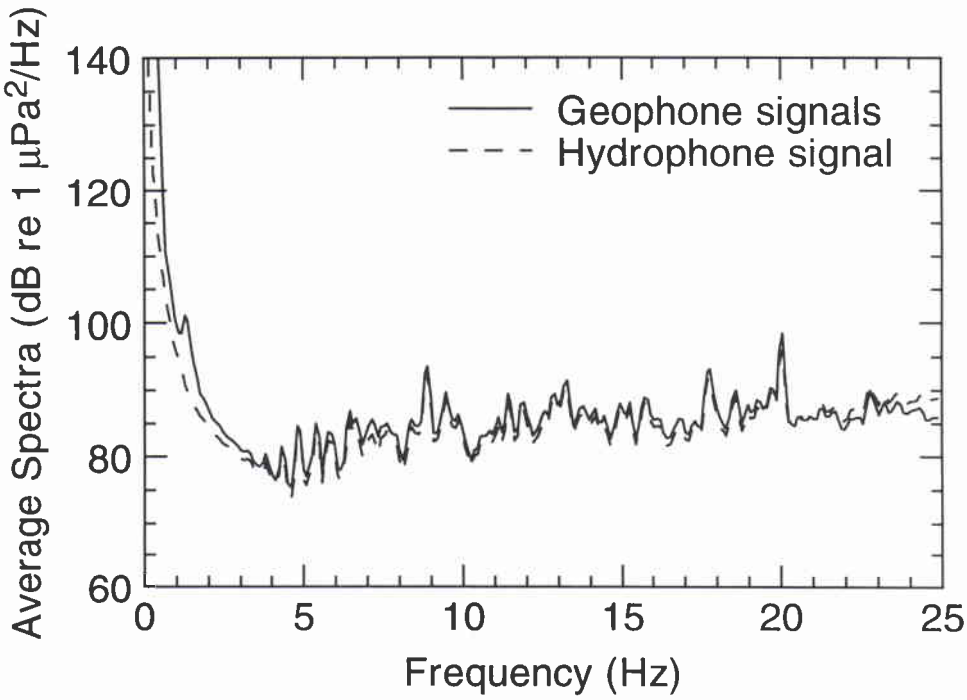

Figure 21a *Float 1, second deployment. 2.5 h time average, starting at record 640: Average hydrophone spectrum (dashed line) and geophone equivalent spectrum (solid line).*

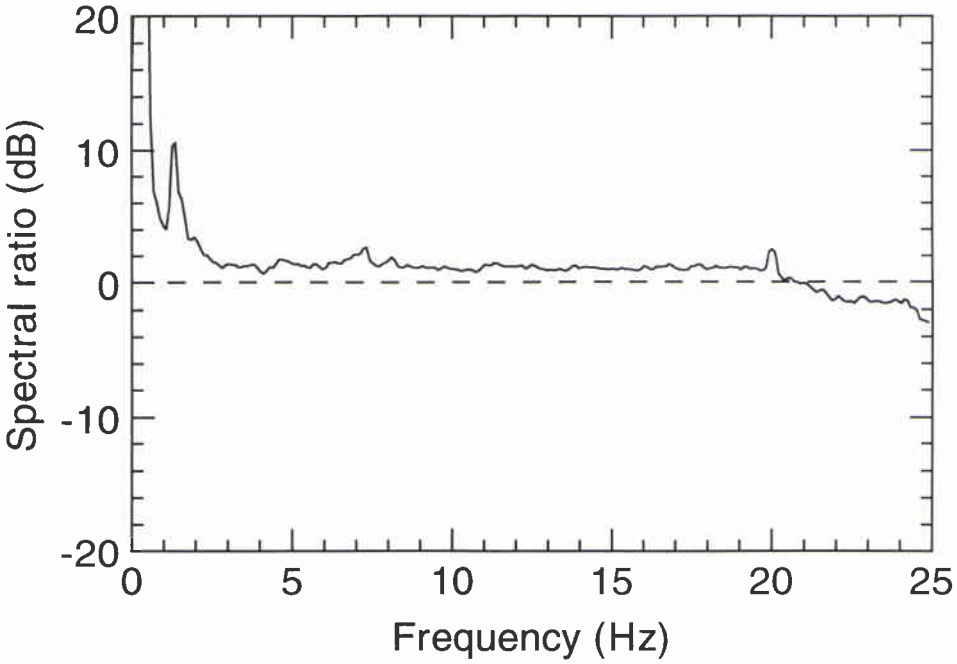

Figure 21b *Float 1, second deployment. 2.5 h time average, starting at record 640: Ratio of averaged geophone to hydrophone spectra (dB).*

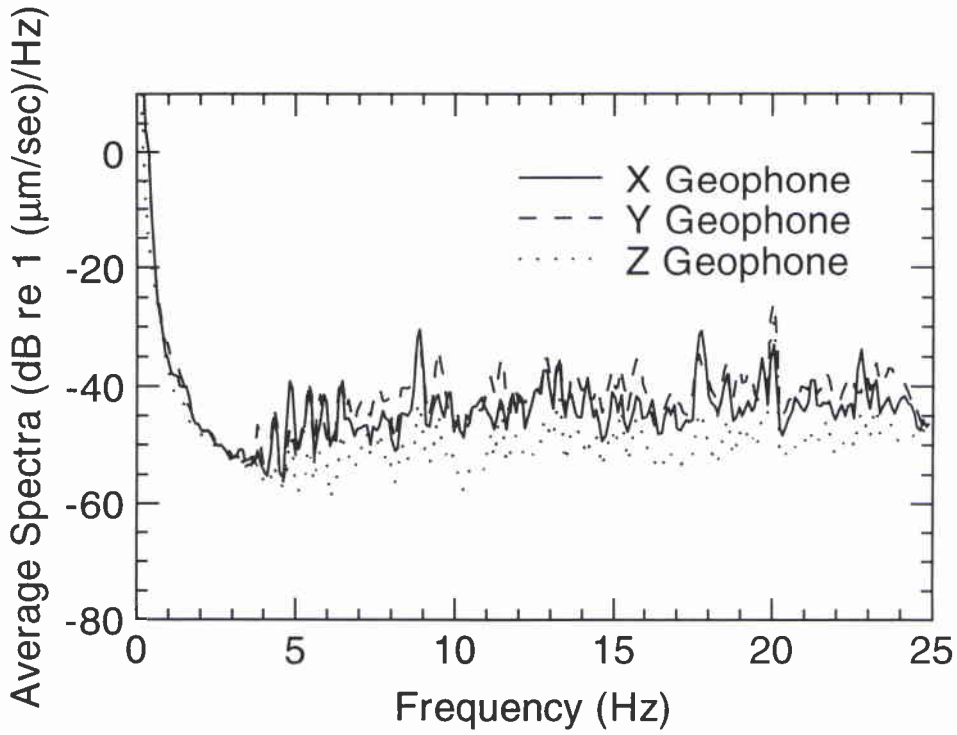

Figure 21c *Float 1, second deployment. 2.5 h time average, starting at record 640: Average geophone spectra in dB re (1 µm/s)/Hz.*

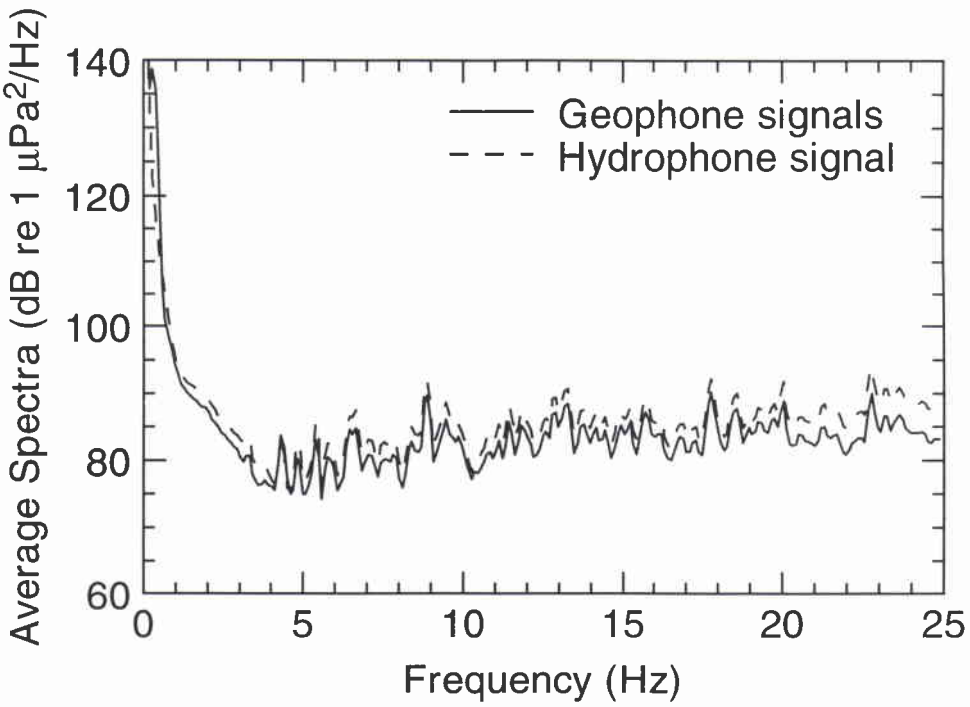

Figure 22a *Float 2, second deployment. 2.5 h time average, starting at record 700: Average hydrophone spectrum (dashed line) and geophone equivalent spectrum (solid line).*

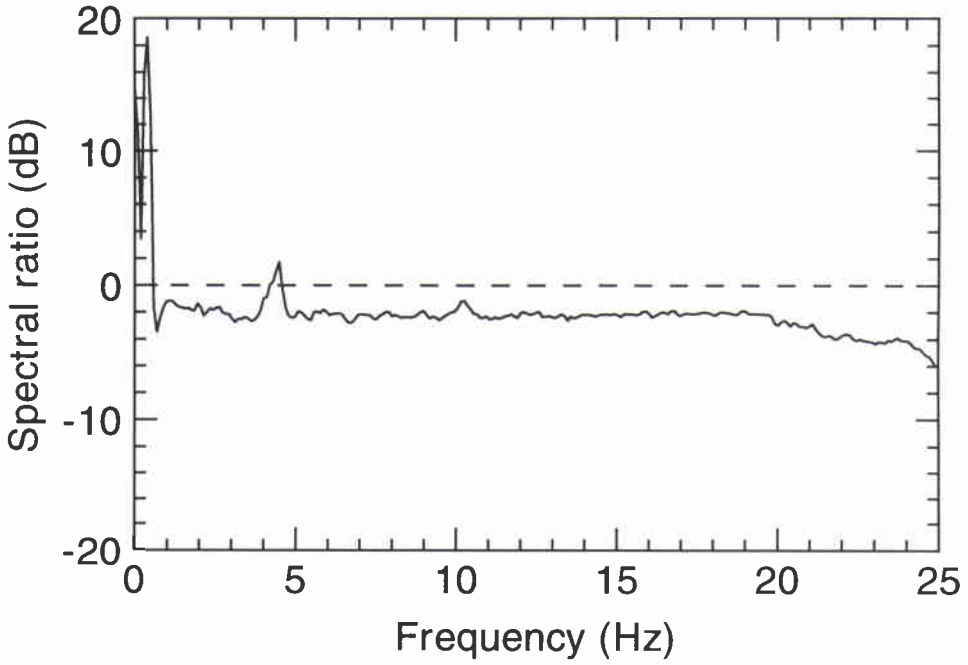

Figure 22b *Float 2, second deployment. 2.5 h time average, starting at record 700: Ratio of averaged geophone to hydrophone spectra (dB).*

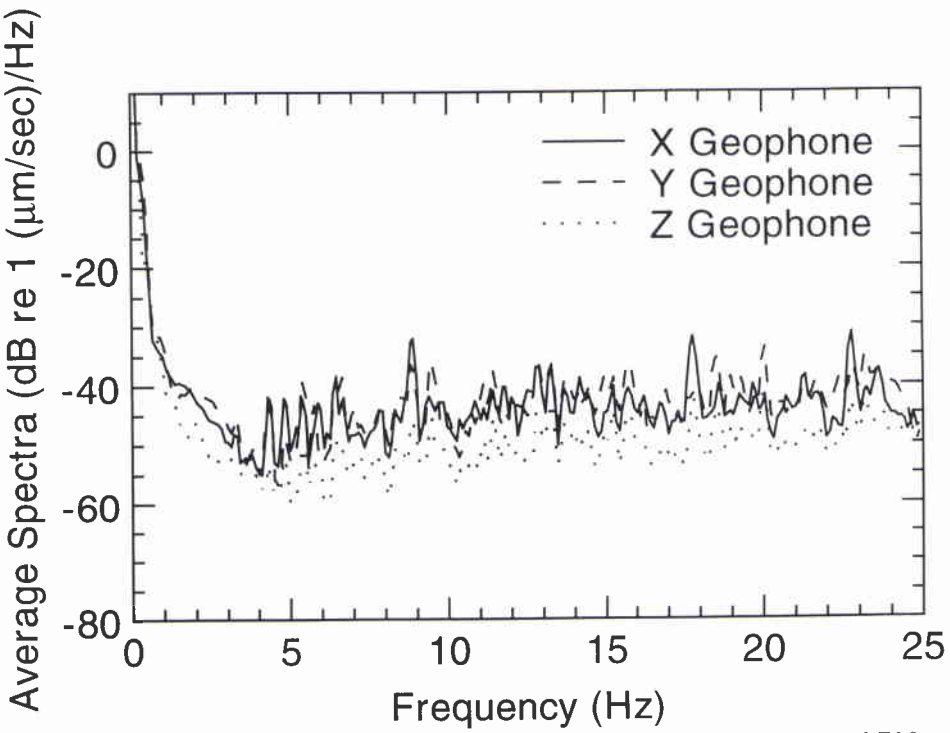

Figure 22c *Float 2, second deployment. 2.5 h time average, starting at record 700: Average geophone spectra in dB re (1 µm/s)/Hz.*

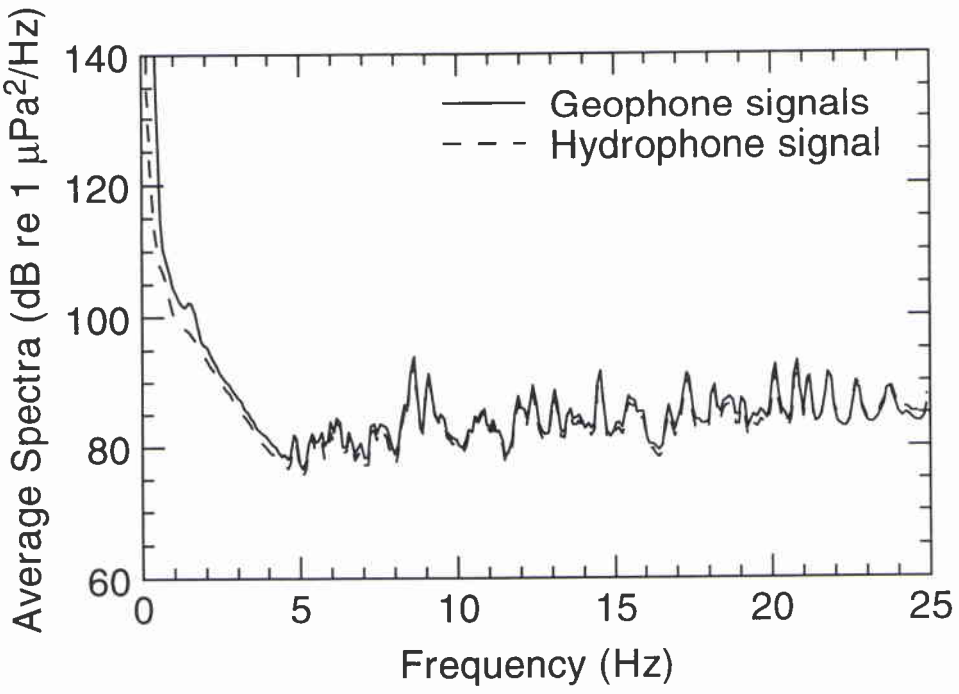

Figure 23a *Float 4, second deployment. 2.5 h time average, starting at record 1952: Average hydrophone spectrum (dashed line) and geophone equivalent spectrum (solid line).*

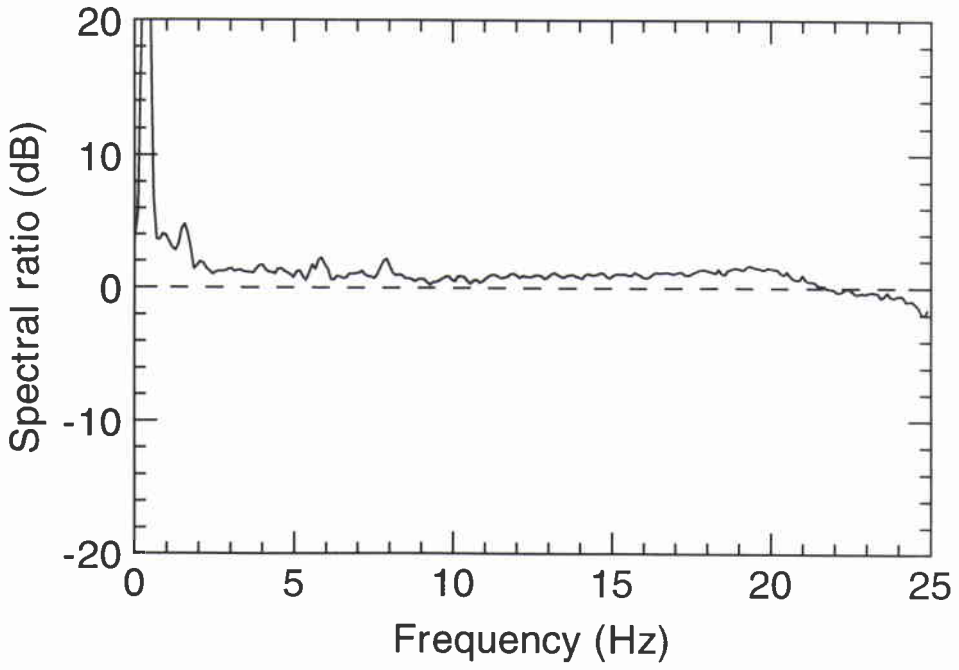

Figure 23b *Float 4, second deployment. 2.5 h time average, starting at record 1952: Ratio of averaged geophone to hydrophone spectra (dB).*

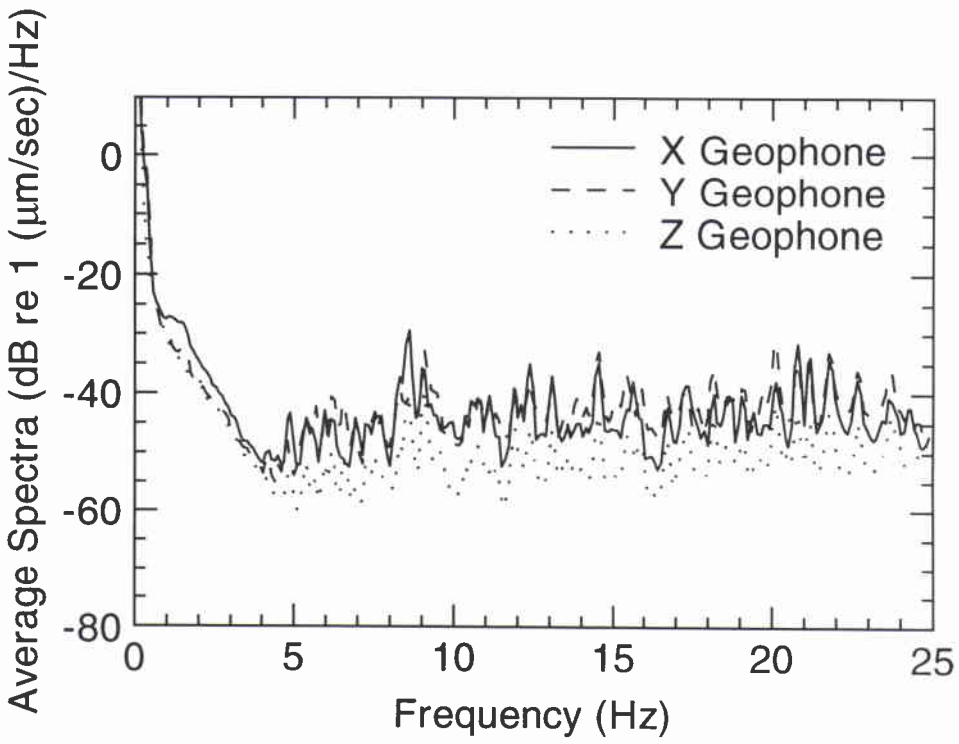

Figure 23c *Float 4, second deployment. 2.5 h time average, starting at record 1952: Average geophone spectra in dB re (1 µm/s)/Hz.*

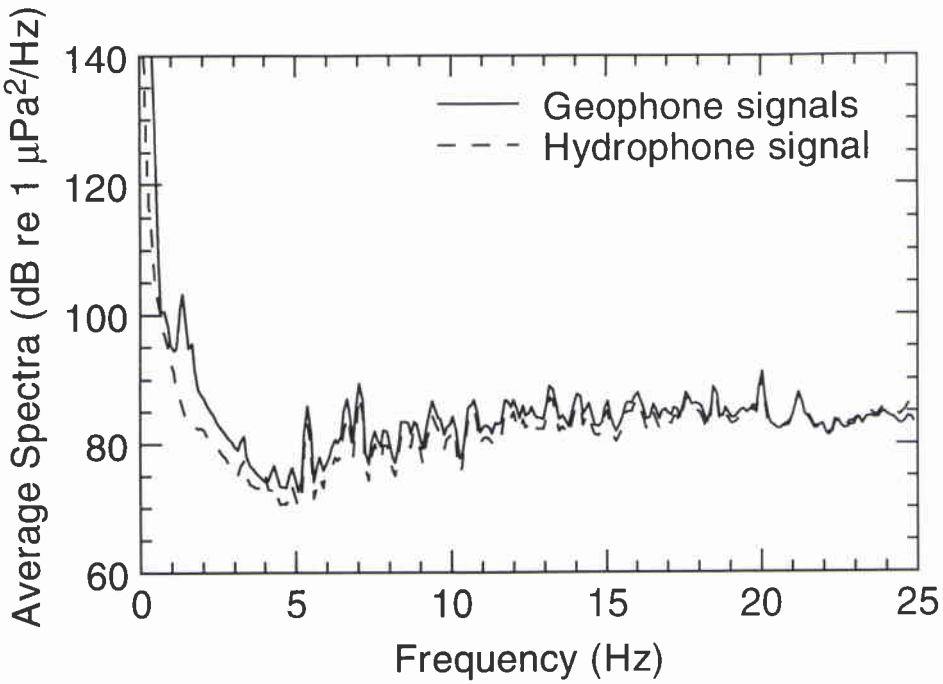

Figure 24a *Float 5, second deployment. 2.5 h time average, starting at record 1148: Average hydrophone spectrum (dashed line) and geophone equivalent spectrum (solid line).*

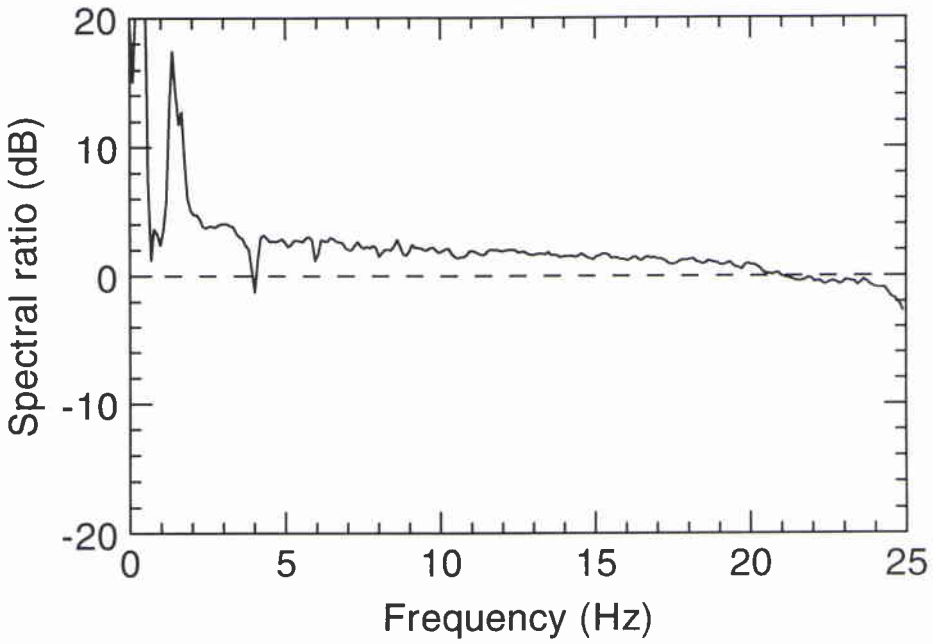

Figure 24b *Float 5, second deployment. 2.5 h time average, starting at record 1148: Ratio of averaged geophone to hydrophone spectrum (dB).*

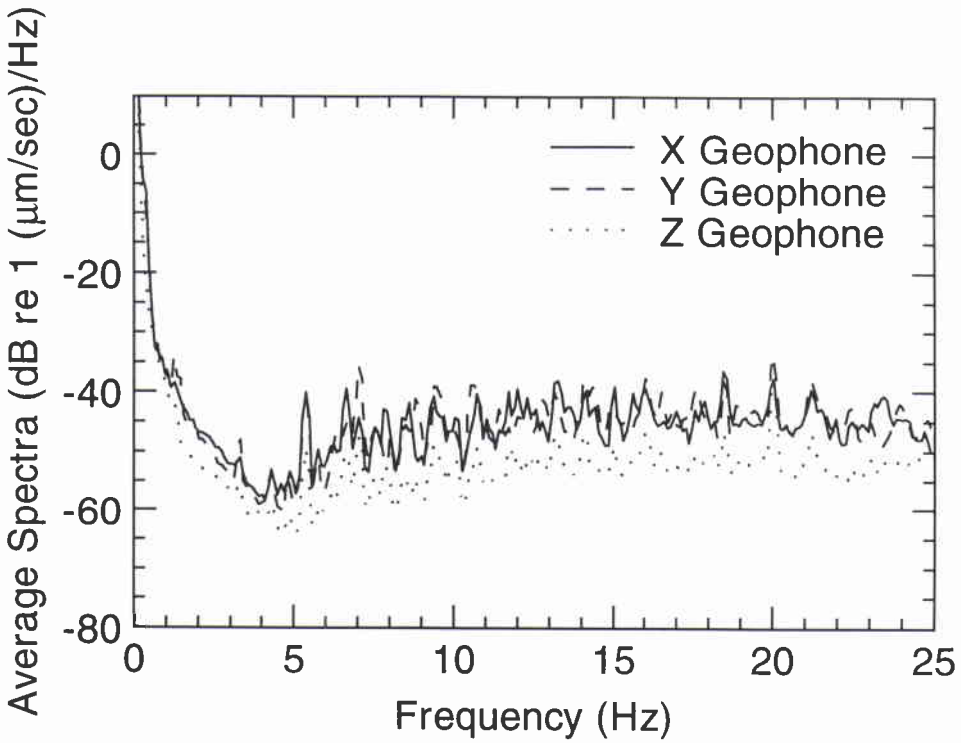

Figure 24c *Float 5, second deployment. 2.5 h time average, starting at record 1148: Average geophone spectrum in dB re (1 µm/s)/Hz.*

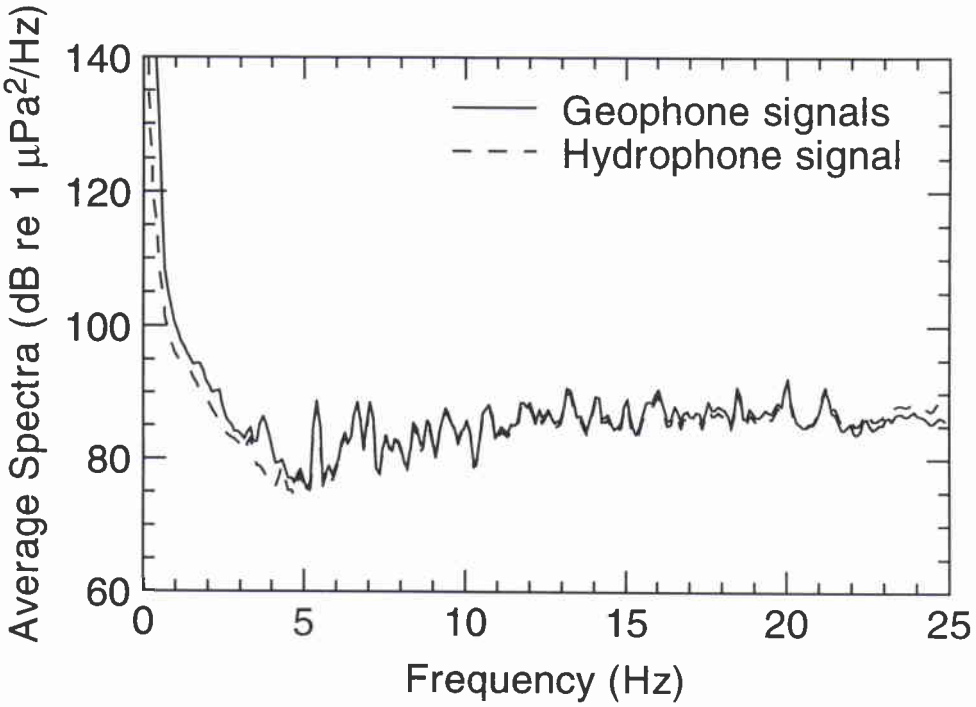

Figure 25a *Float 6, second deployment. 2.5 h time average, starting at record 1148: Average hydrophone spectrum (dashed line) and geophone equivalent spectrum (solid line).*

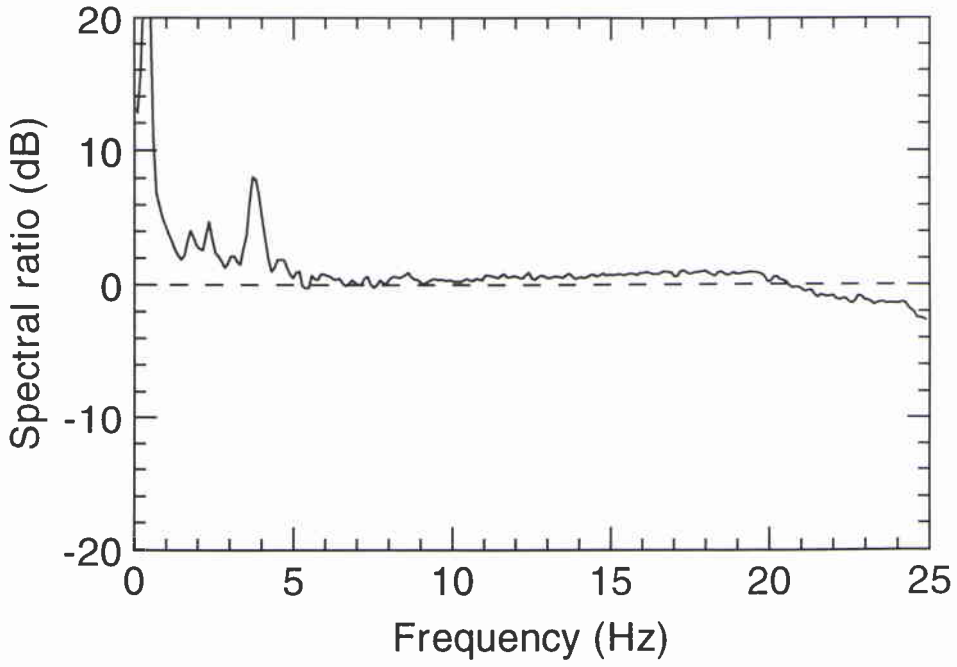

Figure 25b *Float 6, second deployment. 2.5 h time average, starting at record 1148: Ratio of averaged geophone to hydrophone spectrum (dB).*

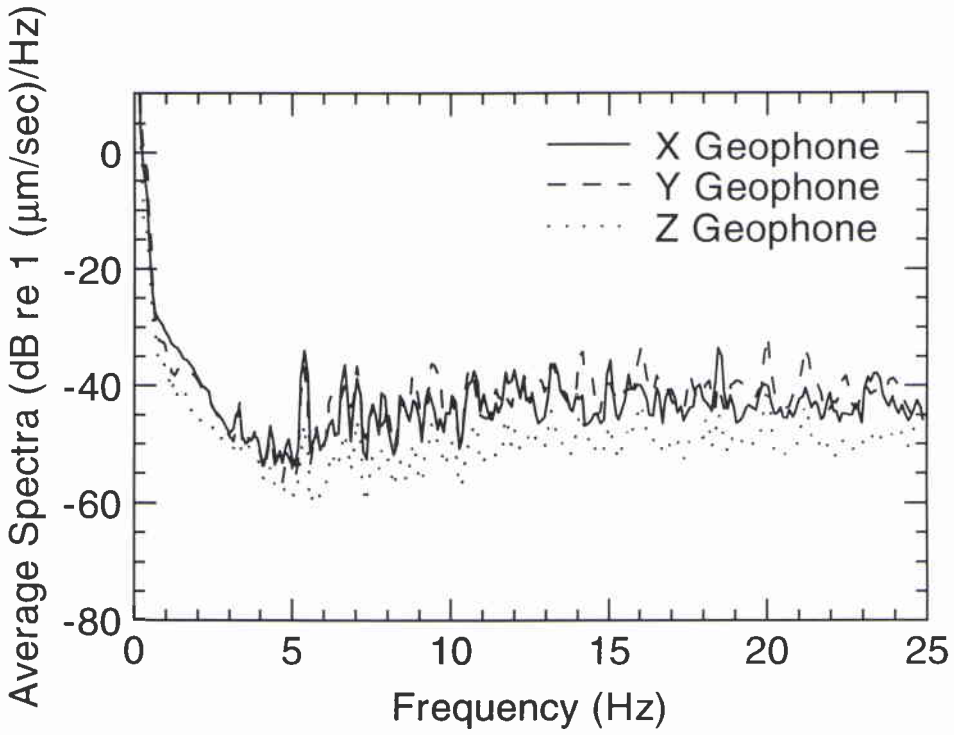

Figure 25c *Float 6, second deployment. 2.5 h time average, starting at record 1148: Average geophone spectrum in dB re (1 µm/s)/Hz.*

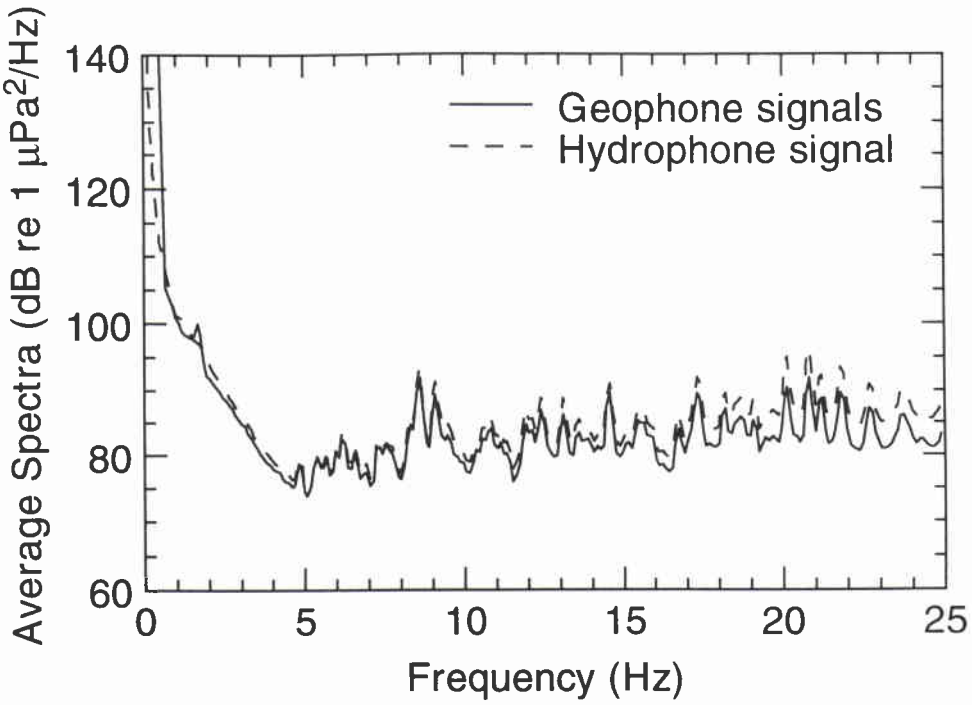

Figure 26a *Float 7, first deployment. 2.5 h time average, starting at record 1964: Average hydrophone spectrum (dashed line) and geophone equivalent spectrum (solid line).*

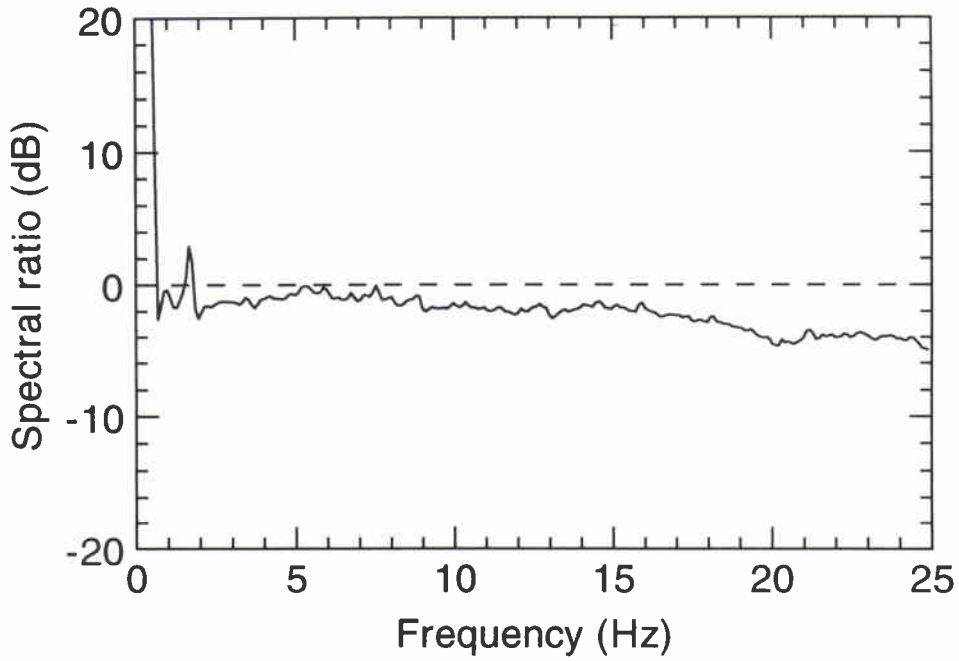

Figure 26b *Float 7, first deployment. 2.5 h time average, starting at record 1964: Ratio of averaged geophone to hydrophone spectrum (dB).*

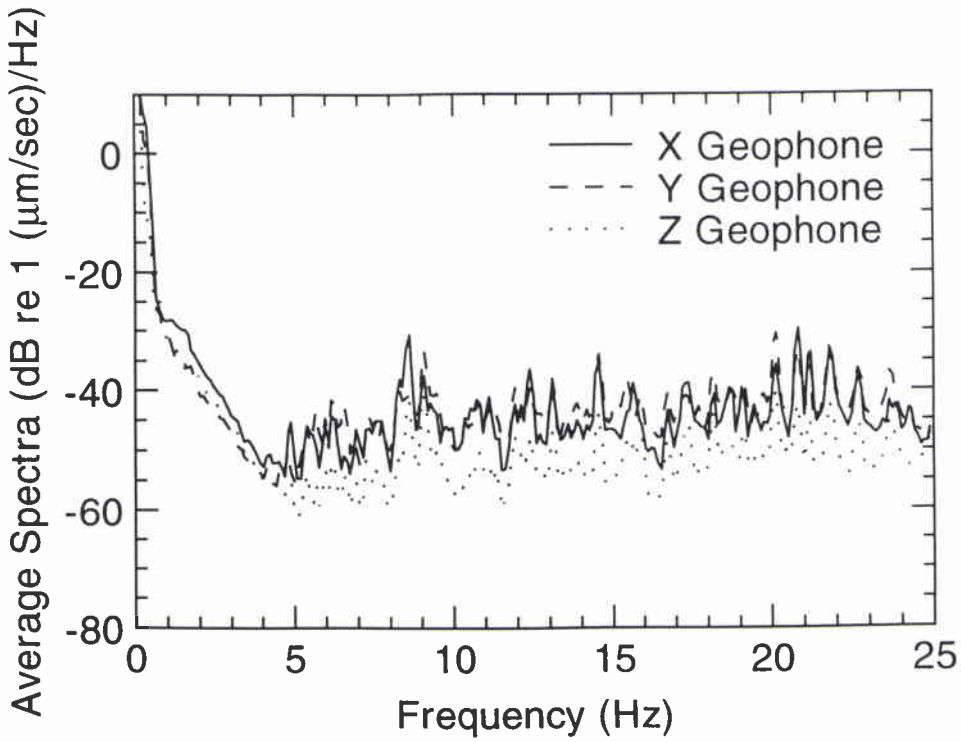

Figure 26c *Float 7, first deployment. 2.5 h time average, starting at record 1964: Average geophone spectrum in dB re (1 µm/s)/Hz.*

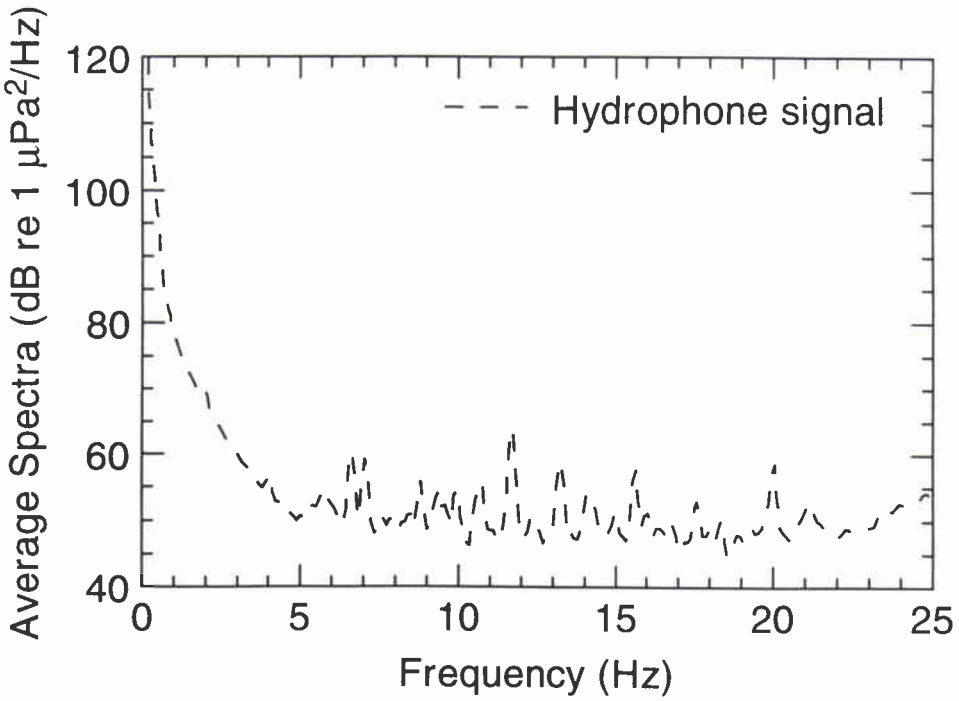

Figure 27a *Float 8, second deployment. 2.5 h time average, starting at record 1500: Average hydrophone spectrum (dashed line).*

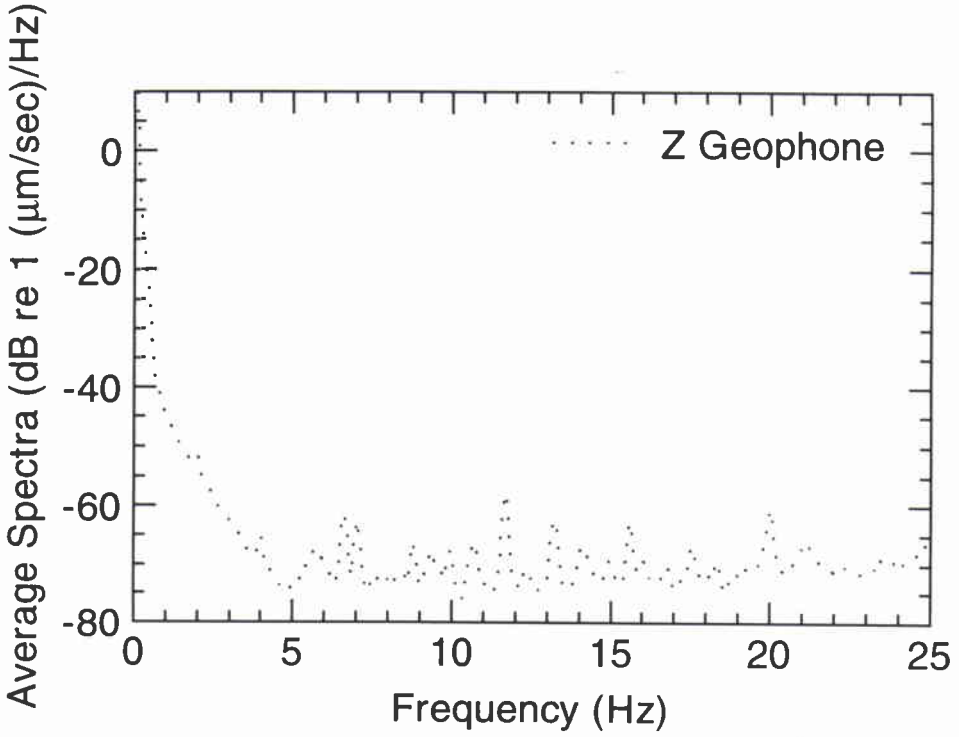

Figure 27b *Float 8, second deployment. 2.5 h time average, starting at record 1500: Average geophone spectrum in dB re (1 µm/s)/Hz.*

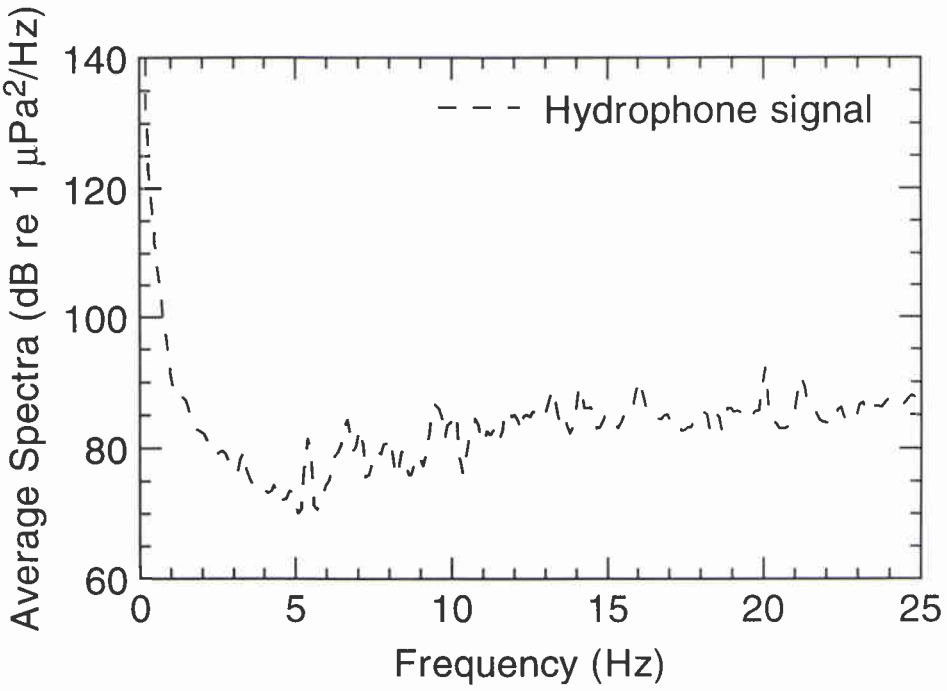

Figure 28a *Float 9, second deployment. 2.5 h time average, starting at record 1100: Average hydrophone spectrum (dashed line).*

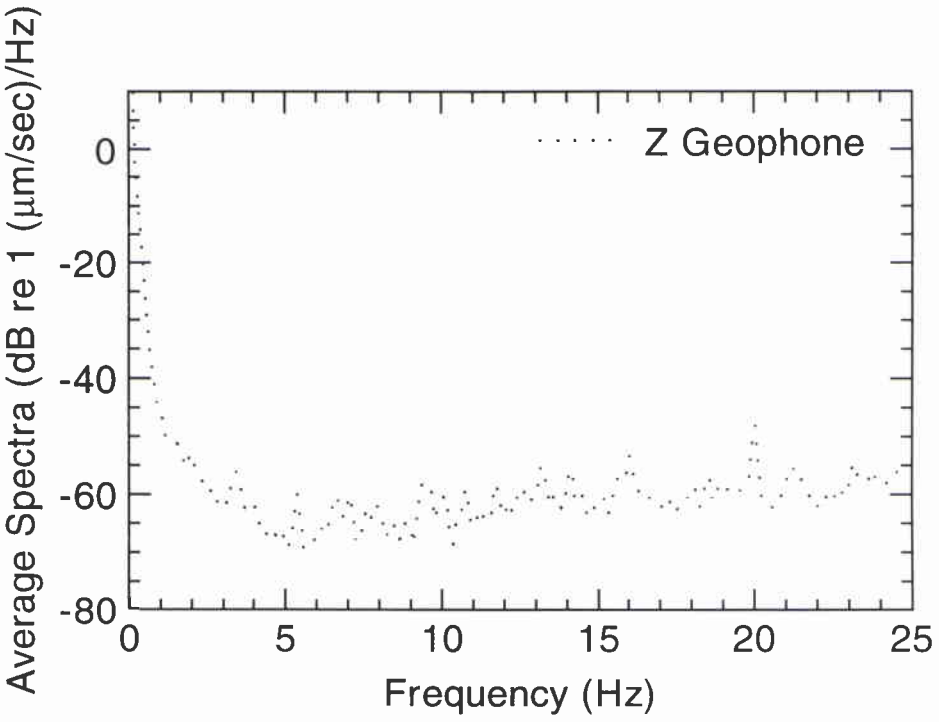

Figure 28b *Float 9, second deployment. 2.5 h time average, starting at record 1100: Average geophone spectrum in dB re (1 µm/s)/Hz.*

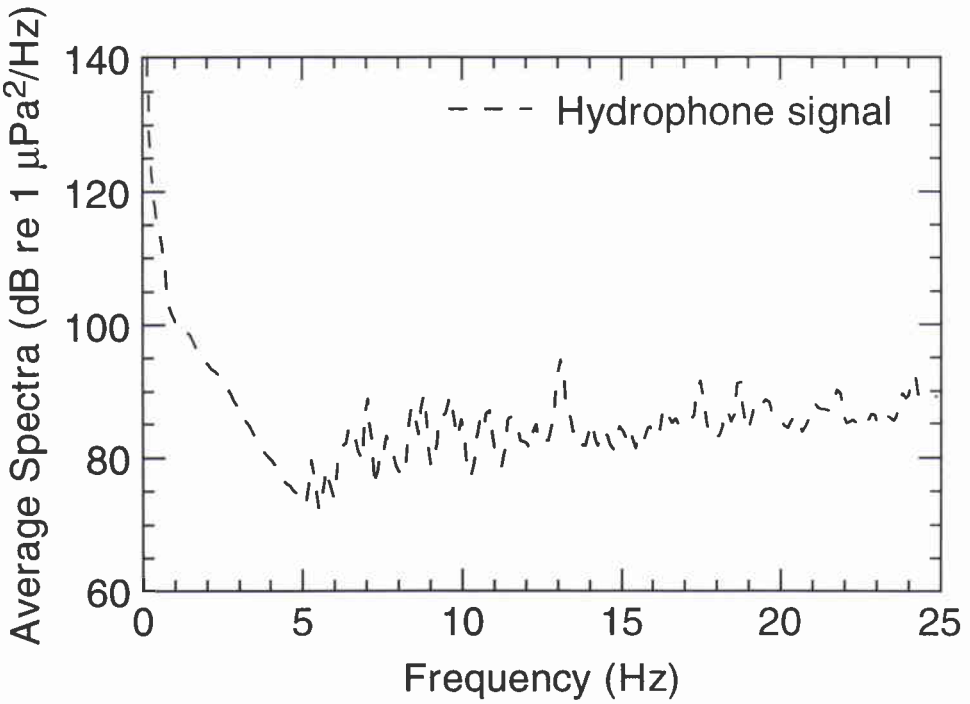

Figure 29a *Float 10, second deployment. 2.5 h time average, starting at record 2004: Average hydrophone spectrum (dashed line).*

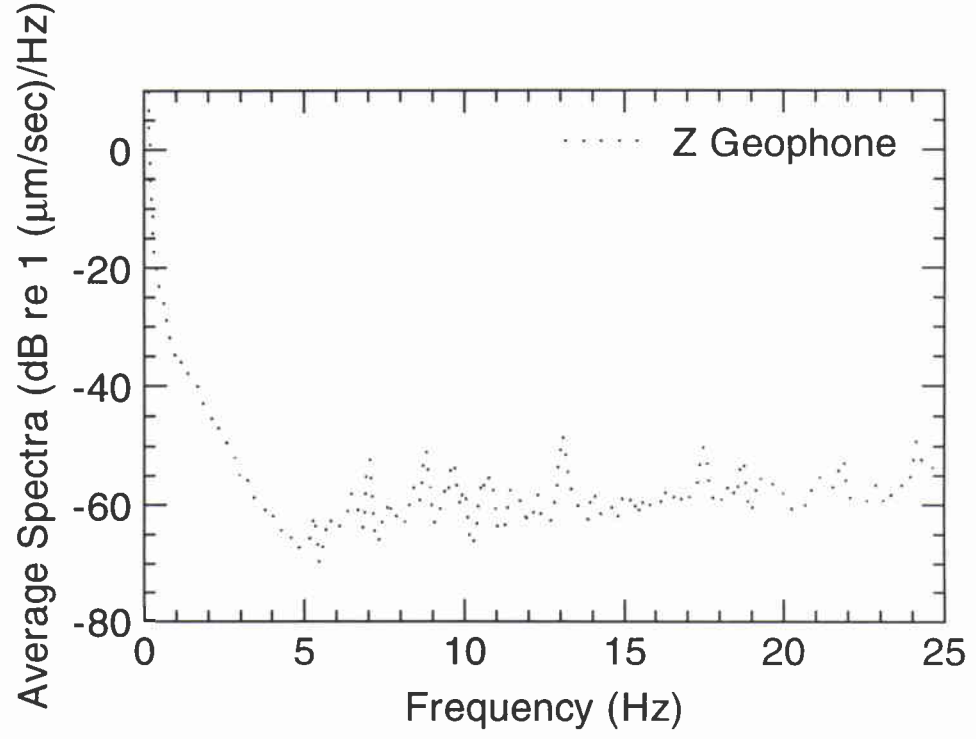

Figure 29b *Float 10, second deployment. 2.5 h time average, starting at record 2004: Average geophone spectrum in dB re (1 µm/s)/Hz.*

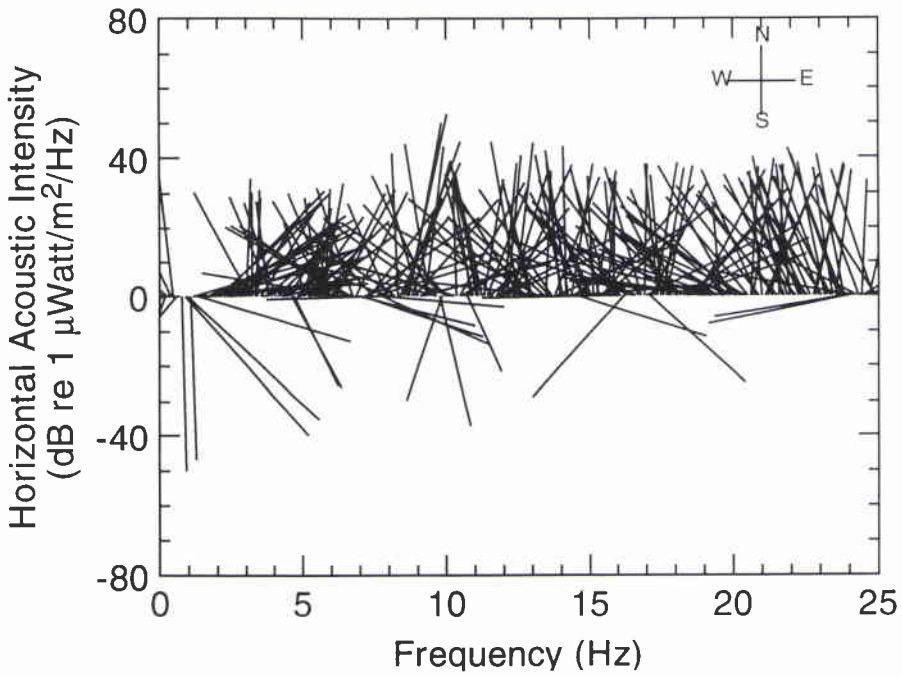

Figure 30 *Horizontal acoustic intensity vectors, representative of the first deployment. The magnitude of the intensity, in dB// 1 µWatt/m²/Hz, is obtained by measuring each vector along the vertical scale, starting at -80 dB.*

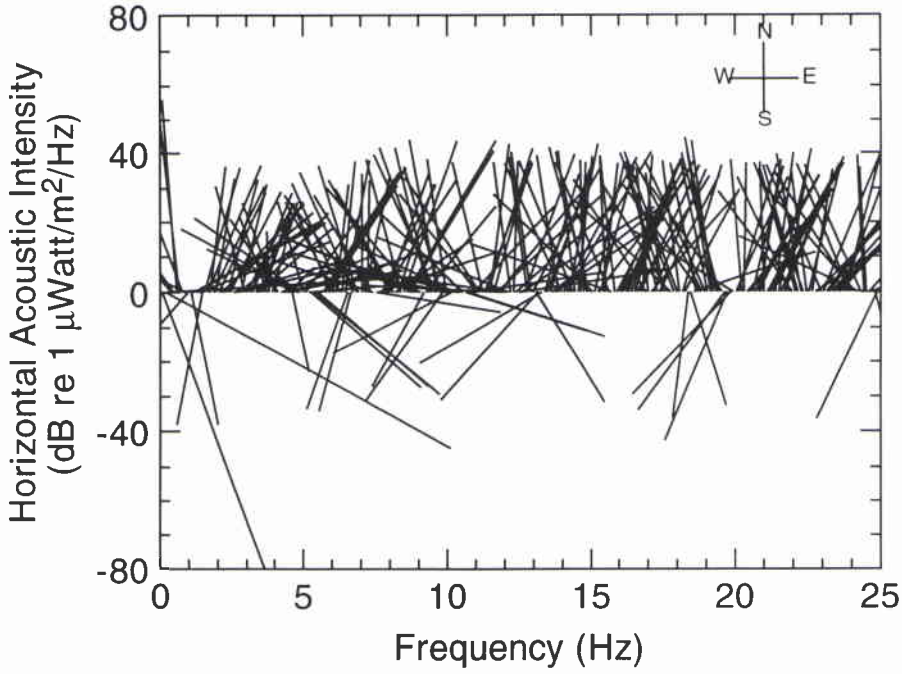

Figure 31 *Horizontal acoustic intensity vectors, representative of the second deployment. The magnitude of the intensity, in dB// 1 µWatt/m²/Hz, is obtained by measuring each vector along the vertical scale, starting at -80 dB.*

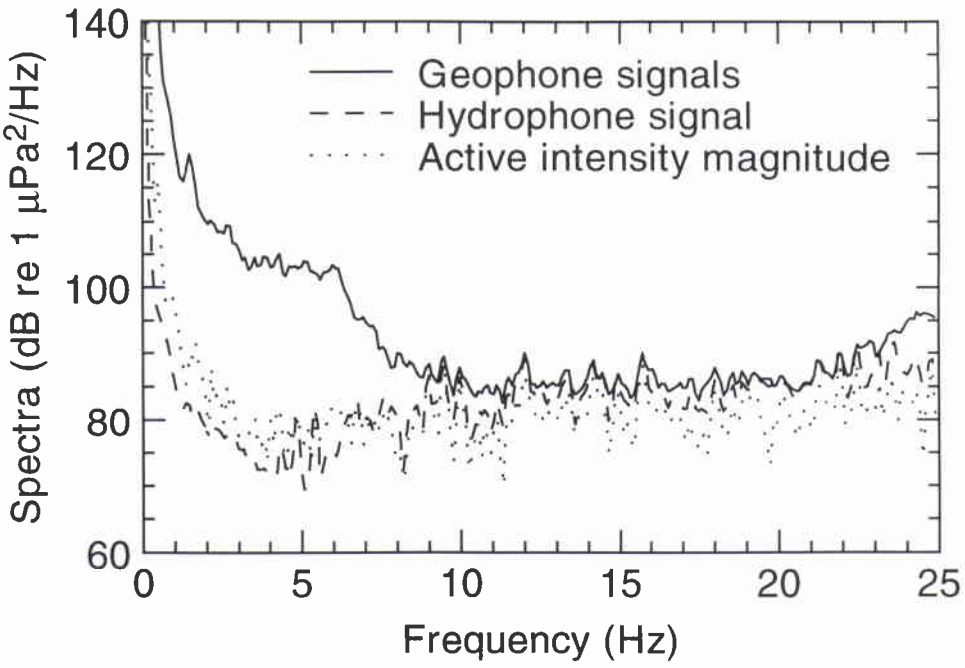

Figure 32 *Average spectra during loud non-acoustic event.*

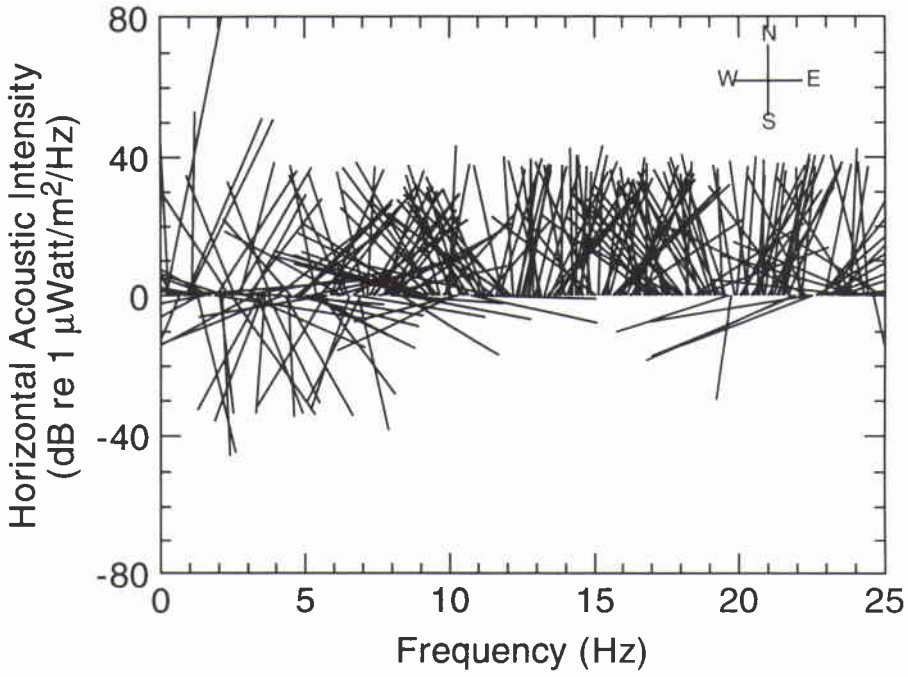

Figure 33 *Horizontal acoustic intensity vectors during loud non-acoustic event. The magnitude of the intensity, in dB// 1 μWatt/m²/Hz, is obtained by measuring each vector along the vertical scale, starting at -80 dB.*

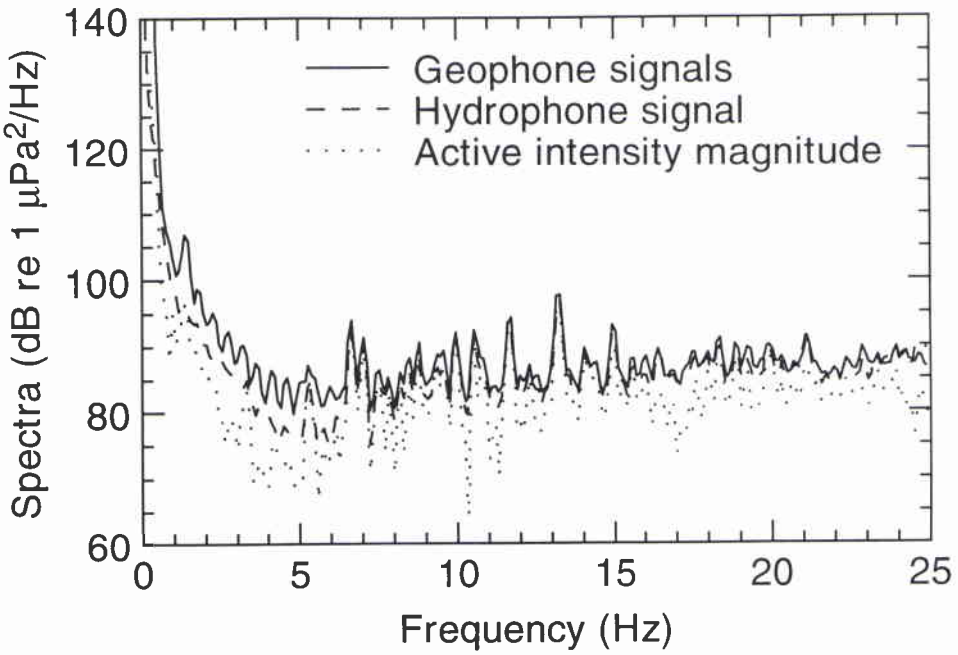

Figure 34 *Average spectra during non-acoustic event.*

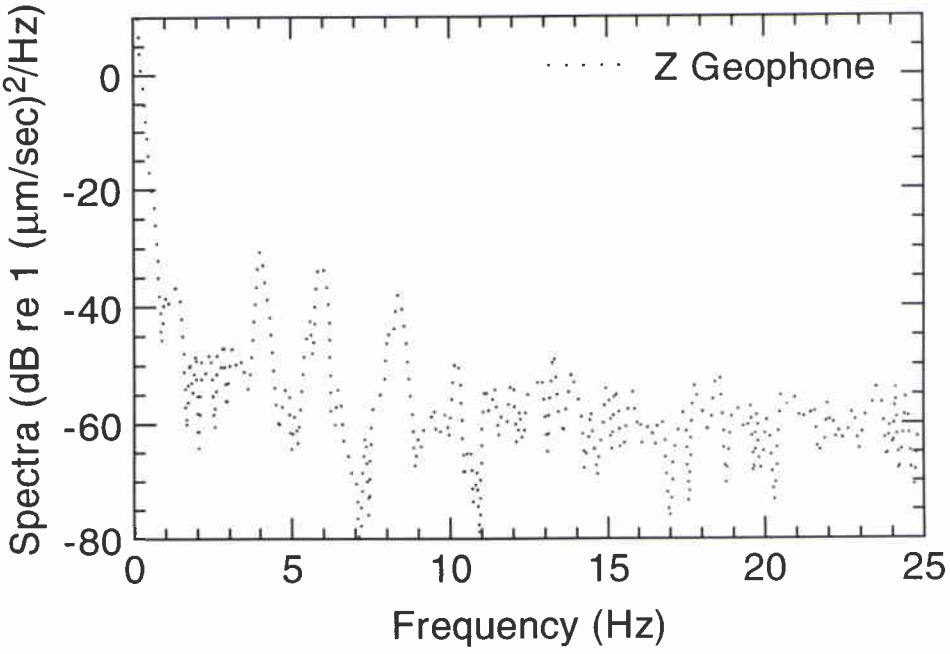

Figure 35 *Average geophone spectrum during non-acoustic event.*

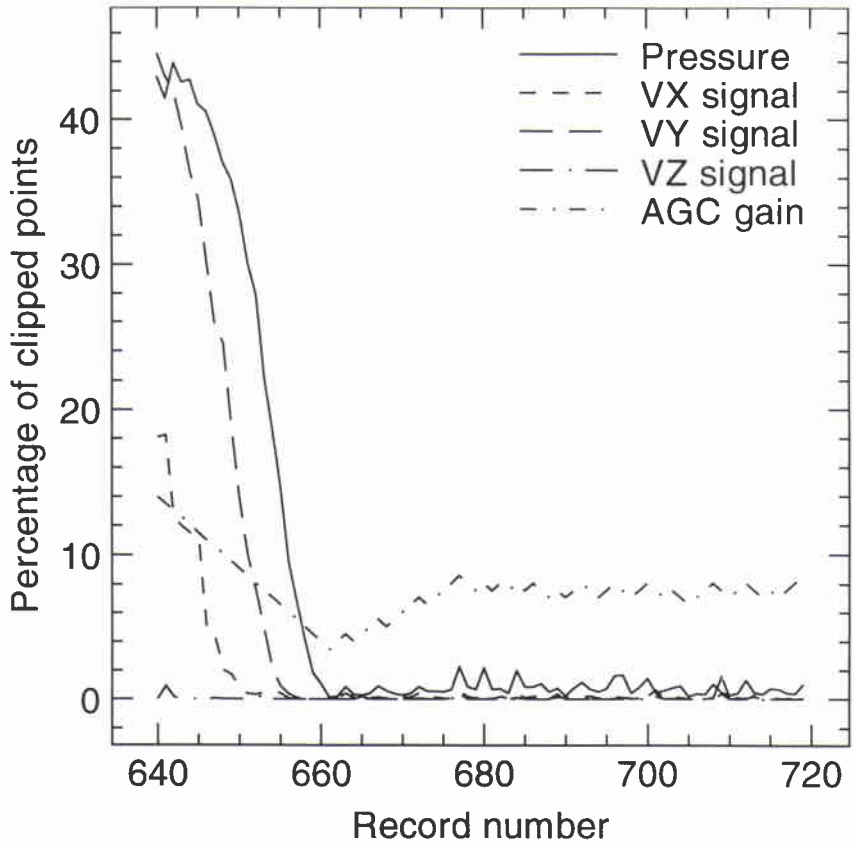

Figure 36 *Percentage of clipped points for the 4 acoustic sensors, and AGC gain for Float 5, second deployment. Record 640 to 720.*

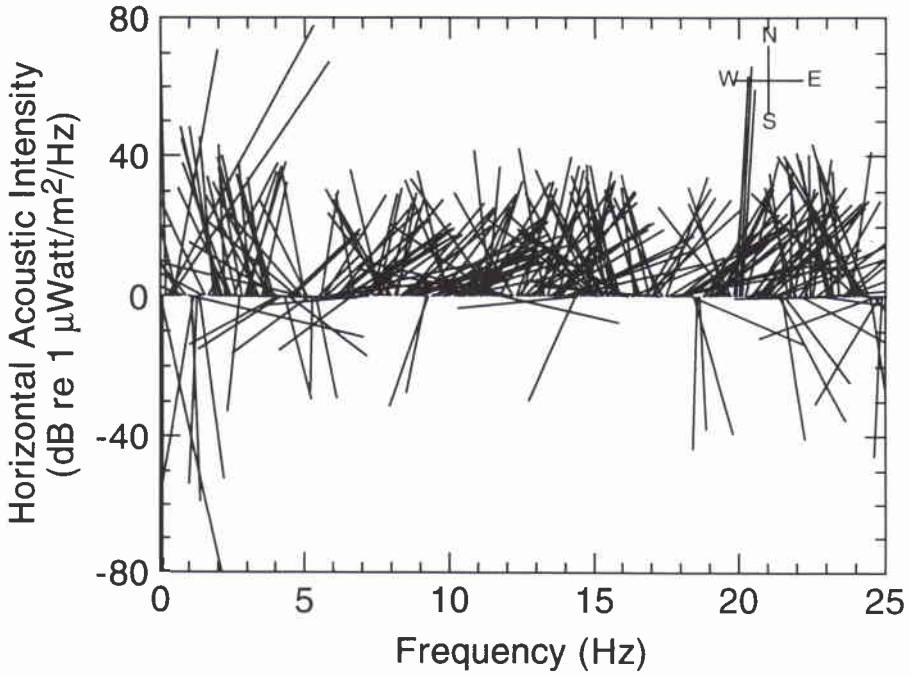

Figure 37a *Horizontal acoustic intensity vectors during transmission of the 20 Hz CW tone (second deployment. The magnitude of the intensity, in dB// 1 μWatt/m²/Hz, is obtained by measuring each vector along the vertical scale, starting at -80 dB. Float 0.*

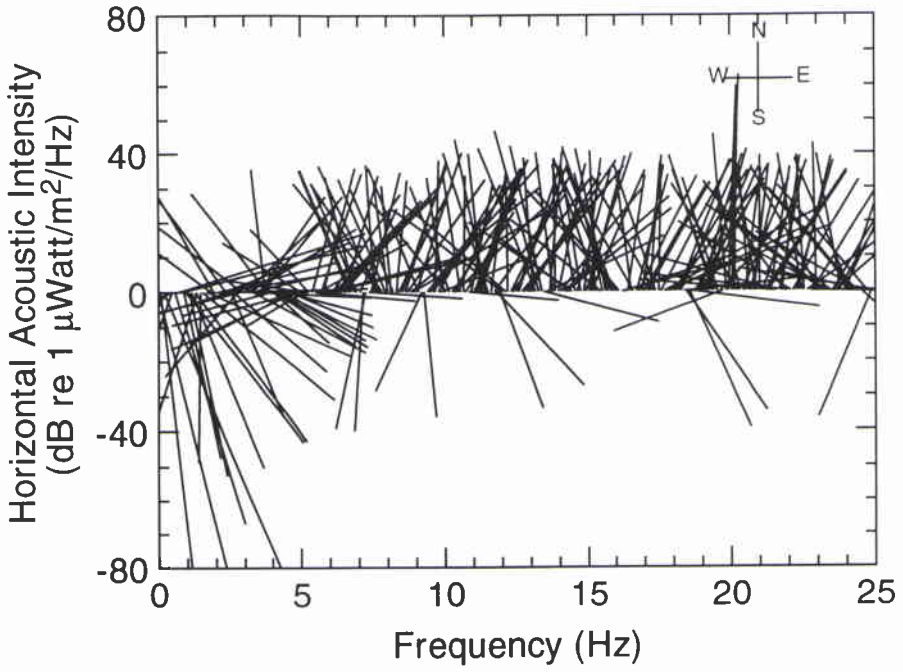

Figure 37b *Horizontal acoustic intensity vectors during transmission of the 20 Hz CW tone (second deployment. The magnitude of the intensity, in dB// 1 μWatt/m²/Hz, is obtained by measuring each vector along the vertical scale, starting at -80 dB. Float 1.*

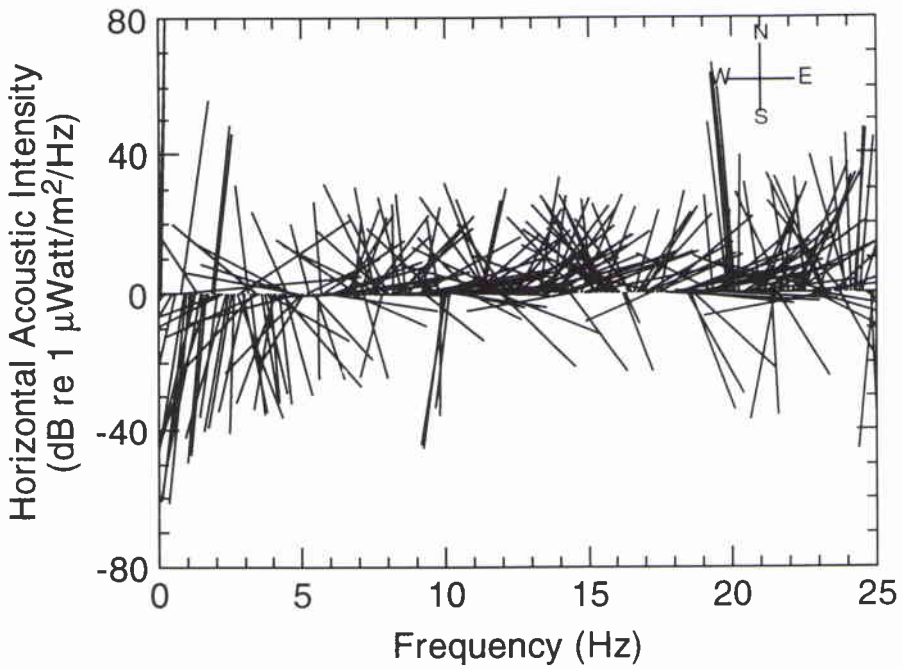

Figure 37c *Horizontal acoustic intensity vectors during transmission of the 20 Hz CW tone (second deployment. The magnitude of the intensity, in dB// 1 μWatt/m²/Hz, is obtained by measuring each vector along the vertical scale, starting at -80 dB. Float 2.*

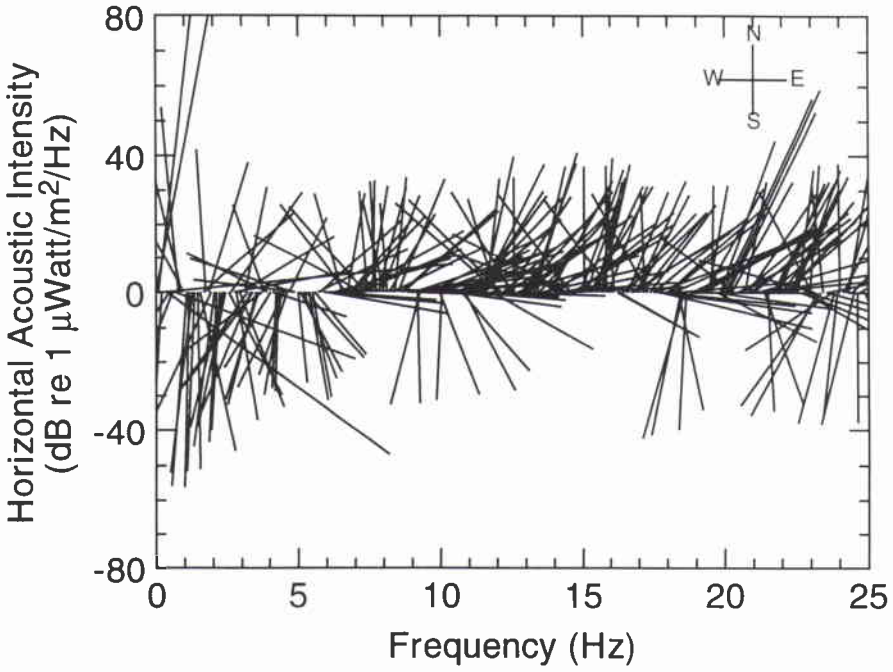

Figure 37d *Horizontal acoustic intensity vectors during transmission of the 20 Hz CW tone (second deployment. The magnitude of the intensity, in dB// 1 μWatt/m²/Hz, is obtained by measuring each vector along the vertical scale, starting at -80 dB. Float 5.*

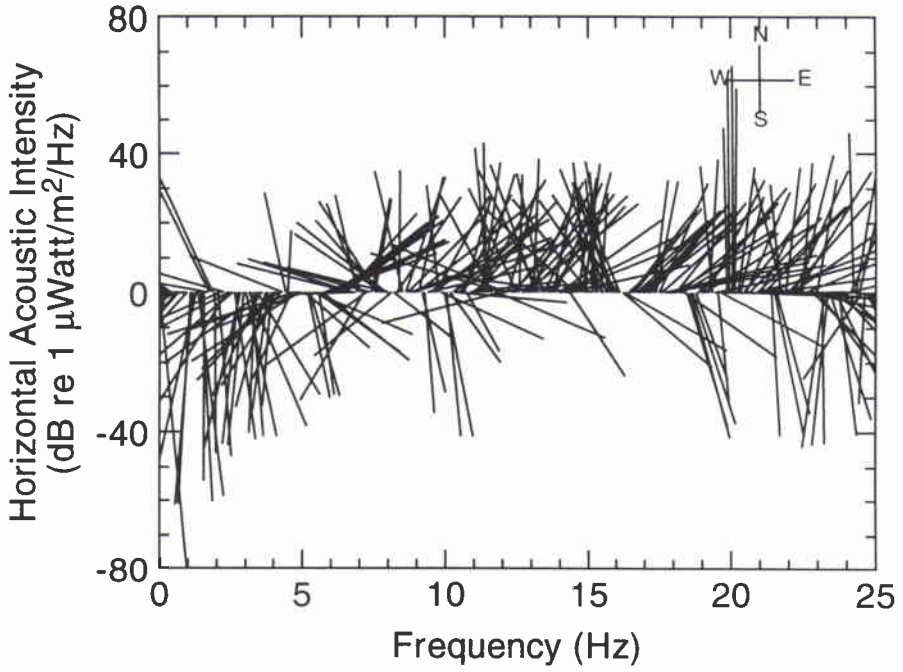

Figure 37e *Horizontal acoustic intensity vectors during transmission of the 20 Hz CW tone (second deployment. The magnitude of the intensity, in dB// 1 μWatt/m²/Hz, is obtained by measuring each vector along the vertical scale, starting at -80 dB. Float 6.*

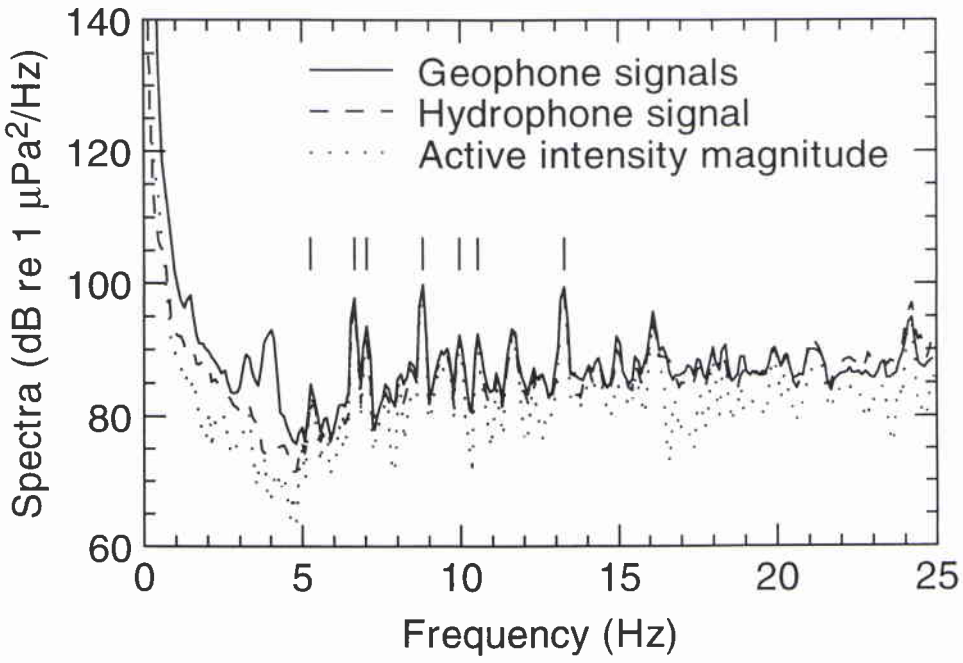

Figure 38a *Average spectra with two sources close by.*

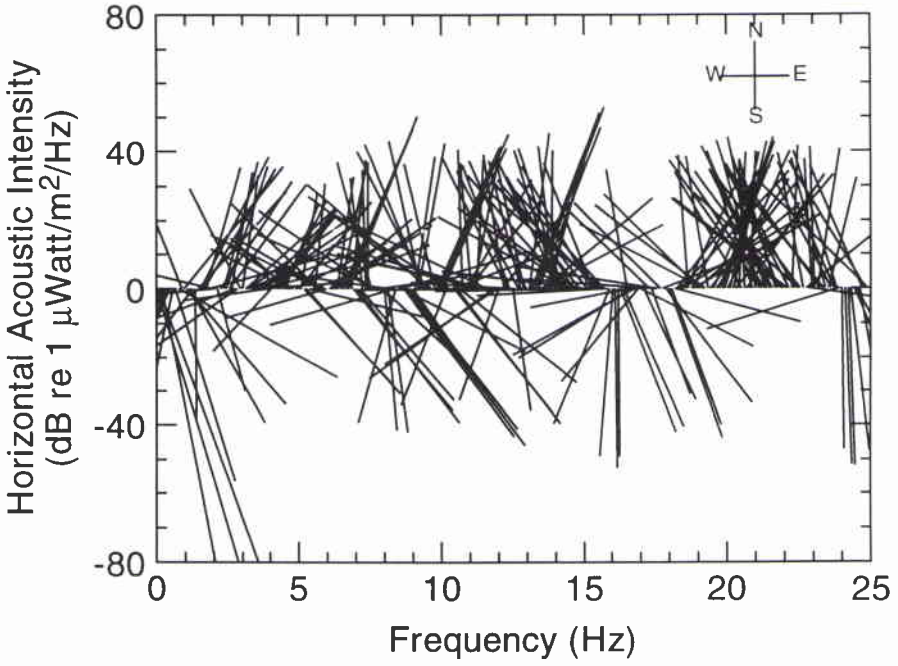

Figure 38b *Horizontal acoustic intensity vectors with two sources close by.*

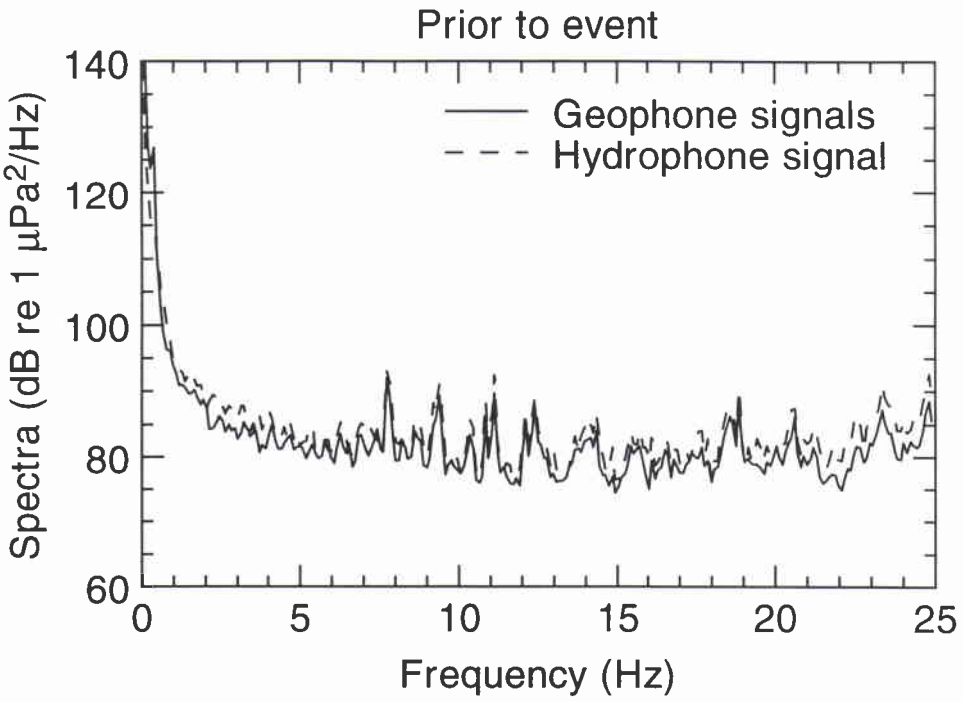

Figure 39a *Average spectra immediately before an earthquake event.*

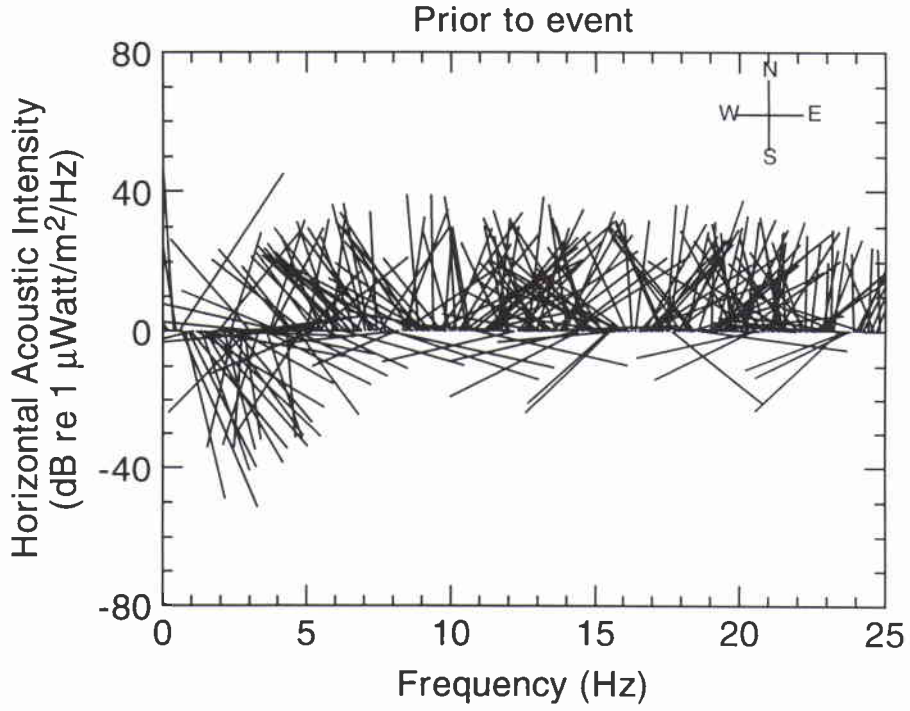

Figure 39b *Horizontal acoustic intensity vectors immediately before an earthquake event.*

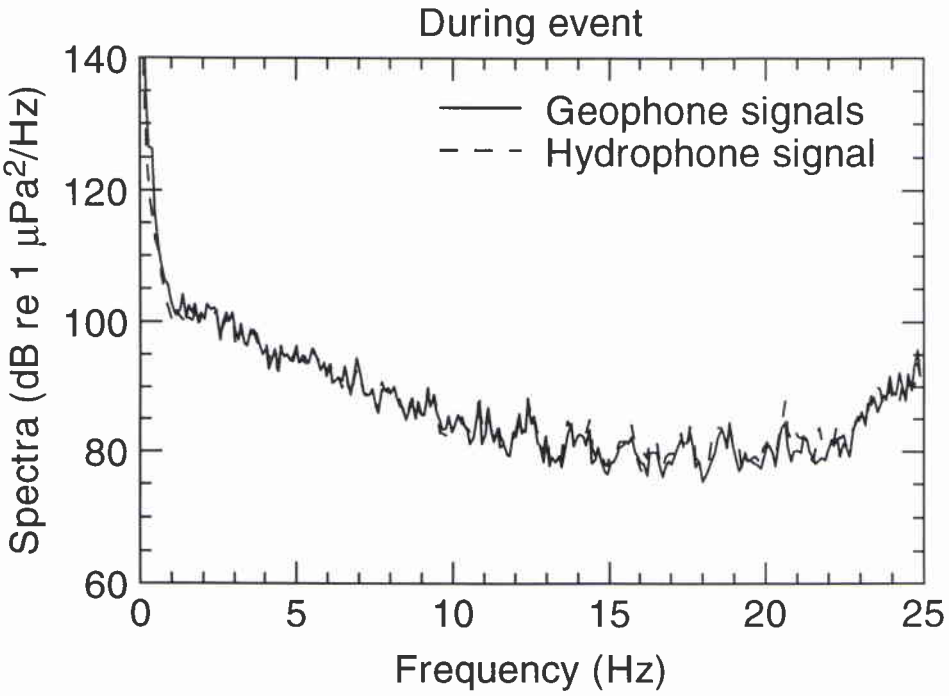

Figure 40a *Average spectra during an earthquake event.*

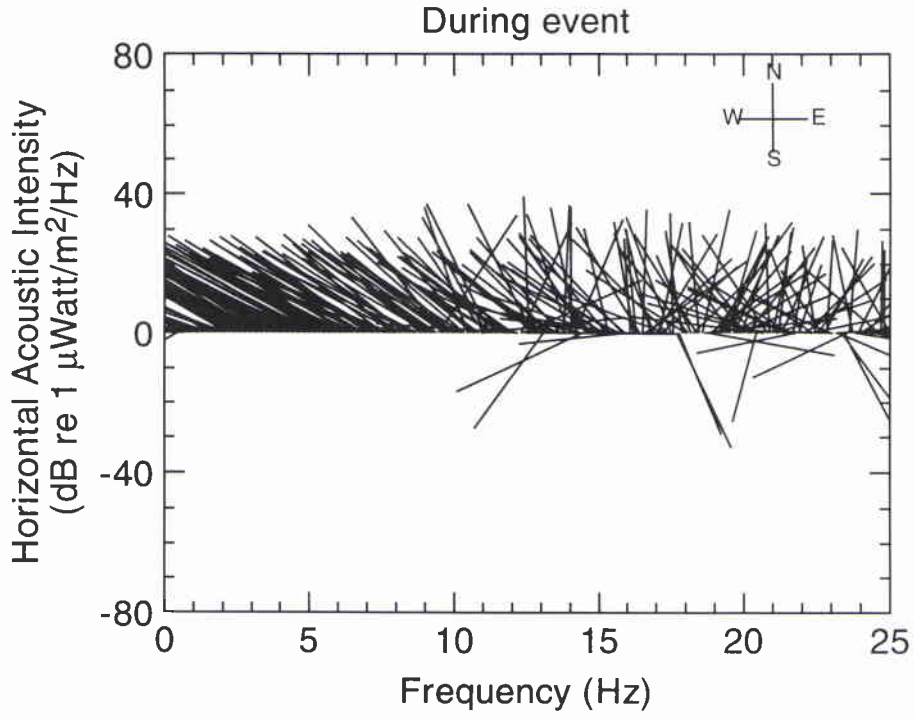

Figure 40b *Horizontal acoustic intensity vectors during an earthquake event.*

Annex A
Time and position tables

The following tables include the time periods of hardware deployments and data recording.

Table A1 *Time table of hardware deployments during IONEX 92*

Equipment deployed	Approx. deployment/ recovery time (UTC)	Approx. recovery time (UTC)	Notes
Vertical array	1 June 7:47	1 June 9:35	
Swallow floats	1 June 11:30	4 June	Recording stopped on 2 June
Sonobuoys	2 June 06:28	-	Also shipping traffic survey
Horizontal array	3 June 13:38	3 June 18:35	
Horizontal array	4 June 9:13	4 June 16:46	
Horizontal array	6 June 9:06	6 June 13:48	
Swallow floats	7 June 7:54	10 June	Projector on occasionally
Sonobuoys	7 June 16:00	-	Also shipping traffic survey
Vertical array	10 June 11:53	10 June 14:50	

Table A2 *Data recording periods with SACLANTCEN vertical array*

Time (UTC)	Nominal position of the array
1 June 1992 08:56 - 09:16	37°39.8' N 18°19.9' E
10 June 1992 12:44 - 13:48	37°44' N 18°28' E

Table A3 *Data recording periods with SACLANTCEN's horizontal array*

Polygon #	Recording time (UTC)	Depth of the array (m)	Approximate position of polygon	Sea state during tow
1	3 June 1992 14:43 - 18:30	102 - 142	37°43N 18°20E	2 to 3
2	4 June 1992 10:13 - 16:06	98 - 130	37°42N 18°20E	1 to 2
3	6 June 1992 09:58 - 13:06	113 - 126	36°50N 18°35E	2

Table A4 *Data recording periods with air-deployed sonobuoys*

Date of deployment	Recording period
2 June	06:54 - 12:15
7 June	16:15 - 20:00

Table A5 *Deployment times with SACLANTCEN's Swallow floats*

Time (UTC)	Initial position of the floats
SF(A) 1 June 11:30 - 2 June 18:54	37°39.99 N 18°20.01 E
SF2 7 June 8:14 - 9 June 11:17	37°39.82 N 18°19.74 E
SF1 7 June 8:17 - 9 June 11:39	37°39.82 N 18°19.72 E

Table A6 *Time window of valid data for the two deployments of MPL Swallow floats*

Deployment	Synchronization time (UTC)	Time of record 640 (UTC)	Time of record 2240 (UTC)
First	1 June 1992 11:00	1 June 19:00	2 June 15:00
Second	7 June 1992 7:37	7 June 15:37	8 June 11:37

Annex B
Environmental data

Six CTD (Conductivity–Temperature–Depth) probes were launched at the experimental site, at the times and positions specified in Table B1. The six sound speed profiles calculated from the CTD data are shown in Fig. B1. Except near the surface, where the daily temperature cycle has a large influence on the sound speed, the profiles are similar and feature a sound channel at approximately 200 m depth.

Table B1 *Time and position of the CTD collection*

CTD#	Date (1992)	Time (UTC)	Latitude	Longitude
1	31 May	23:34	37°40' N	18°20' E
2	1 June	08:08	37°40' N	18°21' E
3	3 June	10:44	37°39' N	18°19' E
4	3 June	19:15	37°39' N	18°21' E
5	4 June	17:28	37°33' N	18°18' E
6	5 June	15:17	37°32' N	18°18' E

The weather was relatively calm during the entire sea trial. Figure B2 shows the 6-hourly wind speed readings. The two Swallow float data collection periods are indicated on the figure. The winds were light during the first deployment (increasing only towards the end of the deployment), and similarly the sea state was calm to moderate (end). During the second deployment, a weather disturbance arrived from the south-east, and the winds increased from light to approximately 15 kn (7.7 m/s) in the second half of the period, and the sea state also changed from low to moderate during the same time period.

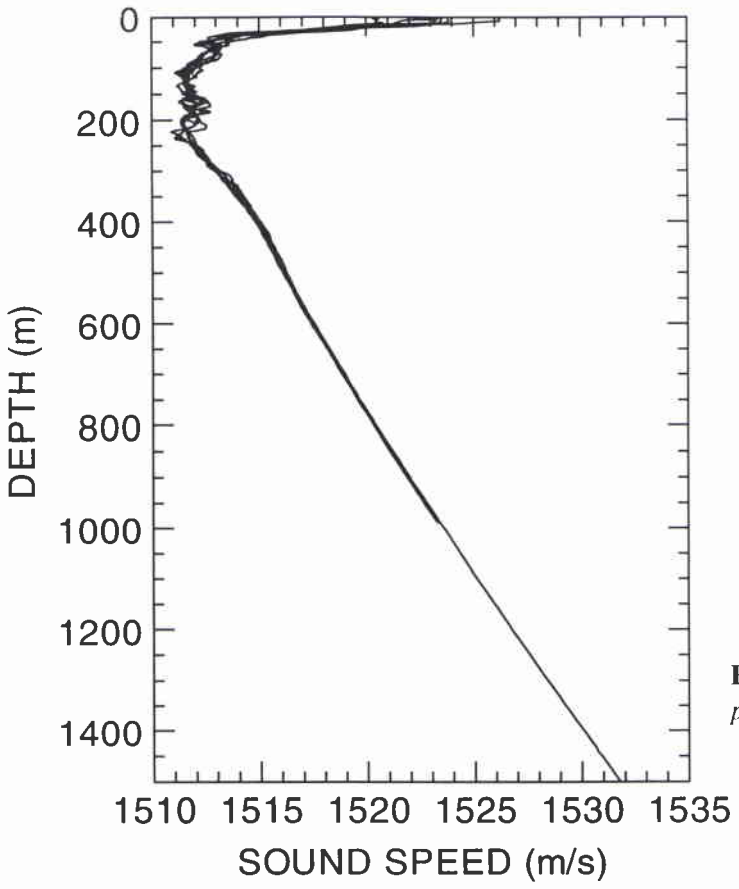

Figure B1 *Sound speed profiles at site location.*

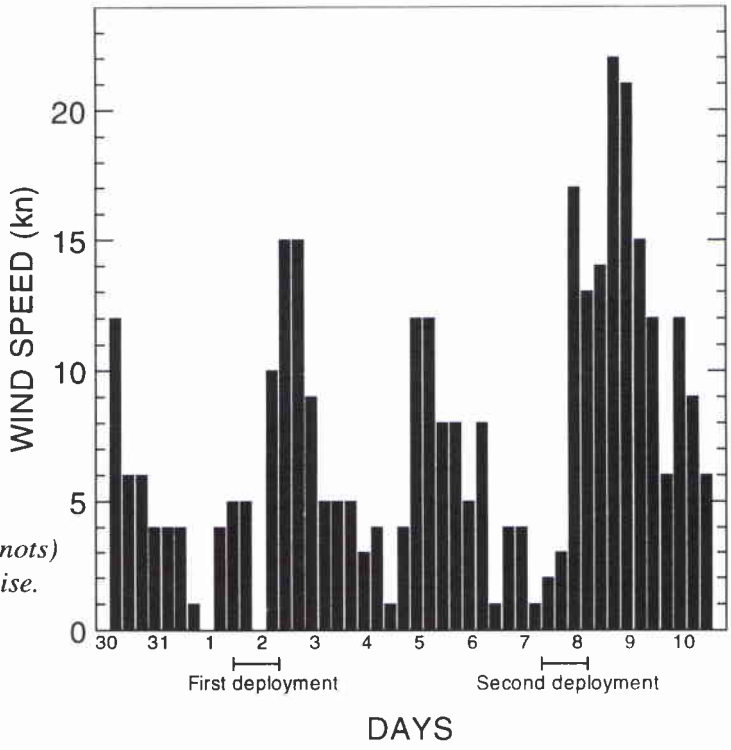

Figure B2 *Wind speed (knots) during the experimental cruise.*

Annex C
Projector log

While the Alliance was steaming south during the second deployment, the VLA acoustic projector was occasionally turned on for a period of approximately 15 minutes. The position of NRV Alliance when the projector was transmitting is shown in Fig. E1, and given in Table C1, along with the estimated distance from the float field at the time, and the accelerometer level of the projector. An accelerometer level of -3.5 dB is equivalent to a source level of 182 dB re 1μPa @ 1 m. The tow depth was 70 m. The tow speed was approximately 10 kn, or 5 m/s.

Table C1 *Projector tow information - second deployment*

Projector time on (7-8 June 92)	Projector time off (7-8 June 92)	Alliance's position	Distance from floats (n. mi.)	Accelero-meter level (dB)
15:20	16:01	37°20.4' N, 18°20.3'E	20	-3.8
18:05	18:21	37°00.2' N, 18°20.0'E	40	-3.5
20:12	20:27	36°40.1' N, 18°19.8'E	60	-3.5
22:56	23:11	36°10.3' N, 18°19.6'E	90	-3.5
01:40	01:56	35°40.2' N, 18°20.0'E	120	-3.5
04:30	04:46	35°10.3' N, 18°19.8'E	150	-3.5
07:20	07:35	34°40.1' N, 18°19.8'E	180	-3.5

Annex D
Shipping traffic

The two support aircraft flights were on 2 and 7 June 1992 respectively (one flight per float deployment). During the periods mentioned in Table D1, the positions of all ships in an opening area of 90° (between 45 and 135°) from the approximate float field location towards Greece were logged once with their estimated speed and course. The periods of shipping surveillance can be compared to the acoustic data collection periods from Table A6. The location of the ships are shown in Fig. D1 for the first deployment, and in Fig. D2 for the second deployment. The word 'station' indicates the approximate location of the float field and was the reference point (37°40' N 18°20' E) to define the surveillance area. The dotted lines from the station indicate the limits of the surveillance area.

Table D1 *Periods of shipping surveillance*

Survey	UTC time period
First	2 June 1992 7:15 - 9:50
Second	7 June 1992 13:15 - 21:00

The surveillance period was much longer for the second deployment, therefore the pattern of two main shipping lanes can be made out. The first one, at an angle of approximately 60° and passing south of the station is the shipping lane used by the traffic going from the canal of Corinth towards the south of Italy. The second one, with a bearing of approximately 115°, shows the traffic going from the south of Greece to Italy. The traffic for the first deployment seems to show similar trends, although fewer ships were logged during the shorter period.

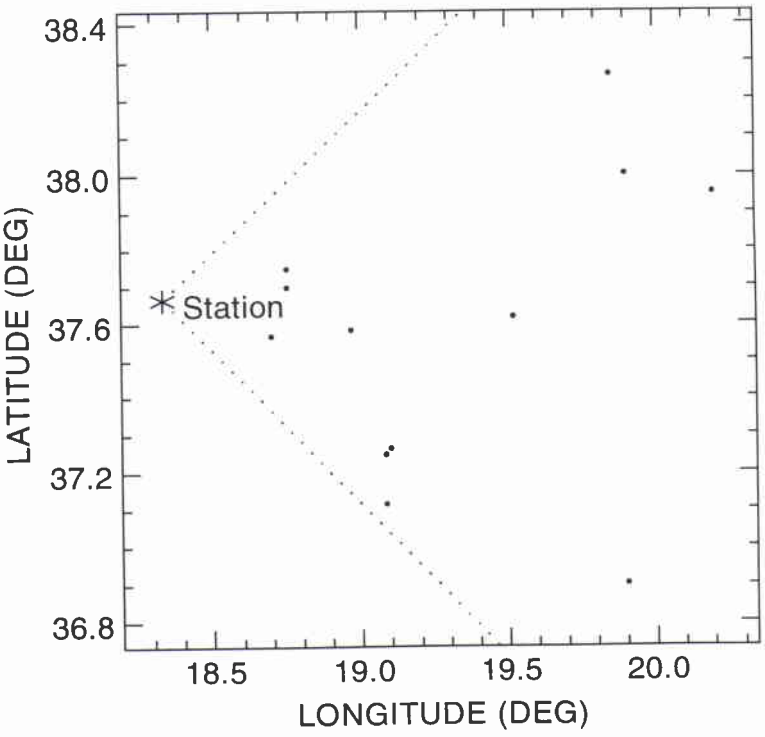

Figure D1 *Shipping traffic during first deployment.*

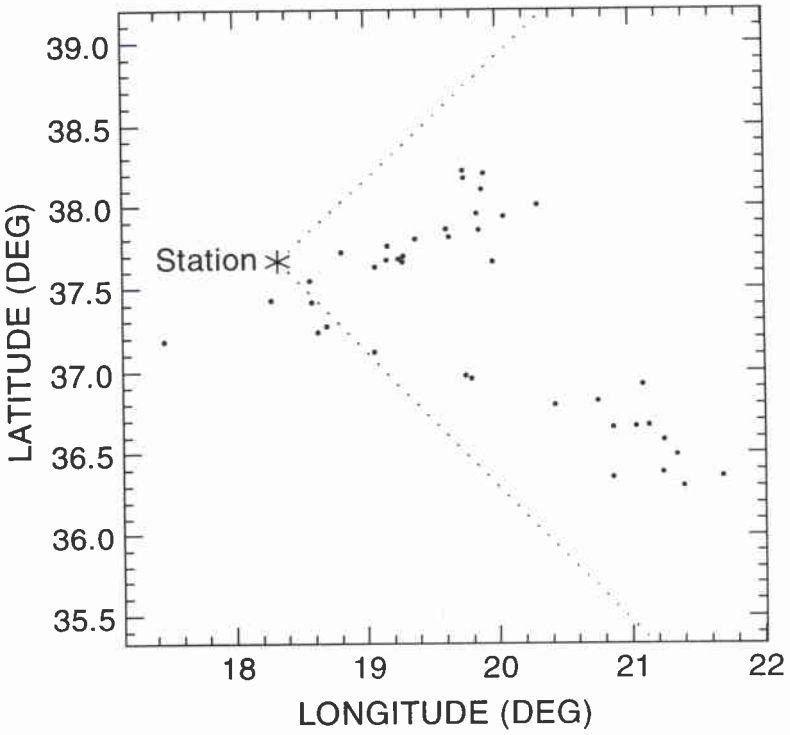

Figure D2 *Shipping traffic during second deployment.*

Annex E
Earthquake information

A listing of earthquakes for the Ionian Sea area was obtained from the Istituto Nazionale di Geofisica, Italy and the National Observatory of Athens (Seismological Institute), Greece. Six earthquakes were listed for the time period covering the data collection; they are repeated in Table E1, with the calculated locations of the hypocenters and initial times of the events. Figure E1 shows the location of five of these six earthquakes with some of the land stations of Italy and Greece.

Table E1 *Earthquake events in the Ionian Sea, data collection period*

Time (UTC)		Latitude (°N)	Longitude (°E)	Approximate range to floats (km)
1 June 92	20:17:32.57	35°09.36	23°01.02	505
1 June 92	23:06:49.07	44°31.8	7°19.2	1200
2 June 92	03:26:45.66	44°28.38	9°49.32	1040
2 June 92	3:47:49.18	44°28.08	9°50.58	1040
2 June 92	8:19:19.50	40°39.84	15°27.9	415
2 June 92	10:50:50.8	43°25.68	10°17.4	935

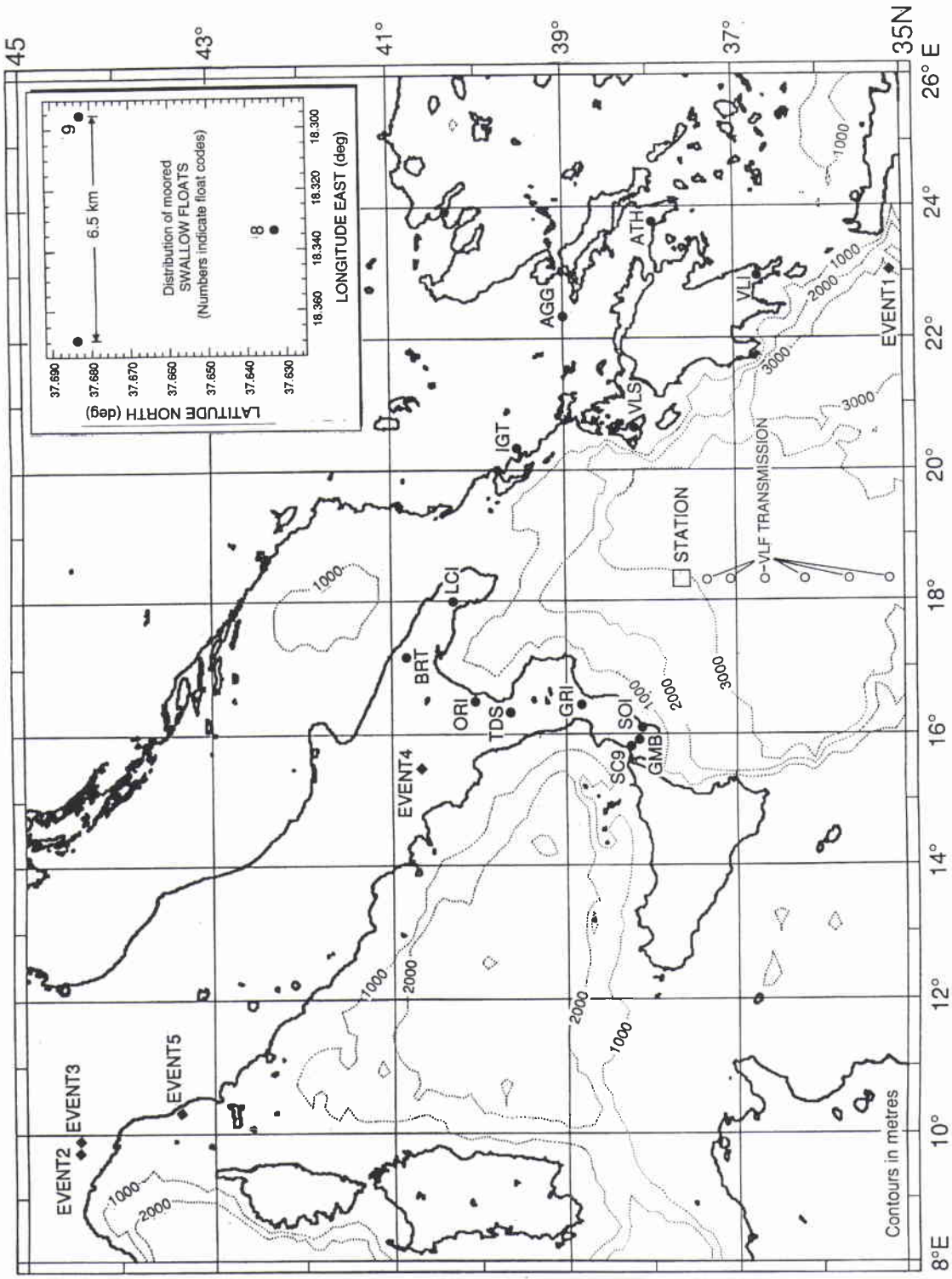

Figure E1 *Location of five of the six earthquake events during that occurred during the two deployments, along with some Italian and Greek land stations (3-letter acronyms). The blowup figure indicates the positions of the 3 bottom floats.*

Annex F
MPL Swallow float deployments–sea trial notes

Figures F1 and F2 give an overview of the periods during which valid data were recorded for each individual float during both deployments. Data can be available outside of these periods, although the quality may not be good since the float may be either settling to depth or returning to the surface. The absolute time can be obtained by using the start times of Table A6, and by counting 80 records per hour.

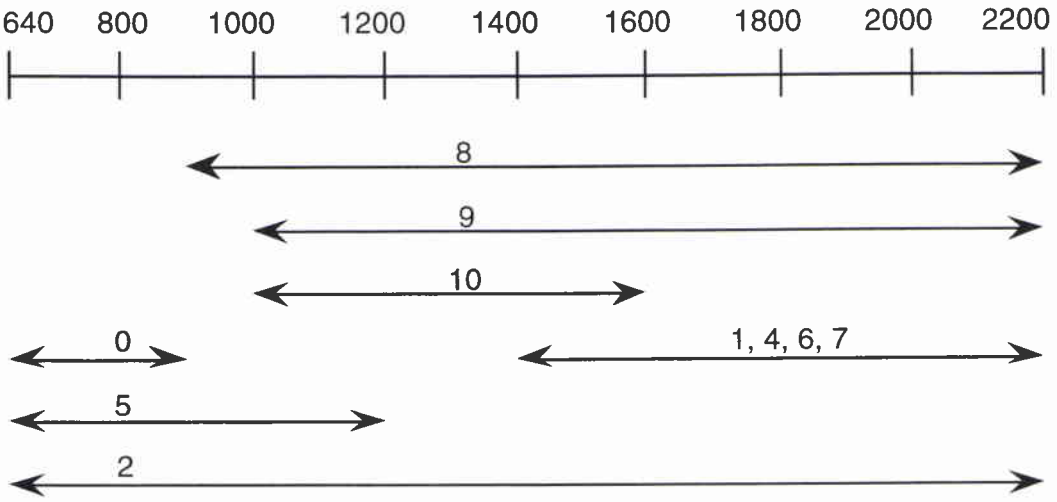

Figure F1 *Periods of valid data (in record numbers) for each float during the first deployment.*

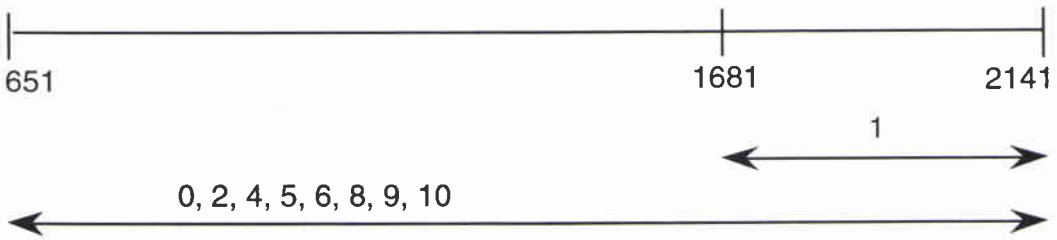

Figure F2 *Periods of valid data (in record numbers) for each float during the second deployment.*

The IONEX 92 sea trial saw the first deployment of the floats in the Mediterranean Sea. It was also the first time that the floats were deployed in such a low sea state (see Annex B). During the first deployment, it was found that when the sea is too calm, the residual air bubbles trapped underneath the float structure will keep the floats from sinking easily. In past experiments, the sea was never quite so calm, and the float rocking due to the wave action would be sufficient to shake the residual air out, and the floats would sink relatively quickly.

In the first deployment, five floats (1,3,4,6,7) did not sink right away, and had to be redeployed later with an extra 58 g of ballast. This explains why no data are available for these floats at the beginning of the experiment (Fig. F1). The floats finally settled to depth at record 1400 approximately (because of the extra weight, the final depths were also different than the planned depths). Float 3 is not shown in Fig. F1 since the float was lost during the first deployment and the data were never recovered. Floats 0, 5 and 10 went back to the surface prematurely because of an internal clock error. In case of failure of the acoustic release system, all floats have an internal clock that triggers an automatic release after a preset number of days. The clocks were incremented by one day, probably due to a physical shock during the manipulation of the floats. Floats 8, 9 and 10 (bottom floats) have noisy data at the beginning of the period since they were still going down to their bottom depth. Floats 3 and 7 could not be recalled acoustically and did not release on their time release system. Float 3 was lost. Float 2's radio beacon behaved differently, and would sometimes broadcast for up to 10 s. It should be mentioned that the audio chip present in the trip container kept overheating and burning up, and excessive self noise was noted.

After the first deployment, the floats were refurbished, and new ballast weights were installed to avoid the problems of the first deployment. Float 7 was not redeployed.

During the second deployment, the combined effects of extra ballast weights and higher sea state contributed to an easy descent of the floats to depth. The main problem during the experiment was with the recovery of the floats. First, the recovery was delayed by 6 h due to high seas. Then some problems arose with the acoustic communication system of the floats. No floats responded to the acoustic release command although they did respond to the transpond command (command to issue a long ping to help localization). The EG&G box was tried to improve the release of the floats. The localization ping of Float 1 was never heard after the return to site at the end of the experiment, and it came up on time release. Float 9 released only after two hours of trials, even though its localization ping was loud and clear.

Report no. changed (Mar 2006): SM-319-UU

Document Data Sheet

NATO UNCLASSIFIED

Security Classification		Project No.
NATO UNCLASSIFIED		042-1
Document Serial No.	**Date of Issue**	**Total Pages**
SM-319	September 1997	98 pp.

Author(s)

F. Desharnais, H. G. Urban, and G. L. D'Spain

Title

Very low frequency ambient noise measurements in the Ionian sea - data report

Abstract

This memorandum describes an experiment and provides a data summary and quality assessment of very low frequency data of ambient noise collected in the Ionian Sea in June 1992. The experiment was a joint operation between SACLANTCEN and the Marine Physical Laboratory (MPL) of Scripps Institution of Oceanography, USA. The sensor system had been supplied by MPL, it consisted of 11 Swallow floats that are neutrally buoyant freely drifting glass spheres which were equipped with sensors to measure acoustic pressure and 3-dimensional particle velocity in the frequency range between 0.5 and 25 Hz. The data of the four sensors can be combined to yield the time averaged acoustic intensity vector, i.e. magnitude and direction of the acoustic propagation obtained in a single point in space. The acoustic data are complemented by a set of environmental data including seismic events, very low frequency propagation and commercial ship surveillance. All the data are of excellent quality, well documented and therefore, can be used to further investigate the very low frequency ambient noise field in the Mediterranean Sea.

Keywords

ambient noise, very low frequency, Swallow floats

Issuing Organization

North Atlantic Treaty Organization
SACLANT Undersea Research Centre
Viale San Bartolomeo 400, 19138 La Spezia, Italy

[From N. America: SACLANTCEN (New York) APO AE 09613]

Tel: +39 (0)187 540 111
Fax:+39 (0)187 524 600

E-mail: library@saclantc.nato.int

NATO UNCLASSIFIED

Initial Distribution for SM 319

Scientific Committee of National Representatives

SCNR Belgium	1
SCNR Canada	1
SCNR Denmark	1
SCNR Germany	1
SCNR Greece	1
SCNR Italy	1
SCNR Netherlands	1
SCNR Norway	1
SCNR Portugal	1
SCNR Spain	1
SCNR Turkey	1
SCNR UK	1
SCNR USA	2
French Delegate	1
SECGEN Rep. SCNR	1
NAMILCOM Rep. SCNR	1

National Liaison Officers

NLO Canada	1
NLO Denmark	1
NLO Germany	1
NLO Italy	1
NLO Netherlands	1
NLO Spain	1
NLO UK	3
NLO USA	4
Sub-total	30
SACLANTCEN library	21
Total	51